DESIGN AND ANALYSIS OF ONBOARD BATTERY CHARGING FOR ELECTRIC VEHICLE

A DISSERTATION SUBMITTED IN THE PARTIAL FULFILMENT OF THE REQUIREMENTS FOR THE AWARD OF THE DEGREE

OF

MASTER OF TECHNOLOGY

IN

POWER SYSTEM

Submitted By:

Chanchal Chaudhary

(2K19/PSY/23)

Under the supervision of

Prof. Uma Nangia

And

Asst. Prof. Saurabh Mishra

Department of Electrical Engineering

Delhi Technological University
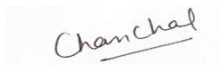(Formerly Delhi College of Engineering)
Bawana Road, Delhi-110042

August 2021

DEPARTMENT OF ELECTRICAL ENGINEERING

DELHI TECHNOLOGICAL UNIVERSITY

(Formerly Delhi College of Engineering)

Bawana Road, Delhi-110042

DECLARATION

I hereby certify that the work contained here in Major Project-II entitled "DESIGN AND ANALYSIS OF ONBOARD BATTERY CHARGING FOR ELECTRIC VEHICLES" in fulfilment of the requirement for the award of the degree of Master of Technology in Power System and submitted to the Electrical Engineering department, Delhi Technological University, Delhi, is a genuine record of my own work which is carried out under supervision of Prof. Uma Nangia and Asst. Prof. Saurabh Mishra during the period of July 2020 to August 2021.

I have not submitted the information contained in this report for any other award of degree or to any other Institute/University.

Chanchal

CHANCHAL CHAUDHARY

(2K19/PSY/23)

CERTIFICATE

To the best of our knowledge this work has not been submitted in part or full for any Degree or Diploma to this University or elsewhere. We also certify that the student's publication and indexing information is accurate.

Prof. Uma Nangia

SUPERVISOR

(Prof. & HOD, EED)

Asst. Prof. Saurabh Mishra

SUPERVISOR

(Asst. Prof., EED)

Place: Delhi

Date: 26-08-2021

ACKNOWLEDGEMENT

Chanchal Chaudhary

Roll No. 2K19/PSY/23

Date: 26-08-2021

ABSTRACT

Electrification of vehicles has become a part of globalisation and modernisation due to the increasing concern for carbon emissions. Global demand for clean fuel energy is increasing rapidly due to fuel scarcity and pollution being important concerns. Consequently, researchers are readily focusing on findings in the electric vehicle (EV) domain. EV is becoming popular in various domains like E-bikes, E-scooters, E-rickshaws, E-cars etc. The ones having lower weight are termed as LEV's i.e., Light electric vehicles. They account for a significant fraction of overall EV and hence cannot be overlooked.

The work in this report deals with the design and analysis of onboard battery charging for electric vehicles with various topologies of DC-DC converters like modified, interleaved, isolated, hybrid etc. which are acting as PFC unit in the charger configuration for better and reliable working of charger thereby reducing total harmonic distortions (THD) within acceptable range as well as improving input current power factor towards unity. In addition to PFC, other DC-DC converters are also used for isolation, and better quality of charging current to be used. In this work, flyback converter is being used due to its simple configuration and excellent isolation properties. Results of interleaved and isolated converters are turned out to be good as compared to other configurations of DC-DC converters. A hybrid configuration is also presented in this report work in which ac supply and solar PV integrated is used for charging in which efficiency of charging is enhanced by use of available solar energy. The unidirectional charging is well elaborated with all the topologies in this work.

The basic charging infrastructure along with the enhanced quality of input current is elaborated in this report work. It involves an AC-DC converter, a PFC unit, an isolated converter and battery as a load. According to the construction and working chargers can be discussed in two categories one is onboard charger and other is offboard charger. Control techniques involves classical linear PI controllers as voltage controller and current controllers. These constants are helpful in the closed loop operation of charger circuit. So, this work compiles a complete view of a better converter topology required for the sound working of onboard battery charger.

TABLE OF CONTENTS

List of Figures

List of Tables

List of Symbols

D	Duty Cycle
S	Switch
f	Switching Frequency
f_{sw}	Flyback converter's switching frequency
f_c	Filter's cut off frequency
n_s	Secondary turns ratio
n_p	Primary turns ratio
C_d	DC link capacitor
L_m	Magnetising Inductance
μ	Battery ripple voltage
V_s	Supply voltage
I_s	Supply current
V_{bat}	Battery voltage
I_{bat}	Battery current
Δi_L	Change in inductor current
Δv_c	Change in capacitor voltage
i_c	Capacitor current
i_D	Diode current

List of Abbreviations

EV	Electric Vehicle
PFC	Power Factor Correction
DCM	Discontinuous Conduction Mode
THD	Total Harmonic Distortion
MOSFET	Metal Oxide Silicon Field Effect Transistor
IGBT	Insulated Gate Bipolar Transistor
MPPT	Maximum Power Point Tracking
PHEV	Plug-in hybrid electric vehicle
DBR	Diode Bridge Rectifier
P&O	Perturb and observe
PV	Photovoltaic
SEPIC	Single ended primary inductance converter
T/F	Transformer
DC	Direct Current
AC	Alternating Current
EMI	Electromagnetic Interference
HFT	High Frequency Transformer
CC-CV	Constant Current-Constant Voltage
V2G	Vehicle to Grid
SOC	State of Charge
DOD	Depth of discharge

CHAPTER-I

INTRODUCTION

In the modern era, as the human population is increasing exponentially and thereby responsible for the rising need of vehicles. Increasing demand of vehicle, large transport dependence on oil that forces to exploit more and more fossil fuels like diesel, petrol etc. The limitation of fossil fuels and pollution caused by them are the big concerns nowadays. Demand is more and stocks are limited on the other hand pollution is playing a major role in damaging environment and its entities. So as a solution to these problems Electric Vehicle (EV) is the vital role player in modernisation and it is the need of the hour. The main advantages of introducing EV majorly involves cutting down the dependence of transport on oil and lowering down carbon emissions. In case of unavailability of any other alternative in transportation may lead to the scarcity of oil resulting in huge price hikes in oil industry.

1.1 Historical Background

First electric locomotive design was invented by Robert Davidson in year 1837 and the use of first locomotive on main line was in 1895 on Baltimore belt line located in USA with a stretch of 4 miles. At the start of 19th century EV started growing and the first experiments were done on electric trams/trolley cars and consequently by the end of 19th century EV became widely usable because of the mass production of rechargeable batteries as batteries came with revolutionary change in EV industry and became an important part player. The first ever regular tram service was started in 1881 in suburbs of Berlin, Germany. Siemens and Halske collaborated on this project. As time passed moving to 20th century, though private cars were rare but electric in nature. Although EV industry was rising but problems related to batteries were also to be bothered as batteries took quite longer time to recharge and they were costlier than the same size IC engines used and as a result in whole 20th century IC engines remained predominant. After it the concept of hybrid vehicle having IC engine combined with one or two electric units. Such a type of hybrid vehicle was introduced by Ferdinand Porsche in 1900 which could run via electricity either from engine or by batteries. In the mid of 20th century electric trains became favourable for railways because of their low maintenance requirement in both the cases i.e., tracks and locomotives. Due to the overhead lines electric trains were a huge success but on the front of   roads electric vehicles had not achieved that much success because they somehow rely on batteries but undoubtedly EV is having certain advantages over

IC engines as first of all EV's do not produce any exhaust emissions and other is that they are inherently quite so these advantages make it suitable for those industries where pollution and noise are the major problems. Coming towards the end of 20th century and start of 21st century where development of high-speed trains was in progress. It all started with the concept of bullet train in Japan whose services started in 1964 from Tokyo to Osaka having capability of travelling 515.4 kms in just 4 hours. More advancements include Maglev trains which uses a special track to run, having a world record of achieving 581kph speed. They are competing with aircrafts in terms of covering distance faster. Major issue in using EV involves using battery and its charging although several manufacturers are producing good quality EV's now. Some of them are Renault, Mitsubishi, Nissan, Tesla. After 1990 electric bicycles became popular and EV two wheelers also gained growth. In recent trends hybrid vehicles, which includes solar as well as AC charging are also new research topics to be explored more.

Promoting EV has become helpful in cutting down hazardous greenhouse emissions and is suitable for the high efficiency demands in vehicular industry with taking care of environmental issues. In addition to this many control strategies are available for motors which enhances the usage of EV in vehicular industry. Above discussion justify the need of EV in present times. Some general examples of EV includes Electric trains, Electric cars, Electric bicycles, Electric rickshaws etc. Government of India is aiming for making India a complete electric vehicle nation by 2030, For this target it has been proposed that all two wheelers having engine capacity below 150cc which has to be sold after 31 march 2025 and all the three wheelers sold after 31 march 2023 should be electric vehicles. Some of the target data set by NITI Aayog concerned to e-mobility can be figured out from Fig.1.1.
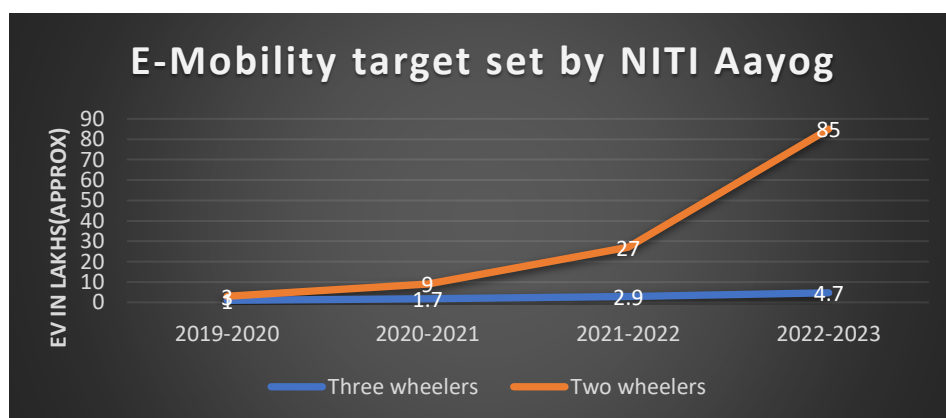
Fig.1.1 Trend showing set target for EV with time (courtesy: timesofindia.indiatimes.com)

1.2 Charging Configuration

The general configuration of a charger as shown in Fig.1.2. It involves an AC-DC conversion unit followed by filter. EV charger needs DC as input so AC-DC conversion unit is required for example basic DBR is mostly used. The usage of DC-DC converter as PFC unit in the circuit is controlled by control algorithm to provide requisite DC level for charging. EV battery gets charged after getting required DC voltage level.
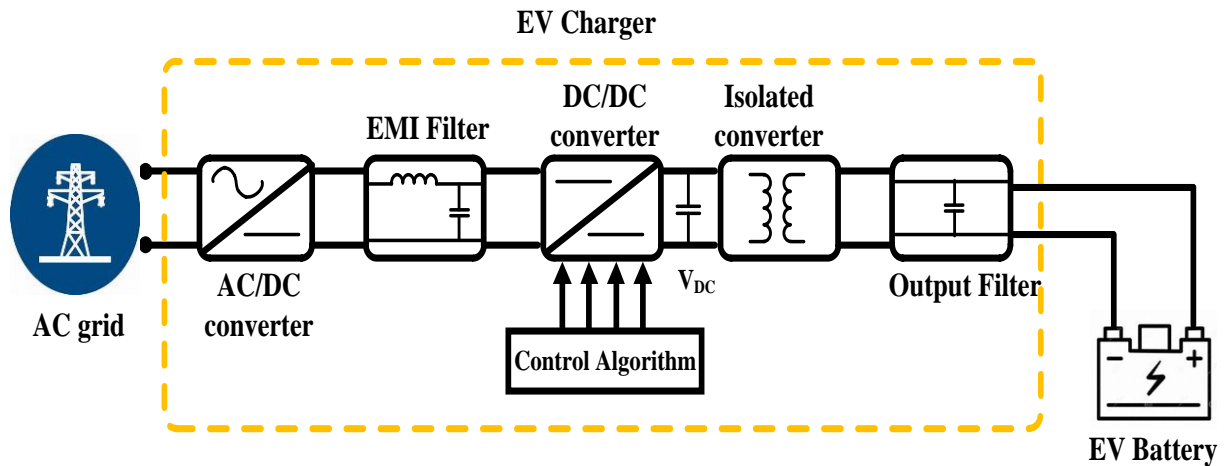
Fig.1.2 Charger configuration

1.3 Existing topologies for EV Charging

Battery charging topologies can be classified as Onboard charging and Offboard charging on the basis of their charging location as shown in Fig 1.3. An onboard charger as illustrated in Fig.1.4 is designed for less rating and are compact, built in within vehicle whereas offboard chargers as per Fig.1.5 are designed for quite high ratings and generally involves charging stations. Offboard charging is served by three phase AC station while onboard charger can be served by single phase supply. There is no reactive power transfer in unidirectional charger and both active as well as reactive power transfer takes place in bidirectional charging. It can be capacitive or inductive operation in latter. Power factor in bidirectional chargers is depending upon their working operation in one of the four quadrants, accordingly it can be lagging, leading, zero or unity.
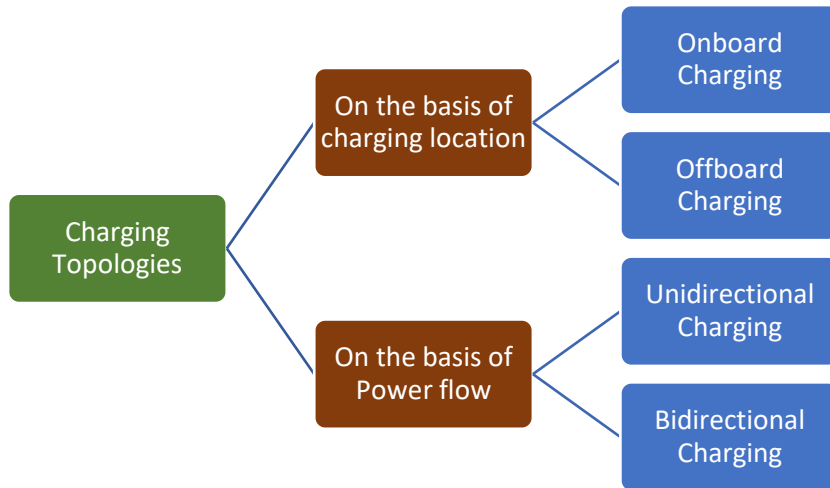
Fig.1.3 Charging Topologies
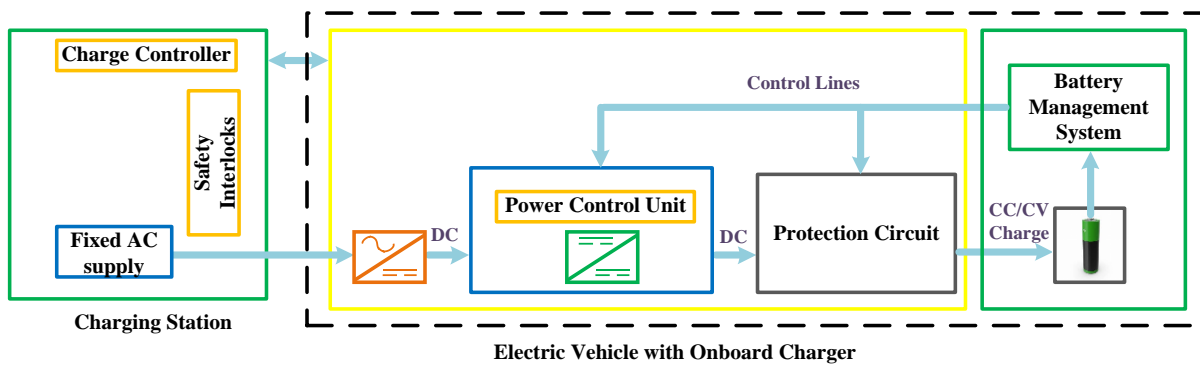
Fig.1.4 Onboard Charger Layout
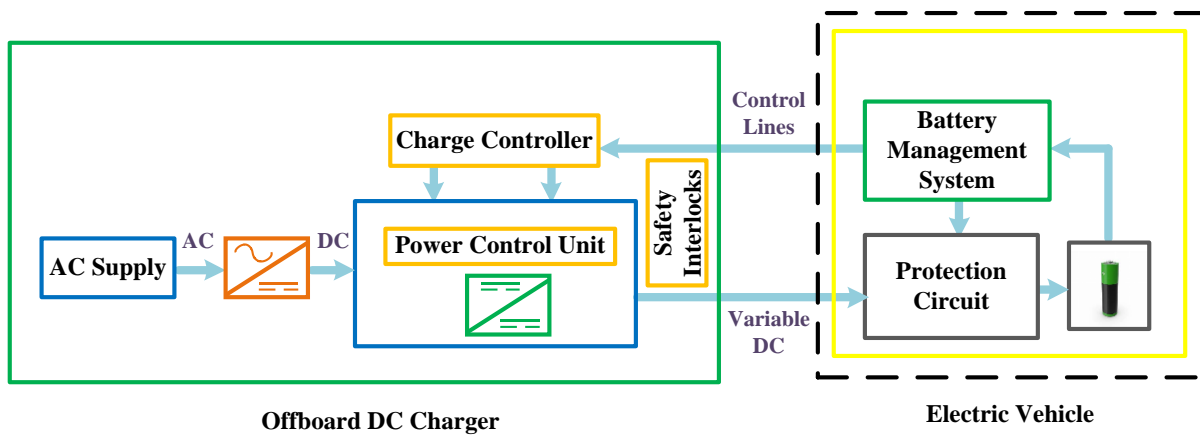
Fig.1.5 Offboard Charger Layout

1.4 Dissertation Outline

- <u>Chapter-I</u> In this chapter brief introduction about EV industry and its rapid rise is discussed along with an outline of historical background and evolution of EV.

4

- <u>Chapter-II</u> Learnings based on the review of many research papers is mentioned in this chapter.

- <u>Chapter-III</u> It comprises of modelling and design analysis of general DC-DC converters that can be utilised as a PFC also. Results along with their simulations are shown in this chapter. This chapter gives an idea about usage of these basic converters and their effectiveness in chargers.

- <u>Chapter-IV</u> The illustration of design as well as analysis of modified DC-DC converters and their usage as PFC in chargers is shown with the help of Simulink results in this section.

- <u>Chapter-V</u> An improved charging topology with improved power factor i.e., Interleaved DC-DC converters as PFC has been discussed in this chapter.

- <u>Chapter-VI</u> After the discussion of all the topologies, a new advancement in this field i.e., hybrid EV charging systems are briefly illustrated in this chapter. A brief discussion about how bridgeless topology is better than conventional topology is represented via simulation results here.

- <u>Chapter-VII</u> This chapter illustrates about conclusion as well as future scope of the whole work discussed here.

CHAPTER-II

LITERATURE REVIEW

2.1 Introduction

The work mentioned in this report is a collective outcome of many research papers which includes the study of EV and its charging. Many new ways and research findings have been found regarding the better efficiency of EV and improved reliability of the vehicle. A general review of these research papers is summarized as per below mentioned areas:

1) Onboard battery charging
2) Need of PFC in Onboard battery Charging
3) Converter selection for PFC converter
4) Various topologies for battery charging
5) New techniques for battery charging

2.1.1 Onboard Charging

Chargers can be of two types i.e., Onboard charger and Offboard charger, former is used generally for the single phase while latter consist of three phase supply being higher in rating as compared to onboard chargers. As per [1] onboard chargers can be used with three phase supply circuits in case of propulsion system integrated with them to make it an integrated onboard charger used for PHEV [2]. Two types of batteries are used in onboard chargers for PHEV and EV, i.e., Auxiliary batteries and propulsion batteries as mentioned in [3]. Propulsion battery supplies high voltage DC for driving the vehicle while auxiliary battery provides with low DC voltage for feeding the electric fields of the vehicle. Onboard charging circuit can be seen in [4],[5] and [6] and clearly shows that it works being inside the vehicle.

2.1.2 Need of PFC in Onboard Charging

In an onboard charger, DC is required for charging the a battery that can be obtained through the use of an AC-DC converter (comparison is given in [7]) at the input of charger. Generally, DBR being basic prototype, is used for this purpose. The basic power electronic rectifiers introduce a huge amount of distortion and harmonics in the circuit. It lowers down the quality of power generated thereby affecting the power factor of the system. THD of system becomes high and power factor goes away from unity leading to the damage in connected system equipment. A general review on power quality in various DC-DC converters is mentioned in

[8] and [9]. This gives rise to the need of PFC in onboard charger. The basic topology as per [10] consists of an AC-DC conversion unit, a PFC unit, an isolated converter and battery which is to be charged. A charger can be single stage charger or two stage as per the rating and requirements of the vehicle. Nowadays, mostly two stage chargers are in use due to their reliable operation and better current wave shaping capability.

2.1.3 Converter selection for PFC

In charger configuration any DC-DC converter is taken to be as PFC unit but as time has passed it is observed that Buck and boost converters are not recommended for PFC as compared to buck-boost converter as given in [11] and [12] rather other modified circuits can be used for boost, one of them is mentioned in [13]. Buck-Boost converter [14] with very simple configuration and less components, is having edge over these two converters due to its wide variable range of duty cycle and that results in operation of converter with a large voltage range also. A comparison for different configurations which can be used in buck-boost is given in [15]. So, these two converters are not suitably used due to the disadvantages as given in [16], of poor current shaping feature as well as low variation availability of duty cycle. Apart from these basic converters there are other converters available like CUK [17], SEPIC [18], Zeta [19], Luo, Landsman converter [20] etc. Out of CUK and SEPIC converters, CUK is a relevant option due to its certain advantages given in [21] i.e., Lower EMI noise, decrease in ripple current at output as   well as at input with an added feature of shielding from start-up inrush current whereas SEPIC deals with the drawback of high ripples in output current along with the discontinuity in output current. An improved battery charger is mentioned in [22] and [23] with requirement of these converters in designing of PFC corrected circuits. Further Zeta converter as per [24] is having certain qualities like good dynamic response, low output ripples, positive voltage at output but it is having high voltage stresses at PFC switches. Luo and Landsman converters are further used due to their added advantage of better current profile, low ripples in current and output voltage as can be observed from [25]. These converters with added elements in comparison to basic buck-boost converter, are more apt in the input current wave shaping and hence acting as a PFC converter in the battery charging system. In addition to these converters one isolated converter can also be used (Flyback converter in this report). One such type of flyback converter is illustrated in [26]. High frequency transformers play an excellent role in the mitigation of ripples in a circuit and though flyback is consisting of HFT, it further improves the current profile at input and also reduces the ripples at output of charger to great extent. Flyback converter is simplest in view of design and provides a large extent

isolation in the converter circuit. It also ensures the CC-CV charging in the circuit as mentioned in [27]. AC-DC converter selection can be understood from [28].

2.1.4 Various topologies for charging

In a charger, at the place of PFC converter various configurations can be used like it can be a conventional converter which we have discussed earlier or it can be a modified configuration of previously discussed converters with some minor changes like rearrangement of diodes and inductors or addition of components to mitigate the problem arisen due to the usage of DBR [29] at the input side. Some of the modified converters are bridgeless converters also due to the absence of DBR as described in [30] and [31]. Modified converters reduce THD to great extent. Apart from modified converters isolated converters [32] are another configuration which can be helpful as it doesn't require another converter such as flyback converter in the circuit as it is already having isolation within the circuit. Some of the examples of isolated configurations with or without bridgeless feature can be seen in [33], [34], [35]. One of them is bridgeless Zeta converter as mentioned in [36] and similarly modified bridgeless Luo converter as per [37]. Though modified and bridgeless isolated configurations give good results as PFC but interleaved converter configuration is another converter type which is very effective in reducing THD and enhancing the performance of the charger. Interleaving means 'multi-phasing'. It is the technique in which two converters are interleaved and made in the combination of single entity. The converters work with a phase shift of 180 degrees. Interleaved converters in Luo and landsman can be seen from [38] and [39]. Interleaved converters are so efficient in the power factor correction that they almost make it unity. Another important quality in these converters is their ripple cancellation within the circuit which makes it suitable for charging circuit. After all these configurations researchers tried for the combinational circuits of different DC-DC converters which can be used in onboard chargers for example: Cuk-SEPIC [40], Zeta-Luo, boost-zeta [41] etc. These circuits combinedly give the advantages of both the converters and makes the combinational useful for charging purpose.

2.1.5 New Techniques for charging

As EV is becoming popular many new techniques are included in research areas. One of them is hybrid configurations i.e., combination of more than one source of charging on grid side. One of them is mentioned further in this report which is solar aided battery charging for bridgeless isolated Zeta converter. From [42], [43] [44] some of the hybrid models can be observed. Hybrid configurations like solar assistance along with grid connected models are

making EV system very much reliable and efficient in case of absence of grid power and in boosting of power along with grid also. Apart from this some other types of hybrid systems are available, one of them is given in [45] and transformer less systems [46] are under research as mentioned in [47]. Supercapacitor is another new system to be used in the charging of EV. Bidirectional DC-DC converter is used in the hybrid system consisting of supercapacitor as per [48] and [49]. Supercapacitors [50] and batteries [51] have hybrid combination in these types of systems. Bidirectional or V2G charging becoming more popular these days one such comparison of unidirectional and bidirectional charging is mentioned in [52]. V2G [53], [54] comes under the concept of microgrid which takes care of energy flow in both the directions i.e., from vehicle to grid as well as grid to vehicle. Bidirectional charging is the future of EV industry and gaining popularity day by day as the research continues in this area. While working with bidirectional charging [55],[56],[57] according to the state of charge and voltage in EV, converter operates accordingly in various modes. With the reduction in passive element number switched capacitor/inductor [58],[59] is also in the race of new techniques discussed for EV chargers. It is a changed topology with rearrangement of diodes and other passive elements. Another solar powered soft switching power converter is technique has been mentioned in [60]. In this way it can be seen that EV batteries are the subject of a lot of research area. onboard and unidirectional battery charger has been covered in this report so far.

2.2 Conclusion

Literature review for the work mentioned in this project report titled "Design and analysis of onboard battery charging for electric vehicles" is mentioned in this chapter. The survey is being carried out to find out the further scope of research in this area and to get the idea of the previously done work. It helped in understanding type of charger and its recommendation for EV, what innovations can be further made in this area to improve EV charging. New techniques which include Hybrid charging systems, switched capacitors/inductors andV2G charging was extremely helpful in drafting the whole major project report.

CHAPTER-III

MODELLING AND ANALYSIS OF CONVENTIONAL DC-DC CONVERTERS FOR BATTERY CHARGING

3.1 Introduction

Nowadays electric vehicle chargers generally consist of DC-DC converter as power factor correction (PFC) unit because without PFC unit the quality of battery charging is quite deteriorated. Total harmonic distortion at supply side remains very high in absence of PFC unit and power factor is also not nearer to unity. So initially conventional DC-DC converters like Buck, Boost, Buck-Boost etc. were used as PFC in battery chargers. Later on, new converters like CUK, Zeta, SEPIC, Luo, Landsman etc. became the part of charger configurations due to their improved input current profiles and added components in their model. This chapter covers the following topics:

- ✓ Boost converter
  - Configuration and working
  - Battery charging using Boost converter as PFC
- ✓ Buck-Boost converter
  - Configuration and working
  - Battery charging using buck-boost converter as PFC
- ✓ CUK converter
  - Configuration and working
  - Battery charging using CUK converter as PFC
- ✓ SEPIC converter
  - Configuration and working
  - Battery charging using SEPIC converter as PFC
- ✓ Zeta converter
  - Configuration and working
  - Battery charging using Zeta converter as PFC

3.2 Boost converter

The boost converter is a simple DC-DC converter that boosts the level of DC voltage to a requisite value by changing the duty ratio 'D'. The supply is connected in series with the inductor in this configuration as shown in Fig 3.1
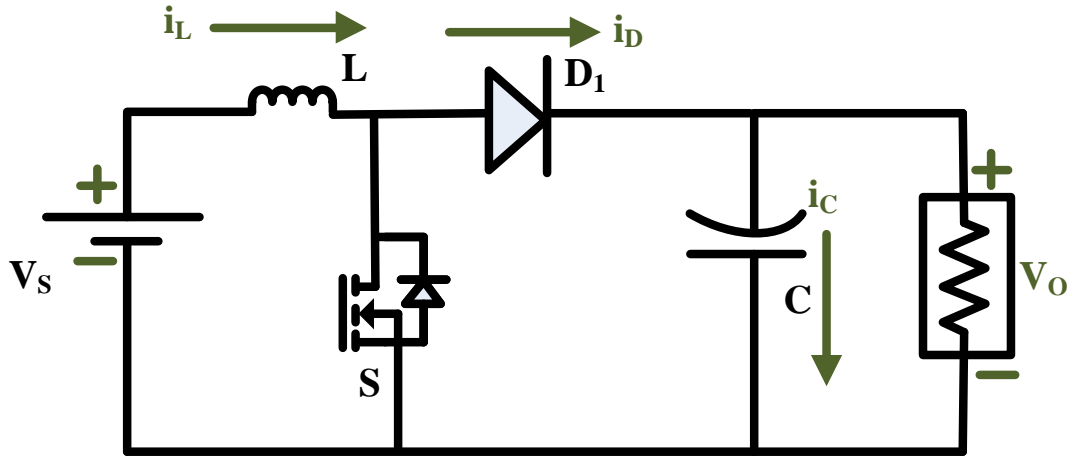
Fig 3.1 Configuration of Boost converter

When Switch (S) is closed

$$V_s = V_L = L\frac{di_L}{dt} \text{ Or } \frac{di_L}{dt} = \frac{V_s}{L} \tag{3.1}$$

For the current increasing in linear manner while switch (S) is closed, inductor current change is calculated as:

$$\left(\Delta i_L\right)_{closed} = \frac{V_s DT}{L} \tag{3.2}$$

When S is open

$$V_L = V_s - V_o = L\frac{di_L}{dt} \tag{3.3}$$

$$\left(\Delta i_L\right)_{open} = \frac{(V_s - V_o)(1-D)T}{L} \tag{3.4}$$

As per volt-sec concept

$$\left(\Delta i_L\right)_{closed} + \left(\Delta i_L\right)_{open} = 0 \tag{3.5}$$

11

On solving equation (3.5), we get: $V_o = \left(\dfrac{V_s}{1-D} \right)$ $\qquad$ (3.6)

In ideal conditions, the source's total power given equals the load's total power received.. So, on equating these we get:

$$\frac{V_o{}^2}{R} = V_s I_s = \frac{V_s{}^2}{(1-D)^2} R \qquad (3.7)$$

Where R is the load resistance.

Solving for I_L, we get:

$$I_L = \frac{V_s}{R(1-D)^2} \qquad (3.8)$$

Maximum and Minimum values for inductor current is given by the following equations:

$$I_{max} = I_L + \frac{\Delta i_L}{2} = \frac{V_s}{R(1-D)^2} + \frac{V_s DT}{2L} \qquad (3.9)$$

$$I_{min} = I_L - \frac{\Delta i_L}{2} = \frac{V_s}{R(1-D)^2} - \frac{V_s DT}{2L} \qquad (3.10)$$

Inductor current remains continuous and so boundary of continuous and discontinuous can be evaluated using $I_{min} = 0$ and from (3.10) we get:

$$L_{min} = \frac{D(1-D)^2 R}{2f} \qquad (3.11)$$

Where f is the switching frequency.

Change in capacitor charge $\quad \Delta Q = C \Delta V_o = \left(\dfrac{V_o}{R} \right) DT$ $\qquad$ (3.12)

Ripple voltage expression is given by using (3.12)

$$\frac{\Delta V_o}{V_o} = \frac{D}{RCf} \qquad (3.13)$$

3.2.1 Battery charging using Boost converter as PFC unit

The configuration of battery charging using boost converter for power factor correction is illustrated in Fig 3.2 which consists of an AC-DC converter unit (AC supply + DBR + EMI Filter), a boost converter and flyback converter for isolation and further improvement in battery current. This system is used to charge the Li-ion battery acting as load.
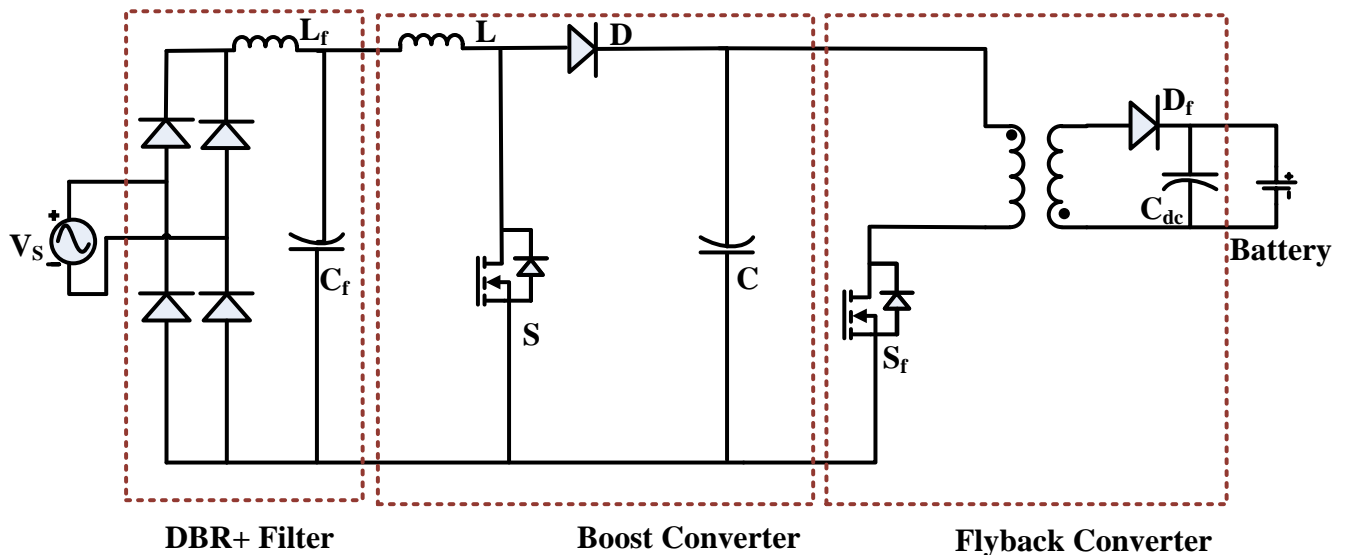
Fig 3.2 Battery charging configuration with Boost converter as PFC

3.2.2 Results & Discussion

The simulation results for charging a Li-ion battery by using Boost converter as a PFC unit is shown in Fig 3.3 below which shows supply voltage (V_s) with a peak voltage of 311V, supply current (I_s) of 14.02A, battery voltage (V_{bat}) with a peak of 53V, battery current (I_{bat}), State of charge (SOC%) and THD% respectively. Increase of current in negative direction shows that battery is in charging mode while in case of positively increasing current, battery is getting discharged. Charging of battery can also be illustrated by increasing SOC% and vice versa is for battery discharging.
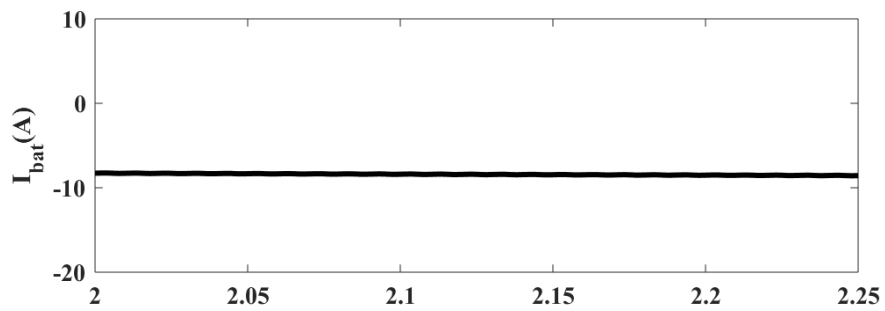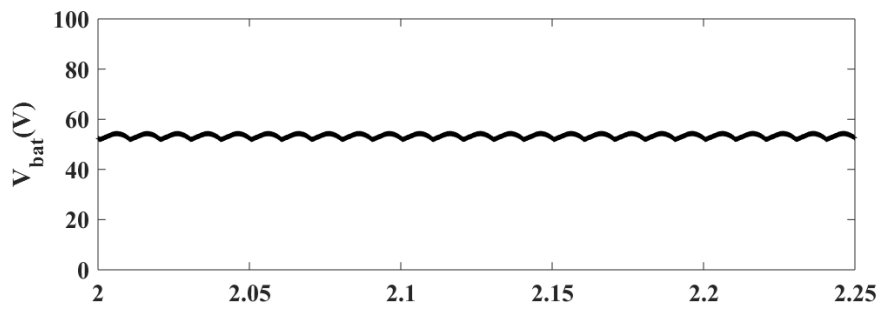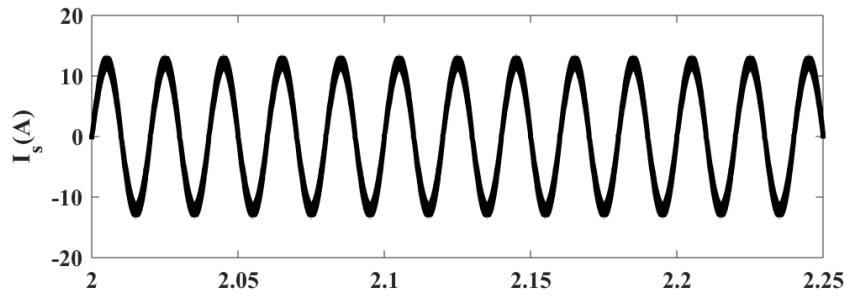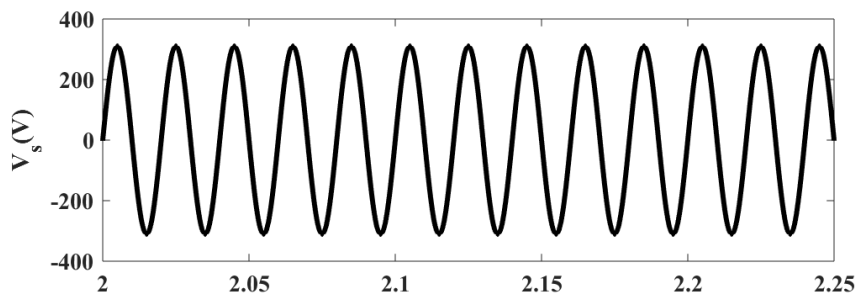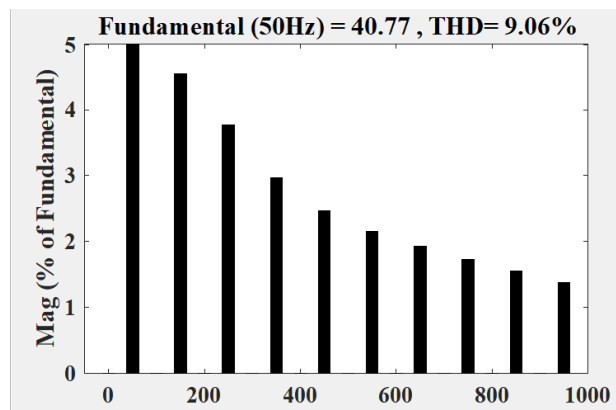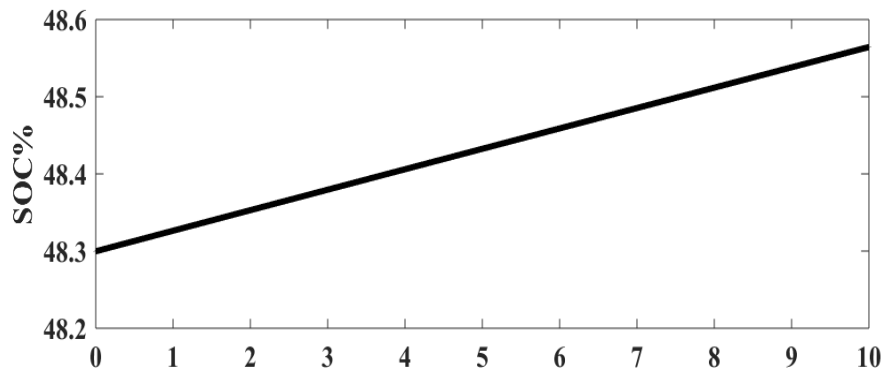
Fig 3.3. Results for Boost as PFC converter for battery charging

3.3 Buck-Boost converter

It is the most basic DC-DC converter which converts DC of certain level to either step up and step down as per the requirement of application and so according to the duty ratio defined for the system. It can give a wide range of output voltages. A schematic of general buck-boost converter is illustrated in Fig 3.4.
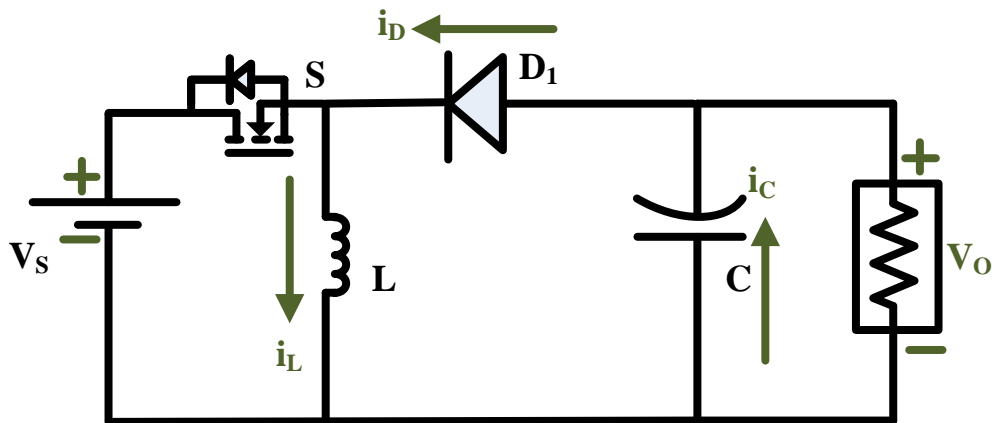
Fig 3.4 Configuration of Buck-Boost converter

15

There are two modes of operation with the Buck-Boost converter.. The voltage at output relies on the how variation in duty ratio 'D' is taking place. If it varies less than 0.5 i.e., for D < 0.5, the voltage at output is more than the voltage at DC input of system whereas for D > 0.5 it is less than the voltage at input.

When S is closed:

$$V_s = V_L = L\frac{di_L}{dt} \text{ Or } \frac{di_L}{dt} = \frac{V_s}{L} \tag{3.14}$$

Considering linear increase in inductor current

$$(\Delta i_L)_{closed} = \frac{V_s DT}{L} \tag{3.15}$$

When S is open:

$$V_o = V_L = L\frac{di_L}{dt} \text{ Or } \frac{di_L}{dt} = \frac{V_o}{L} \tag{3.16}$$

$$(\Delta i_L)_{open} = \frac{V_s(1-D)T}{L} \tag{3.17}$$

The net change in the current of the inductor in steady state operation must remain zero over one period. From equations (3.15) and (3.17)

$$(\Delta i_L)_{closed} + (\Delta i_L)_{open} = 0 \tag{3.18}$$

On solving equation. (3.18) we get: $\quad V_o = -V_s\left(\frac{D}{1-D}\right) \tag{3.19}$

Where negative sign in equation (3.19) indicates that voltage at output is having opposite polarity than voltage at input. Energy storage takes place when switch is closed while it is transferred to the load as switch is open. Buck-Boost converter is also referred as an "Indirect converter".

We know that power absorbed by load is equal to the source power supplied. Hence:

$$\frac{V_o^2}{R} = V_s I_s \tag{3.20}$$

$$I_s = I_L D \tag{3.21}$$

From (3.20) and (3.21):
$$\frac{V_o{}^2}{R} = V_s I_L D \tag{3.22}$$

From (3.20), (3.21), (3.22)
$$I_L = \frac{V_s D}{R(1-D)^2} \tag{3.23}$$

Inductor's maximum and minimum current can be calculated as per (2.24)

$$I_{max} = I_L + \frac{\Delta i_L}{2} = \frac{V_s D}{R(1-D)^2} + \frac{V_s DT}{2L} \tag{3.24}$$

$$I_{min} = I_L - \frac{\Delta i_L}{2} = \frac{V_s D}{R(1-D)^2} - \frac{V_s DT}{2L} \tag{3.25}$$

For finding out limiting value of inductor, at boundary conditions I_{min} is zero.

$$L_{min} = \frac{R(1-D)^2}{2f} \tag{3.26}$$

Where f is the switching frequency.

The voltage ripple at output is given by:

$$\frac{\Delta V_o}{V_o} = \frac{D}{RCf} \tag{3.27}$$

3.3.1 Battery charging using Buck-Boost as PFC unit

The configuration of battery charging using buck-boost converter for power factor correction in illustrated in Fig 3.5 which consists of an AC-DC converter unit (AC supply + DBR + EMI Filter), a buck-boost converter and flyback converter for isolation and further improvement in battery current. This system is used to charge Li-ion battery acting as load. Buck-Boost converter acts better during PFC operation as compared to boost converter in charging of EV battery.
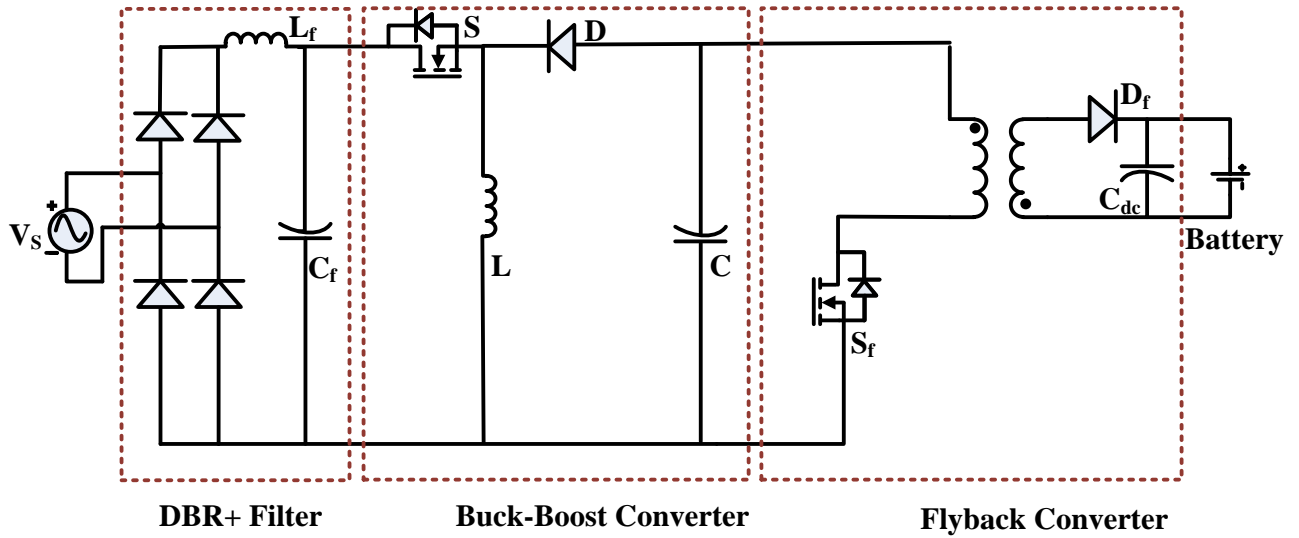
Fig 3.5 Battery charging configuration with Buck-Boost converter as PFC

3.3.2 Results & Discussion

The simulation results for charging a Li-ion battery by using Buck-Boost converter as a PFC unit is shown in Fig 3.6 below which shows supply voltage (V_s) with peak of 311V, supply current (I_s) with a peak of 13.32A, Diode current (I_d), Inductor current (I_l), battery voltage (V_{bat}) with a peak of 53.3V, battery current (I_{bat}), State of charge (SOC%) and THD% respectively.
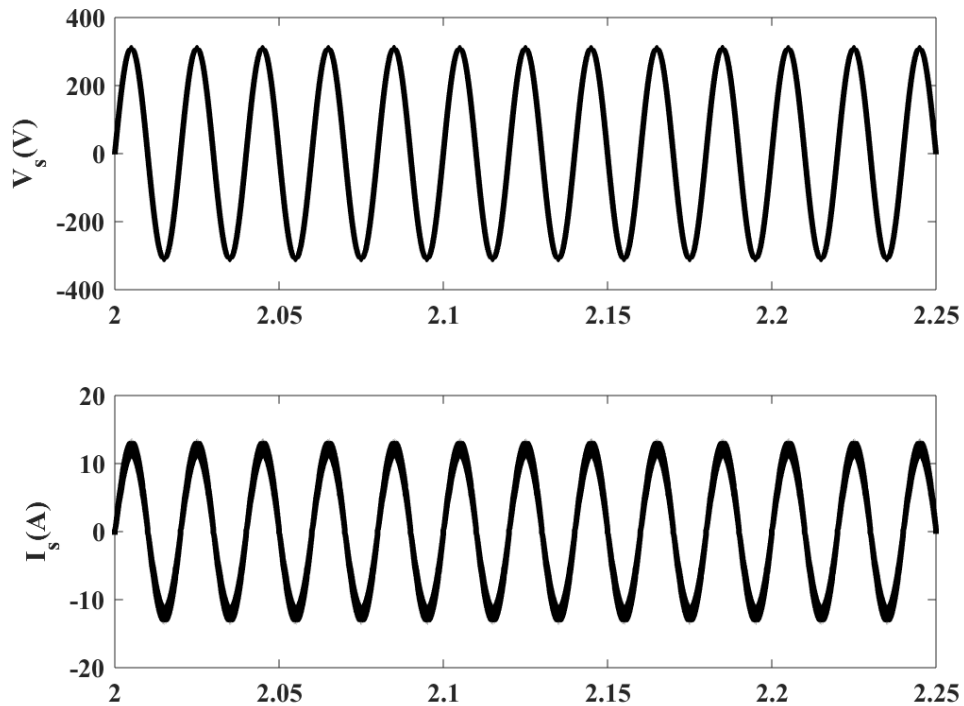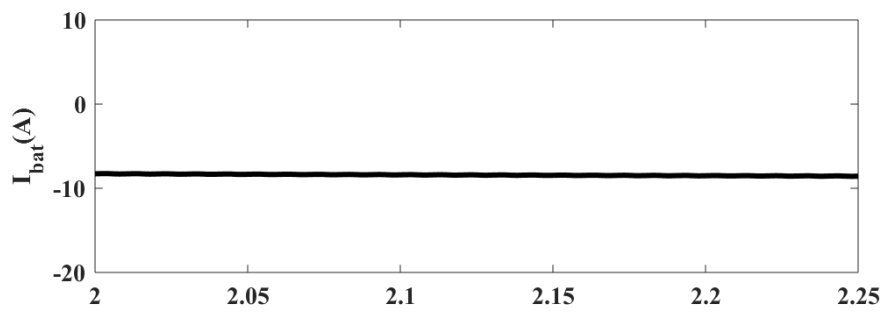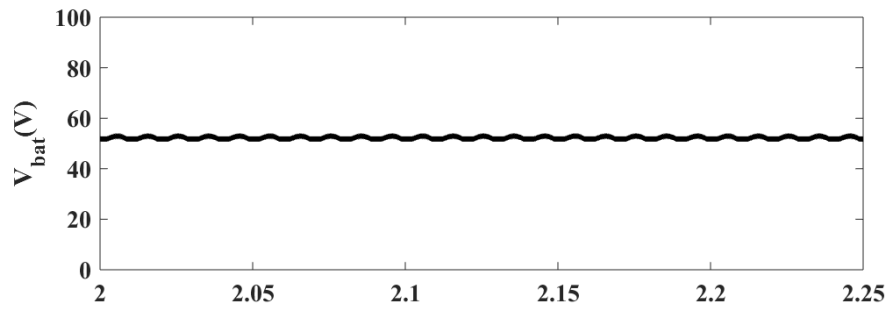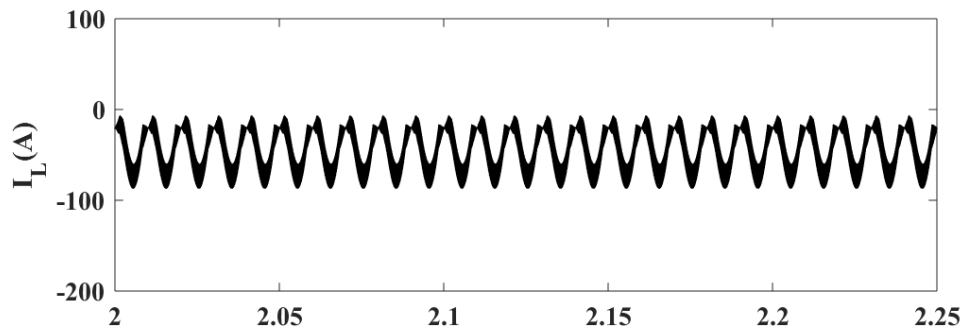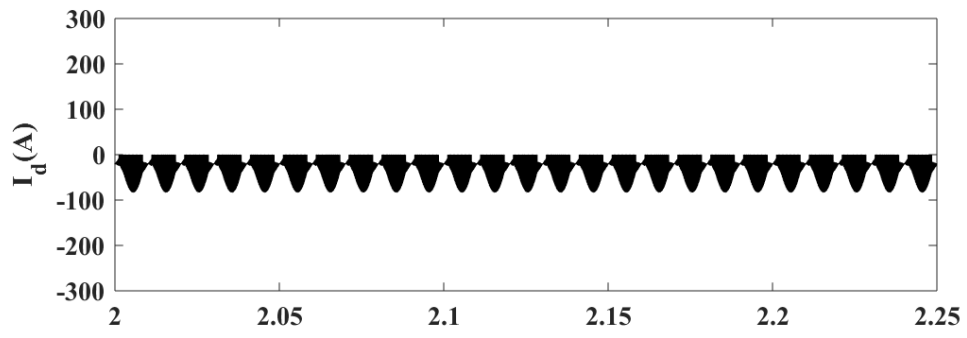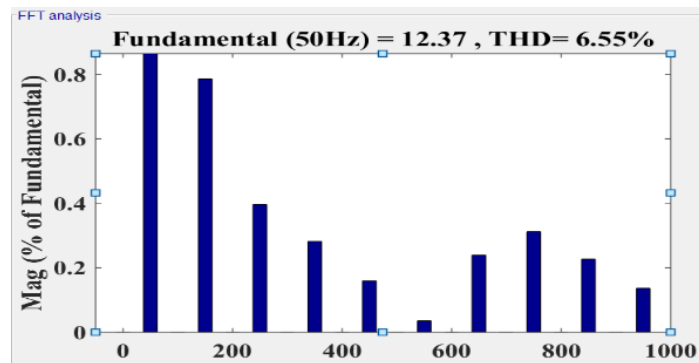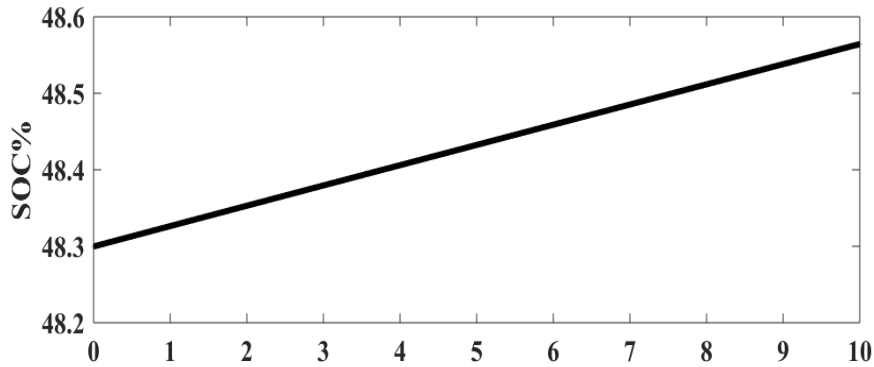
Fig 3.6. Results for Buck-Boost as PFC converter for battery charging

3.4 CUK converter

CUK converter as per Fig 3.7, is a little bit improved configuration than buck-boost converter. Two capacitors and two inductors make up the system.. The process of energy transfer depends on capacitor C_1 while in above topologies transfer of energy was dependent on inductor. Input side inductor behaves as filter for the circuit. At the output, the polarity of the signal is reversed. whereas the output voltage can be lower or higher than the input voltage.
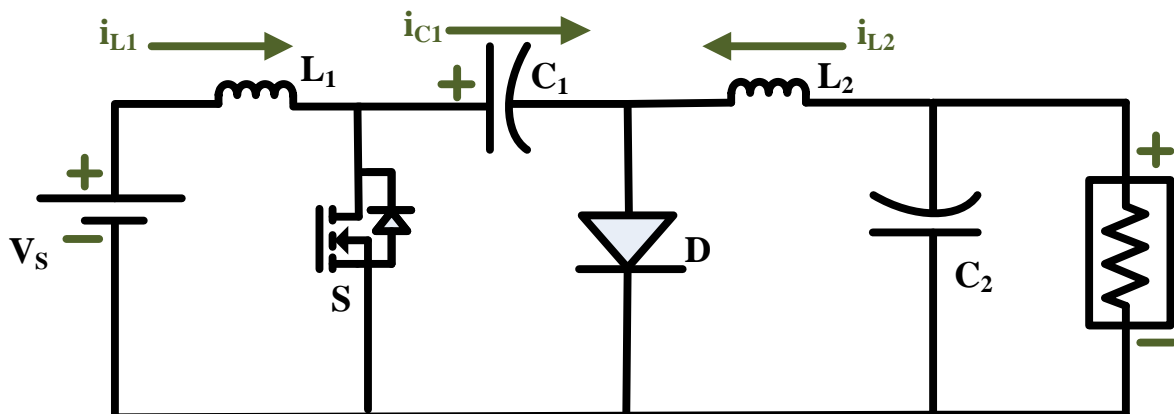
Fig 3.7 CUK converter configuration

20

When switch S is closed, diode is reverse biased and capacitor current in C_1 is given by:

$$(i_{C_1})_{closed} = -I_{L_2} \tag{3.28}$$

When switch S is open, diode is turned on by the action of inductors L_1 and L_2.

$$(i_{C_1})_{open} = I_{L_1} \tag{3.29}$$

The average current in capacitor will be zero over a period,

$$(i_{C_1})_{closed} DT + (i_{C_1})_{open}(1-D)T = 0 \tag{3.30}$$

From equations (3.28) and (3.29) we get:

$$\frac{I_{L_1}}{I_{L_2}} = \frac{D}{1-D} \tag{3.31}$$

As Input power = Output power i.e., $V_s I_{L_1} = -V_o I_{L_2}$ \hfill (3.32)

From (3.31) and (3.32) we get: $\qquad V_o = -V_s\left(\dfrac{D}{1-D}\right)$ \hfill (3.33)

Where polarity reversal is shown by negative sign in equation (3.33).

Output ripple voltage relation is given by:

$$\frac{\Delta V_o}{V_o} = \frac{1-D}{8L_2 C_2 f^2} \tag{3.34}$$

$$i_{L_1} = i_{C_1} \tag{3.35}$$

Where f is the switching frequency.

From equation (3.34) and (3.35) voltage at capacitor C_1 is given by:

$$V_{C_1} = \frac{1}{C_1}\int I_{L_1} dt \tag{3.36}$$

$$\Delta V_{C_1} \approx \frac{V_o D}{R C_1 f} \tag{3.37}$$

In closed switch mode, $\qquad V_s = V_{L_1} = L_1 \dfrac{di_{L_1}}{dt}$ (3.38)

$$\Delta i_{L_1} = \frac{V_s D}{L_1 f}$$ (3.39)

Similarly $\qquad V_{L_2} = V_s = L_2 \dfrac{di_{L_2}}{dt}$ (3.40)

$$\Delta i_{L_2} = \frac{V_s D}{L_2 f}$$ (3.41)

Minimum value for inductors can be evaluated by the same method as for buck-boost converter by boundary conditions and by using above equations.

$$L_{1\min} = \frac{R(1-D)^2}{2Df}$$ (3.42)

$$L_{2\min} = \frac{R(1-D)}{2f}$$ (3.43)

3.4.1 Battery charging using CUK as PFC unit

The configuration of battery charging using CUK converter for power factor correction is illustrated in Fig 3.8 which is having an AC-DC converter unit (AC supply + DBR + EMI Filter), a CUK converter and flyback converter for isolation resulting in further improvement in battery current. This system is used to charge Li-ion battery acting as load.

Fig 3.8 Battery charging configuration with CUK converter as PFC

3.4.2 Results

The simulation results for charging battery by using CUK converter as a PFC unit is shown in Fig 3.9 below which shows supply voltage (V_s) with a peak value of 311V, supply current (I_s) with a peak of 18.56A, State of charge (SOC%), battery voltage (V_{bat}), battery current (I_{bat}) and THD% as 7.43% respectively.
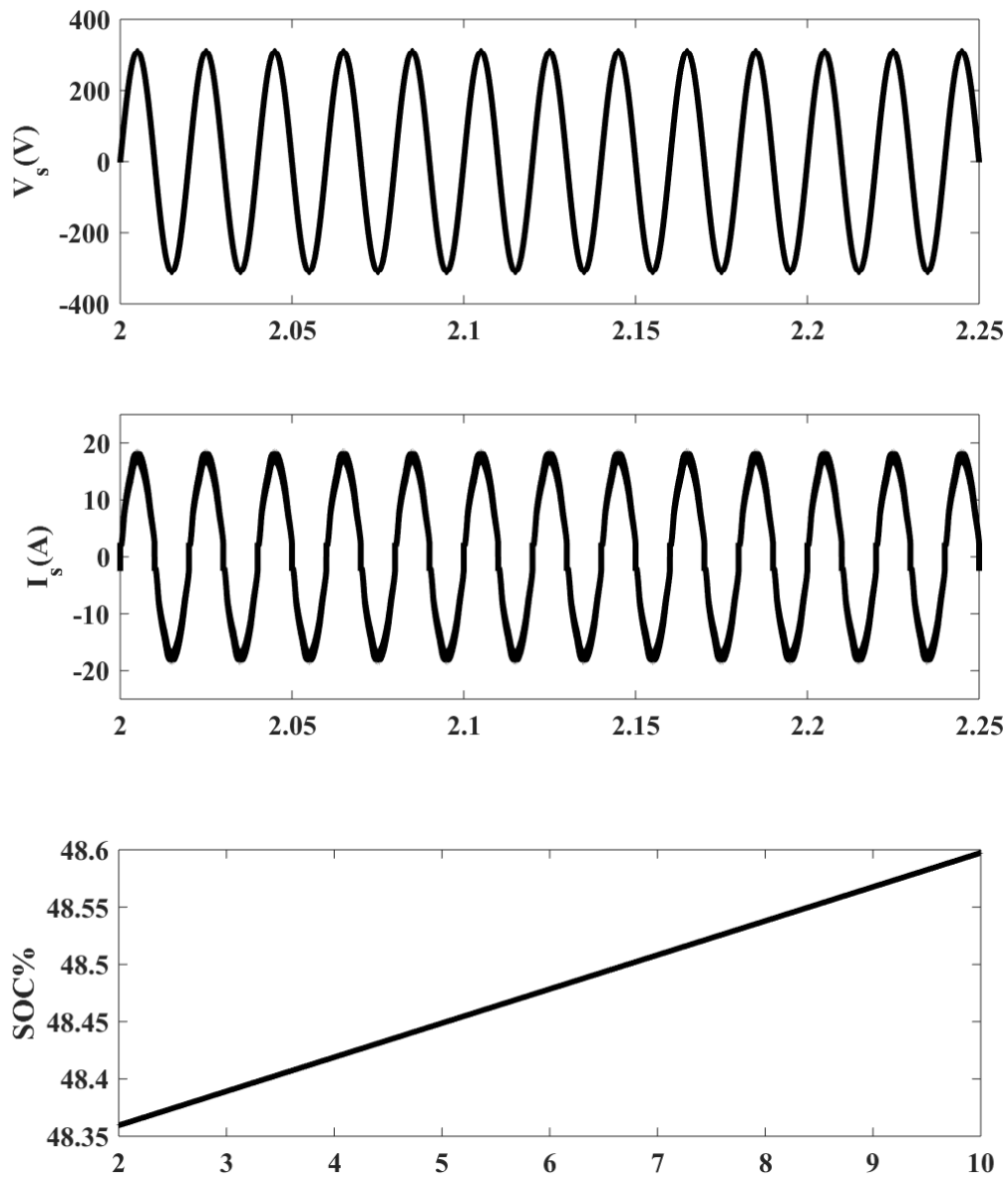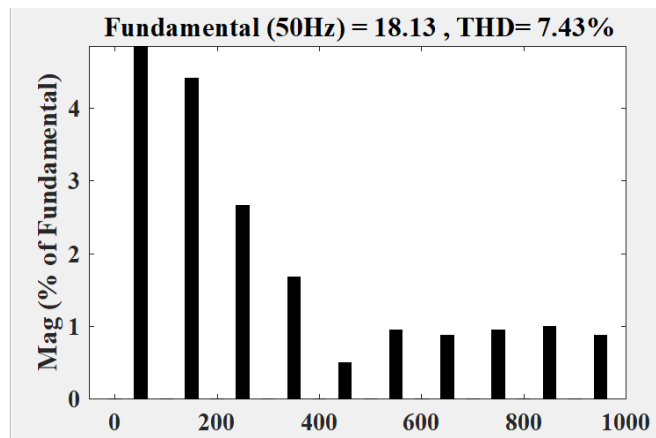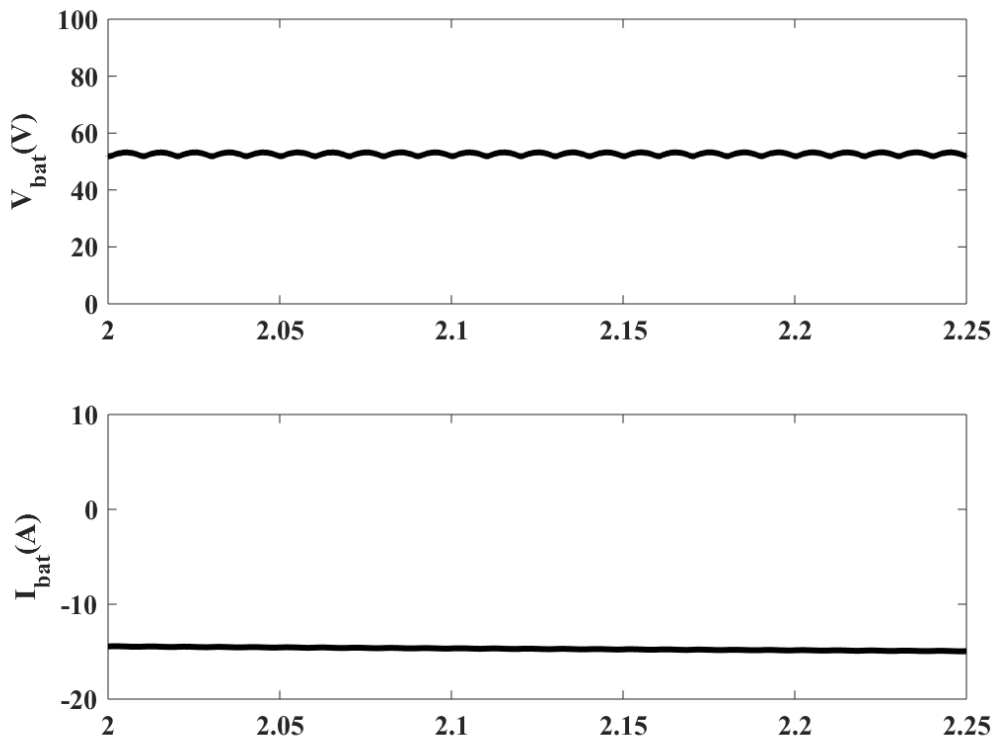
Fig 3.9. Results for CUK converter as PFC for battery charging

3.5 SEPIC Converter

A single ended primary inductance converter (SEPIC) is illustrated in Fig 3.10. which is quite similar to CUK converter in design. The output produced is similar to CUK converter either less than or greater than the voltage at input end but it has no reversal of polarity.
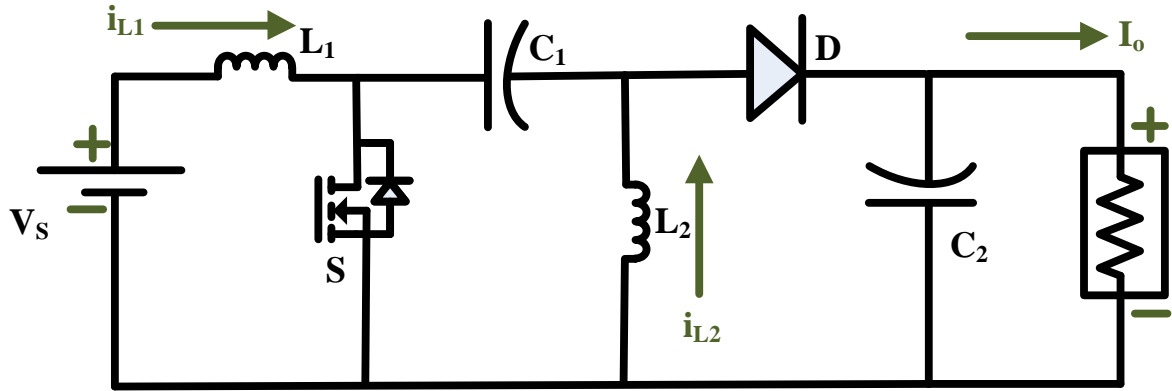
Fig 3.10 SEPIC converter

In steady state operating condition inductor's average current and capacitor's average voltage remain zero. From using Kirchhoff's law:

$$-V_s + v_{L_1} + v_{C_1} - v_{L_2} = 0 \qquad (3.44)$$

As average voltages are zero, So
$$v_{C_1} = V_s \qquad (3.45)$$

When S is closed, diode is reversed biased and inductor voltage is given by:

$$v_{L_1} = V_s \qquad (3.46)$$

When S is open, diode is working and following Kirchhoff's law we get:

$$v_{L_1} = -V_o \qquad (3.47)$$

From (3.46) and (3.47) we get:

$$V_s(DT) - V_o(1-D)T = 0 \qquad (3.48)$$

From (3.48), relation can be obtained as

$$V_o = V_s\left(\frac{D}{1-D}\right) \qquad (3.49)$$

Using power balance equation

$$i_{L_1} = \frac{V_o^2}{RV_s} \qquad (3.50)$$

$$\Delta i_{L_1} = \frac{V_s D}{L_1 f} \tag{3.51}$$

Where f is the switching frequency.

Applying Kirchhoff's law and continuous current rule for inductor, we get:

$$i_{L_2} = I_o \tag{3.52}$$

$$\Delta i_{L_2} = \frac{V_s D}{L_2 f} \tag{3.53}$$

Load side is similar to boost converter so ripple voltage at output is:

$$\Delta V_o = \Delta V_{C_2} = \frac{V_o D}{R C_2 f} \tag{3.54}$$

$$C_2 = \frac{D}{V_o/\Delta V_o \ R f} \tag{3.55}$$

$$\Delta V_{C_1} = \frac{V_o D}{R C_1 f} \tag{3.56}$$

$$C_1 = \frac{D}{V_o/\Delta V_{C_1} \ R f} \tag{3.57}$$

3.5.1 Battery charging using SEPIC as PFC unit

The configuration of battery charging using SEPIC converter for power factor correction in illustrated in Fig 3.11 which consists of an AC-DC converter unit (AC supply + DBR + EMI Filter), a SEPIC converter and flyback converter for isolation and further improvement in battery current. This system is used to charge Li-ion battery acting as load as shown in Fig 3.11.
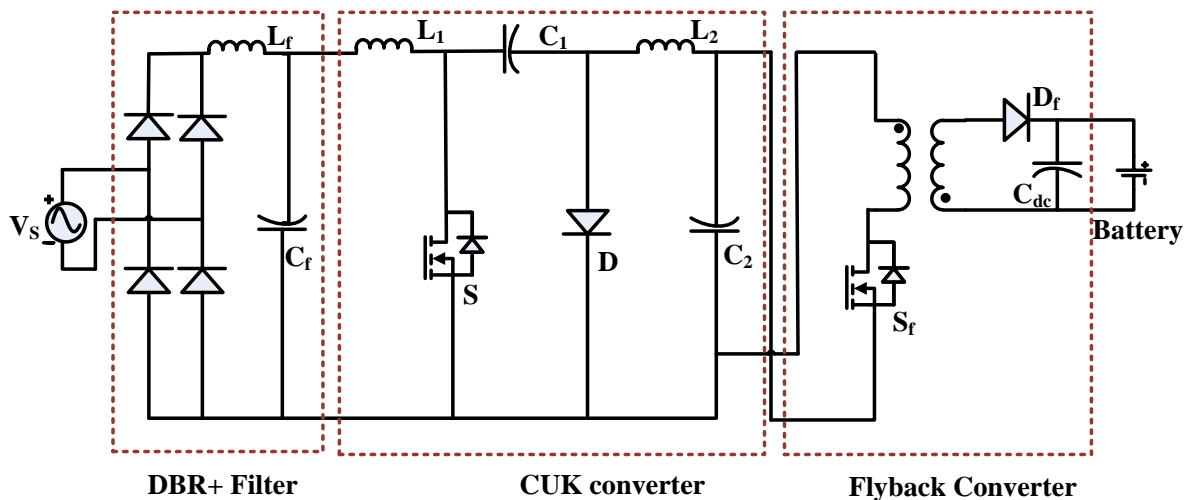
Fig 3.11 Battery charging configuration with SEPIC converter as PFC

3.5.2 Results & Discussion

The simulation results for charging battery by using SEPIC converter as a PFC unit is shown in Fig 3.12 below which shows supply voltage (V_s) with a peak voltage of 311V, supply current (I_s) with a peak current of 13.3A, battery voltage (V_{bat}) of 52.7V, battery current (I_{bat}), increasing State of charge (SOC%) showing charging of battery and THD% of 7.66% respectively.
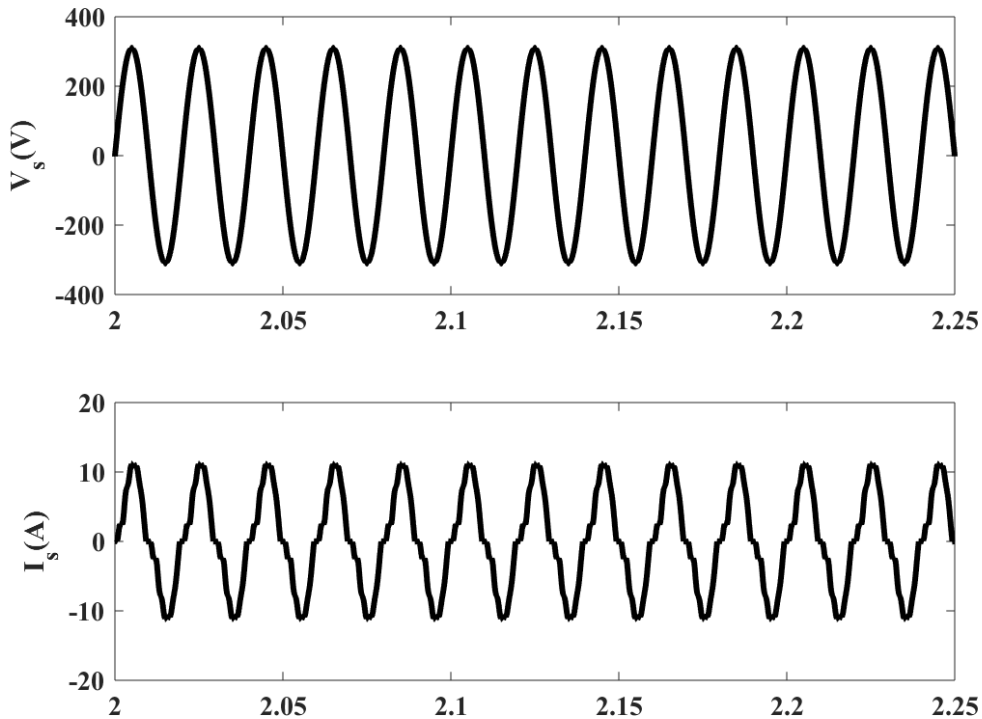
Fig 3.12 Results for SEPIC converter as PFC for battery charging

3.6 Zeta Converter

Zeta converter generates a non-inverting output voltage along with either lower or higher voltage at output as compared to the input voltage. A general circuit diagram of Zeta converter is shown in Fig 3.13.
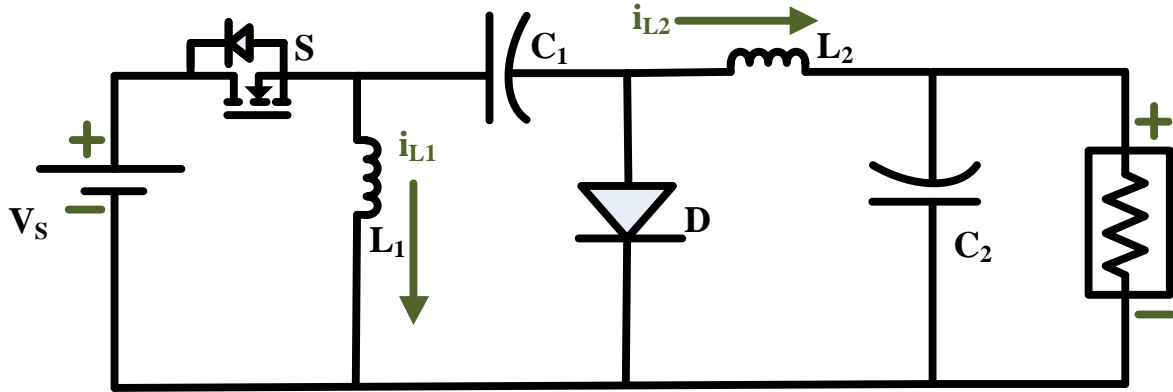
Fig 3.13 Zeta converter

On applying separate Kirchhoff's law on switching of Zeta converter in two modes following equations are used to calculated various parameters useful in designing of converter:

Output in terms of input is given by: $V_o = V_s \left(\dfrac{D}{1-D} \right)$ (3.58)

Ripple in Inductor currents: $\Delta I_{L_1} = \dfrac{V_s D}{f L_1}$ (3.59)

$$\Delta I_{L_2} = \dfrac{V_s D}{f L_2}$$ (3.60)

Minimum Value of inductors can be calculated as per equations (3.61) and (3.62)

$$L_{1\min} = \dfrac{(1-D)^2 R}{2Df}$$ (3.61)

$$L_{2\min} = \dfrac{(1-D)R}{2f}$$ (2.62)

Ripple in voltages at both the capacitors is given by equations (3.63) and (3.64).

$$\Delta V_{C_1} = \dfrac{V_s D}{8f^2 C_1 L_1}$$ (3.63)

29

$$\Delta V_{C_2} = \frac{V_s D}{8 f^2 C_2 L_2} \tag{3.64}$$

Minimum value of capacitors can be evaluated by following equations:

$$C_{1\min} = \frac{D}{8 f (1 - D) R} \tag{3.65}$$

$$C_{2\min} = \frac{1}{8 fR} \tag{3.66}$$

3.6.1 Battery charging using Zeta as PFC unit

The configuration of battery charging using Zeta converter for power factor correction in illustrated in Fig 3.14 which consists of an AC-DC converter unit (AC supply + DBR + EMI Filter), a Zeta converter and flyback converter for isolation and further improvement in battery current. This system is used to charge Li-ion battery acting as load as shown in Fig 3.14.
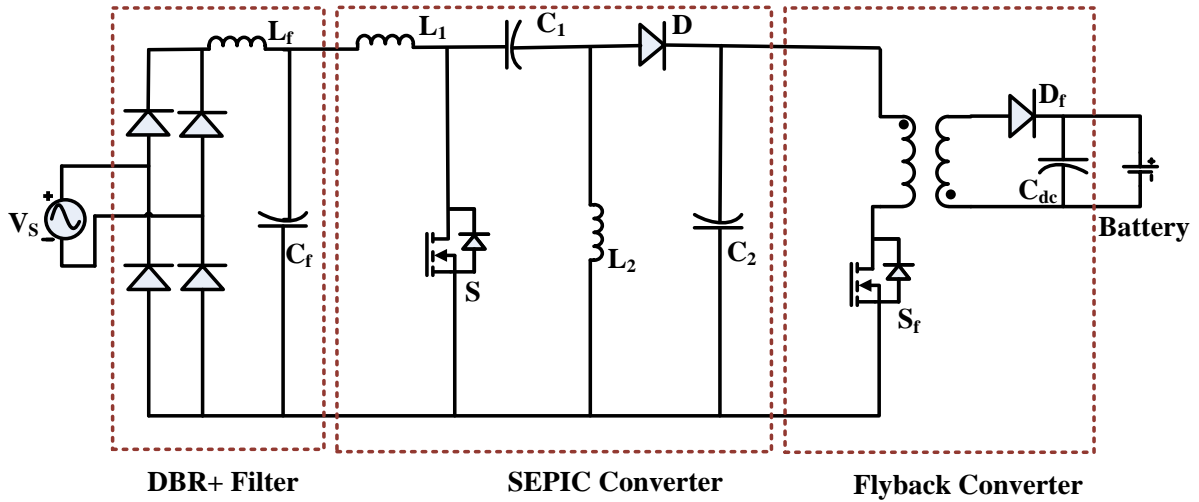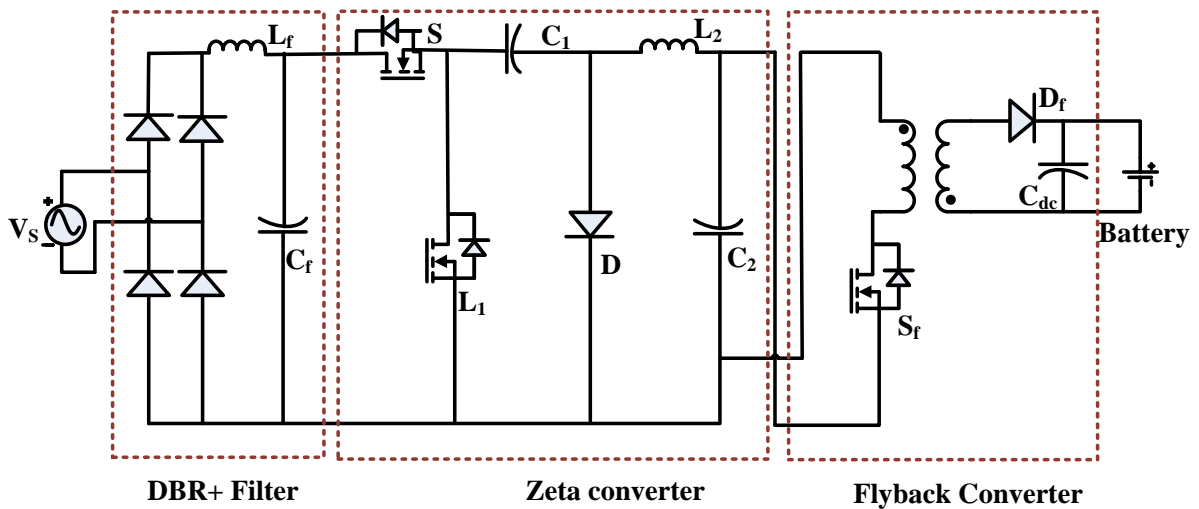

Fig 3.14. Battery charging configuration with Zeta converter as PFC

3.6.2 Results & Discussion

The simulation results for charging battery by using Zeta converter as a PFC unit is shown in Fig 3.15 below which shows supply voltage (V_s) with a peak value of 311V, supply current (I_s) with a peak value of 14.42A, Inductor 2 current (I_{l2}) with 47.82A as peak value, Capacitor 2 voltage (V_{C2}), battery voltage (V_{bat}) with a peak value of 55.03A, battery current (I_{bat}), increasing State of charge (SOC%) showing charging of battery and THD% as 5% respectively.
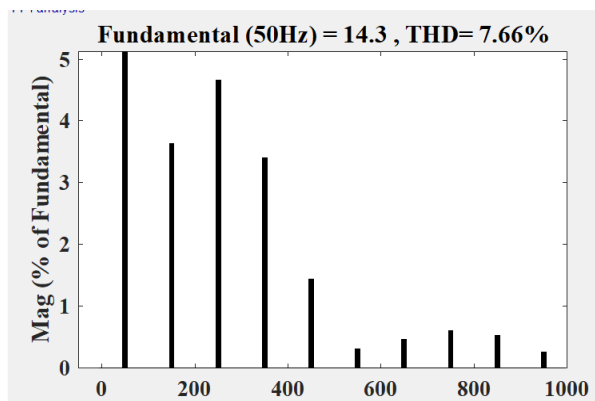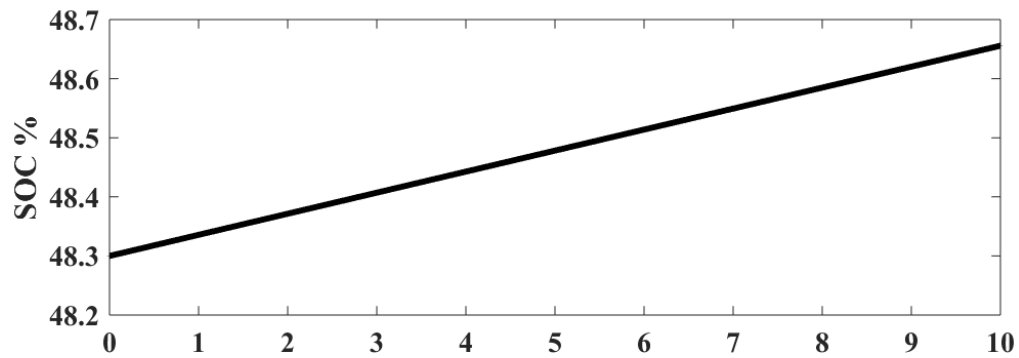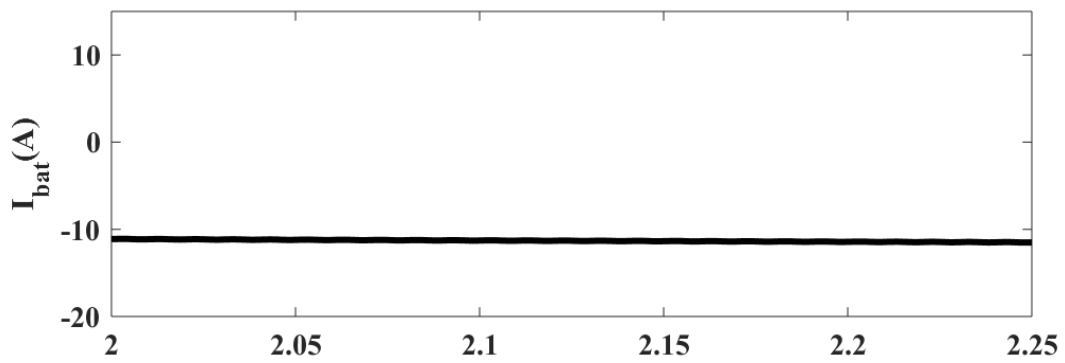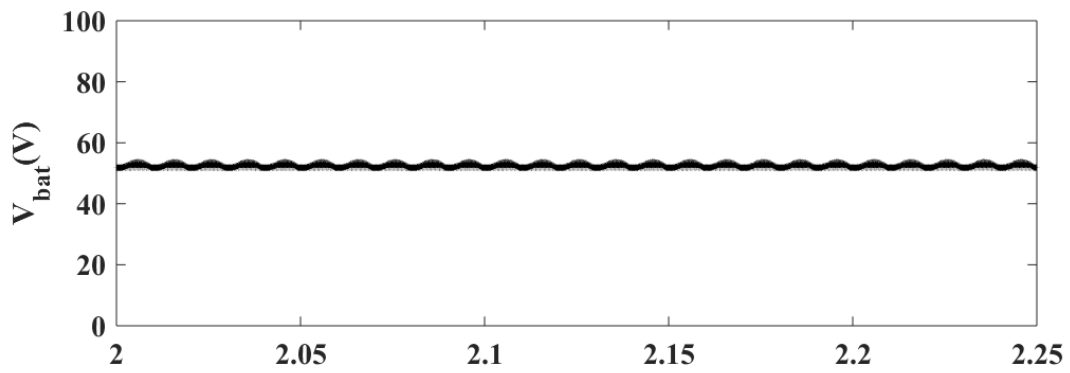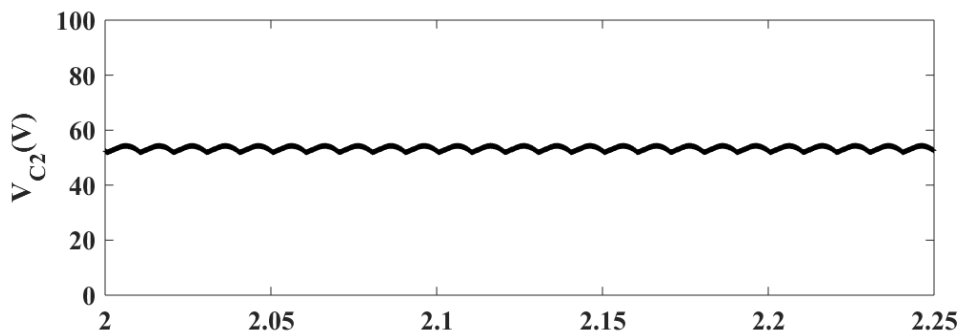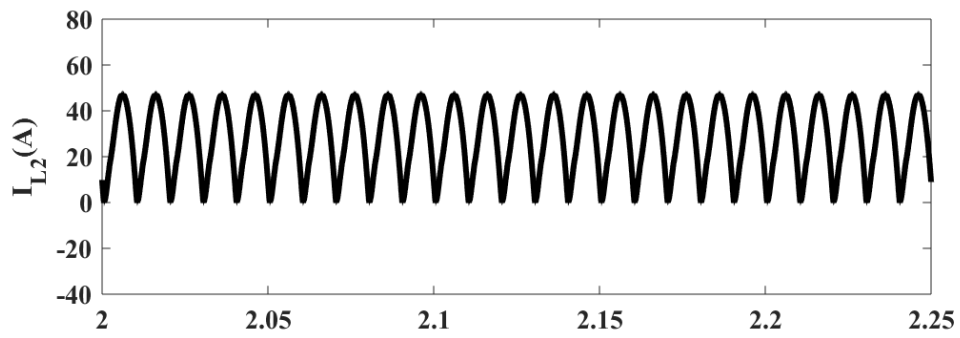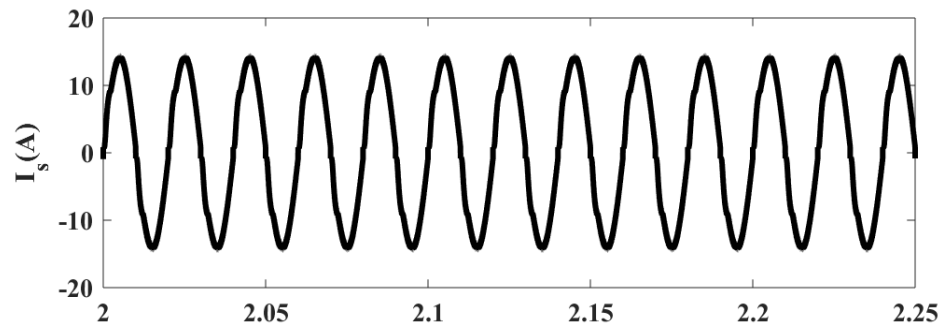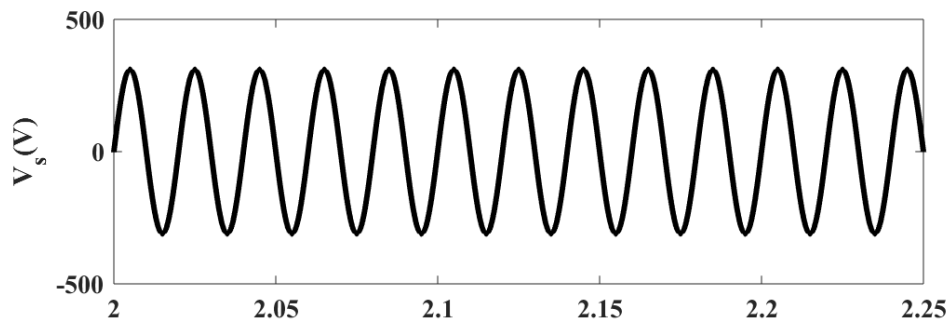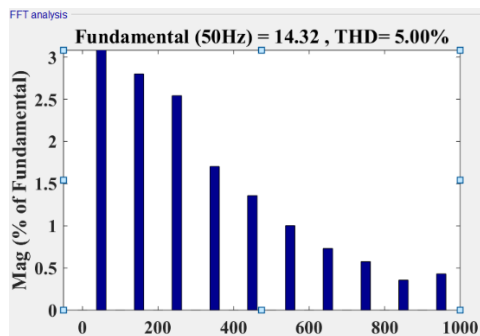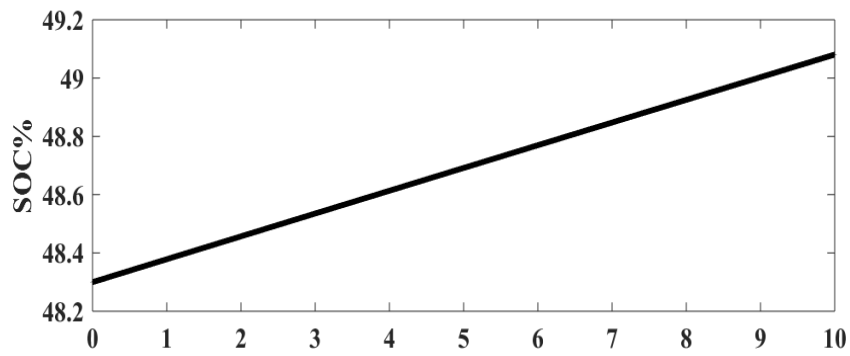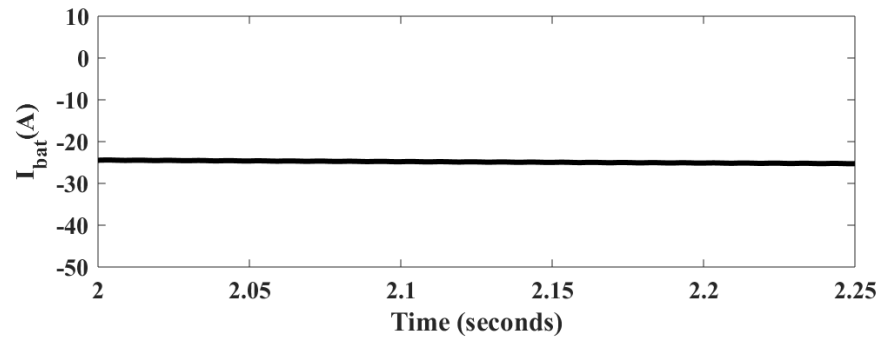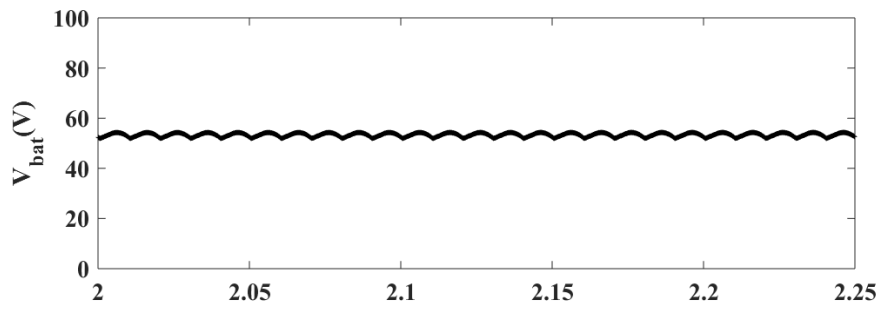
Fig 3.15. Results for Zeta converter as PFC for battery charging

3.7 Conclusion

The usage of DBR already introduces large number of harmonics in the charger circuit. So, by using conventional DC-DC converters as PFC in charger configuration. The ripple reduction is better as compared to the circuit not using PFC for EV charging. These converters usage decreases THD to below 10%. Only Boost converter works not so apt in reducing input current ripple, rest of the converters work well under specified THD levels. Buck-Boost converter perform well as compared to boost converter whereas SEPIC, CUK and Zeta converters works with better efficiency due to the added inductors and capacitors and hence improving the current profile. Out of these best converters who works most efficiently is CUK converter in terms of THD reduction as PFC converter.

CHAPTER-IV

MODELLING AND ANALYSIS OF MODIFIED CONVERTERS

4.1 Introduction

Charging quality with conventional converters needs to be improved and requires more advanced and efficient converters in the charging configuration and consequently modified DC-DC converters are better than conventional converters in terms of improving power factor of the system and reducing total harmonic distortion in the circuit. Modified converters are configurations with rearrangement or addition of components like diodes and inductors to improve the line current at input side. Some of the modified configurations like modified CUK and modified Zeta have been discussed here in this chapter.

4.2 Modified CUK Converter

CUK converter has been considered as a best choice over other basic chargers as it has low input and low output ripple in current and moreover with the modified structure of CUK converter, better charging efficiency can be achieved. Low input current, lower electromagnetic interference (EMI) noise, and decrease in ripple current at output along with shielding against start up inrush current are the features of modified CUK converter. It consists of less conduction losses as well due to the input side elimination of DBR. Overall modified CUK converter is preferrable because it offers incorporated PFC features.

4.2.1 Working and Design considerations

The circuit of modified CUK converter with a rearrangement of diodes and inductors as illustrated in Fig.4.1. consists of a Li-ion battery as a load getting charged with the help of a modified Cuk converter. The flyback DC-DC converter follows power factor correcting device for the better isolation properties and reduced THD. In design of modified CUK converter there is an advantage of elimination of DBR as the modification. Due to this the input conduction losses reduces thereby improving the battery charging system.
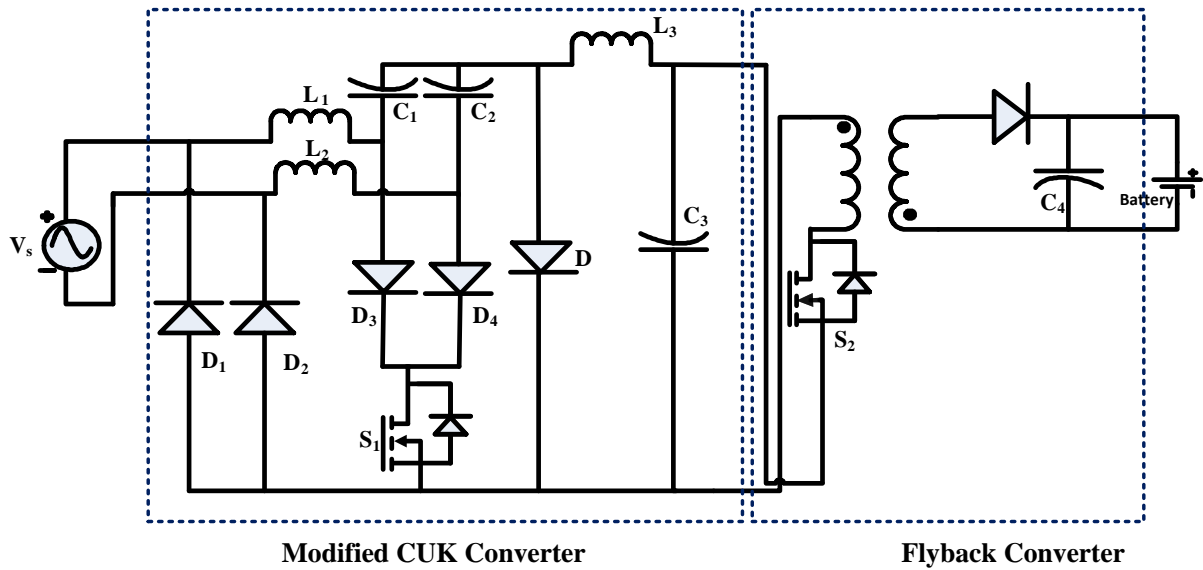
Fig 4.1 Battery charging with modified CUK converter

4.2.2 Modes of charging

This converter has three modes of charging. Circuit is independently analysed in half-cycles of operation (positive and negative).

> ➤ **Mode-1:** When Switch 'S_1' is turned on, current flowing through the inductor starts to rise, and it continues to charge, as shown in Fig 4.2 (a). The charging path includes an inductor L_1, a diode D_3, a switch S_1, and D_2 diode. A charging path for the capacitor includes an inductor and a switch.
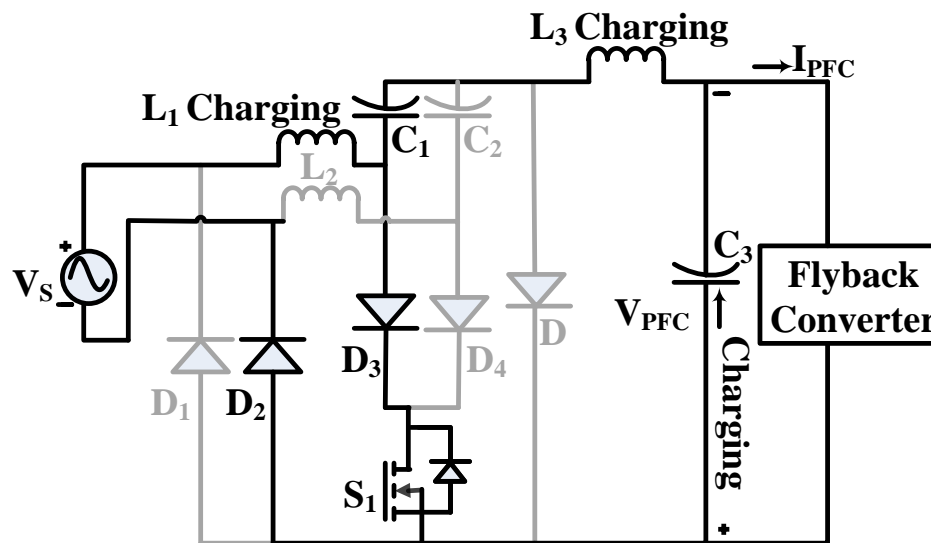
Fig 4.2 (a) Mode 1 of modified CUK converter

➢ **Mode-2:** When the switch S_1 is switched off ,mode 2 begins immediately at an instant t_2 When the inductor starts discharging via capacitor C_3 and diode D, the polarity of the voltage changes at the capacitor C_3. As a result, C_3 is charging and L_1, L_3 being discharged in this manner.
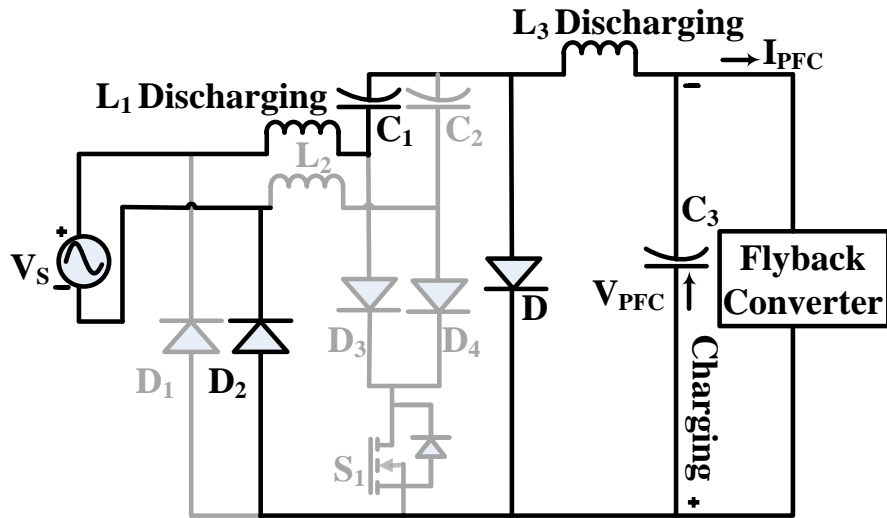
Fig 4.2 (b) Mode 2 of modified CUK converter

➢ **Mode-3**: This mode illustrates that inductor L_3 is completely discharged and enters in discontinuous mode whereas inductor L_1 is getting discharged by diode D and capacitor C_1.
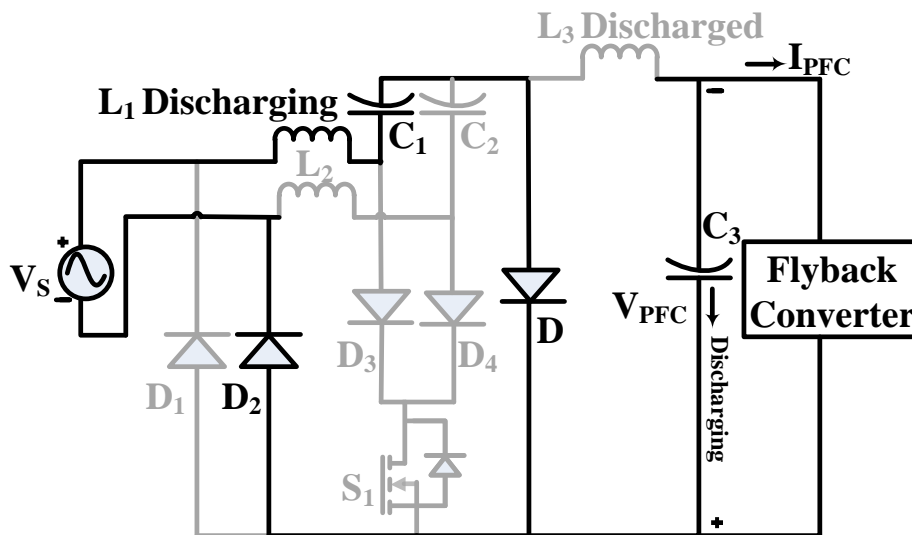
Fig 4.2 (c) Mode 3 of modified CUK converter

The redesigned CUK converter's DC connection is managed to achieve unity power factor. Parameters of modified converter can be designed by the following equations:

Duty cycle for instantaneous operation of converter is defined by equation:

$$D = \frac{V_{PFC}}{V_{PFC} + V_i} \tag{4.1}$$

where $V_i = V_p \sin(\omega_L t)$; $\omega_L = 2\pi f$.

In DCM mode 'D' varies between 0.5700 to o.4493. During steady state operation of converter,current in both the inductors increases. The values for inductors can be evaluated as given by following equation:

$$L_{1,2} = \left(\frac{V_{in}^2}{P_{in}}\right)\frac{1}{0.2f_s}\frac{V_{PFC}}{V_{PFC} + V_i} \tag{4.2}$$

Mid capacitors C_1 and C_2 can be calculated as per equation (4.3).

$$C_{1,2} = \left(\frac{V_{PFC}}{\lambda f_s V_i}\right)\frac{1}{(V_{PFC}^2/P_i)}\frac{V_{PFC}}{V_{PFC} + V_i} \tag{4.3}$$

Where λ is the input current ripple . Output inductor is designed in DCM mode to get unity power factor and is given by:

$$L_3 = \frac{V_{PFC}(1-D)}{2f_s L_3} \tag{4.4}$$

For reducing the size of converter output inductor is chosen to be 1/3 of the value calculated.

Capacitor C_3 is helpful in elimination of second harmonics in the converter.

$$C_3 = \frac{I_{PFC}}{2\omega V_{PFC}} \tag{4.5}$$

Flyback converter produces a higher potential at the output to provide the required voltage for battery charging. This is operated in CC-CV charging mode. This converter is made to work in discontinuous mode by choosing magnetising inductance in such a manner that reduces current drawn in CV mode. The turn ratio of high frequency transformer is taken as 'n_f'. Flyback converter design includes following equations:

37

$$V_4 = \frac{n_f D}{(1-D)} V_b \tag{4.6}$$

Where 'V_b' is the input voltage at flyback converter.

Magnetising current defined by 'L_m' and is calculated as:

$$L_m = \frac{D V_b}{f_s I_m} \tag{4.7}$$

DC link Capacitor 'C_4' at output is given by:

$$C_4 = \frac{D V_b}{f_s k V_b (V_b{}^2 / P_i)} \tag{4.8}$$

Where k is the ripple factor at output of DC link capacitor.

All designed values for modified CUK converter is mentioned in Table 4.1.

Table 4.1- Designed values for modified CUK converter

S.No.	Parameters of Modified CUK Converter	Designed Values
1.	Duty Cycle 'D'	0.57-0.493
2.	Input Inductance '$L_{1,2}$'	4.17mH
3.	Middle Capacitors '$C_{1,2}$'	0.9533μF
4.	Output Inductor 'L_3'	356.61μH
5.	DC Link Capacitor 'C_3'	1.5mF
6.	Switching Frequency 'f'	20KHz
7.	Switching Frequency for flyback converter 'f_{sw}'	50KHz
8.	Magnetizing Inductance of flyback converter 'L_m'	164.37μF

4.2.3 Control technique

As converter switches require distinct controls, the control techniques for both converters are illustrated in Fig 4.3(a) and Fig 4.3(b) (b). As shown in Fig 4.3 (a), the switch of the flyback converter is assigned to the dual loop PI scheme, which tracks battery voltage and compares it to the reference signal, thereby providing error signal to the current PI controller, whereas the modified CUK converter switch is simply assigned to the current PI controller.
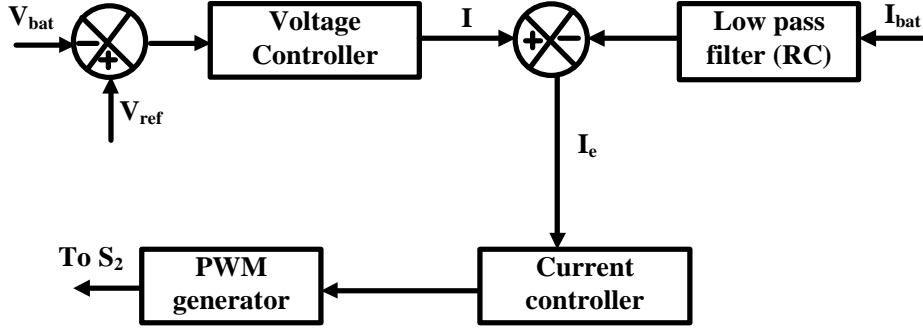
Fig 4.3(a) Control for Flyback converter
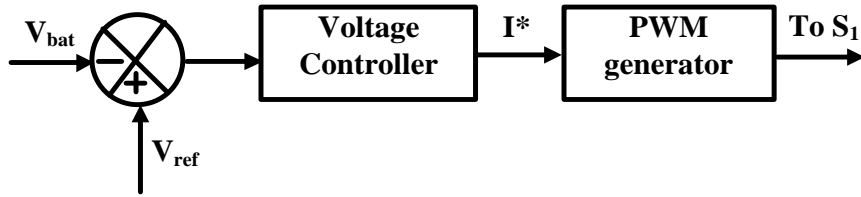
Fig 4.3(b) Control for modified CUK converter

4.2.4 Calculations of K_P and K_I

Let A_1, A_2, A_3 be the state space matrix of mode-1, mode-2 and mode-3 respectively. For state space matrix inductor currents and capacitor voltages are chosen as variables. Using KVL and KCL equations for each mode state space matrix can be generated.

Let $x_1 = I_{L_1}$; $x_2 = I_{L_3}$; $x_3 = V_{C_1}$; $x_4 = V_{C_3}$ $\qquad$ (4.9)

A_1 can be calculated for mode-1 with the help of following equation and can be represented in matrix form also.

$$x_1 = A_1 x + B_1 \qquad (4.10)$$

$$
\begin{bmatrix} \dot{x}_1 \\ \dot{x}_2 \\ \dot{x}_3 \\ \dot{x}_4 \end{bmatrix} =
\begin{bmatrix}
0 & 0 & 0 & 0 \\
0 & 0 & \dfrac{-1}{L_3} & \dfrac{-1}{L_3} \\
0 & \dfrac{1}{C_1} & 0 & 0 \\
0 & \dfrac{1}{C_3} & 0 & \dfrac{1}{RC_3}
\end{bmatrix}
\begin{bmatrix} x_1 \\ x_2 \\ x_3 \\ x_4 \end{bmatrix}
+
\begin{bmatrix} \dfrac{1}{L_1} \\ 0 \\ 0 \\ 0 \end{bmatrix} V_s
$$

For mode 2, A_2 can be evaluated as per equation (4.11):

$$x_2 = A_2 x + B_2 \qquad (4.11)$$

$$\begin{bmatrix} \dot{x}_1 \\ \dot{x}_2 \\ \dot{x}_3 \\ \dot{x}_4 \end{bmatrix} = \begin{bmatrix} 0 & 0 & \dfrac{-1}{L_1} & 0 \\ 0 & 0 & 0 & \dfrac{-1}{L_3} \\ \dfrac{1}{C_1} & 0 & 0 & 0 \\ 0 & \dfrac{1}{C_3} & 0 & \dfrac{1}{RC_3} \end{bmatrix} \begin{bmatrix} x_1 \\ x_2 \\ x_3 \\ x_4 \end{bmatrix} + \begin{bmatrix} \dfrac{1}{L_1} \\ 0 \\ 0 \\ 0 \end{bmatrix} V_s$$

For mode 3, A_3 can be calculated as per equation (4.12):

$$x_3 = A_3 x + B_3 \tag{3.12}$$

$$\begin{bmatrix} \dot{x}_1 \\ \dot{x}_2 \\ \dot{x}_3 \\ \dot{x}_4 \end{bmatrix} = \begin{bmatrix} 0 & 0 & \dfrac{-1}{L_1} & 0 \\ 0 & 0 & 0 & \dfrac{-1}{L_3} \\ \dfrac{1}{C_1} & 0 & 0 & 0 \\ 0 & 0 & 0 & \dfrac{1}{RC_3} \end{bmatrix} \begin{bmatrix} x_1 \\ x_2 \\ x_3 \\ x_4 \end{bmatrix} + \begin{bmatrix} \dfrac{1}{L_1} \\ 0 \\ 0 \\ 0 \end{bmatrix} V_s$$

For DCM mode, $A = A_1 d_1 + A_2 d_2 + A_3(1 - d_1 - d_2)$ \hfill (4.13)

where d_1 and d_2 are duty cycles for mode 1 and mode 2.

$$\begin{bmatrix} \dot{x}_1 \\ \dot{x}_2 \\ \dot{x}_3 \\ \dot{x}_4 \end{bmatrix} = \begin{bmatrix} 0 & 0 & \dfrac{-1}{L_1} & 0 \\ 0 & 0 & 0 & \dfrac{-1}{L_3} \\ \dfrac{1}{C_1} & 0 & 0 & 0 \\ 0 & \dfrac{d_1}{C_3} + \dfrac{d_2}{C_3} & 0 & \dfrac{1}{RC_3} \end{bmatrix} \begin{bmatrix} x_1 \\ x_2 \\ x_3 \\ x_4 \end{bmatrix} + \begin{bmatrix} \dfrac{1}{L_1} \\ 0 \\ 0 \\ 0 \end{bmatrix} V_s$$

After performing steady state analysis of above state matrix equations, transfer function can be found out and using routh Hurwitz method critical value K_{cr} can be find out easily and further values of K_P and K_I can evaluated.

$$K_P = 0.45 K_{cr} \qquad (4.14)$$

$$K_I = \frac{1.2 K_P}{T_{cr}} \qquad (4.15)$$

$$T_{cr} = \frac{2\pi}{\omega_{cr}} \qquad (4.16)$$

4.2.5 Simulation Results

The simulation results for charging battery by using modified CUK converter as a PFC unit is shown in Fig 4.4 below which illustrates supply voltage (V_s), supply current (I_s), battery voltage (V_{bat}), battery current (I_{bat}), State of charge (SOC%) and THD% respectively.
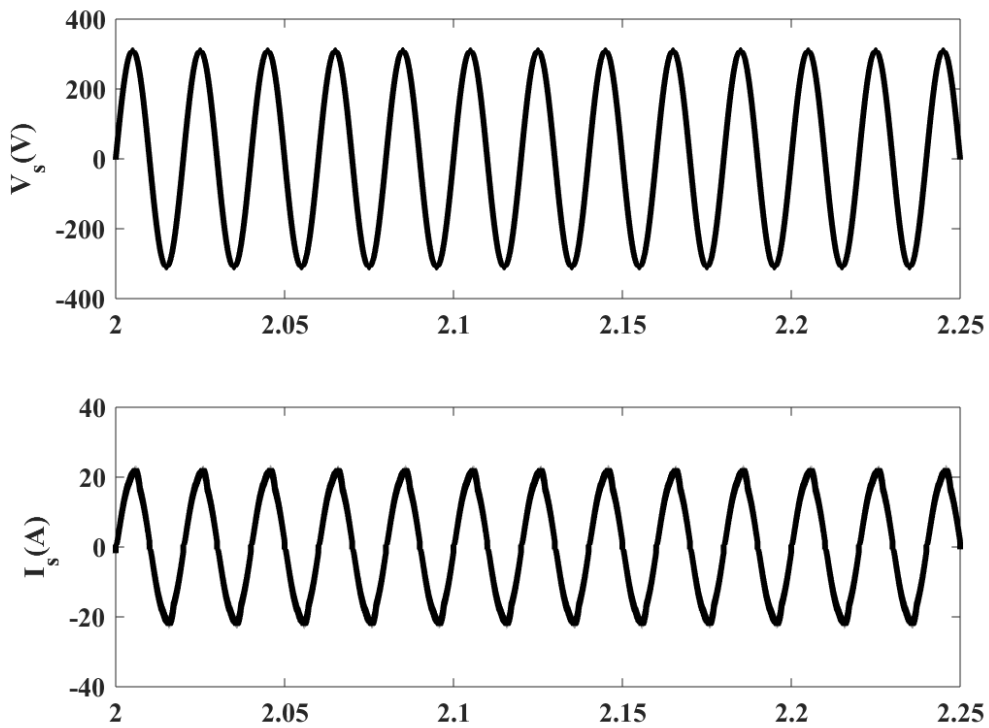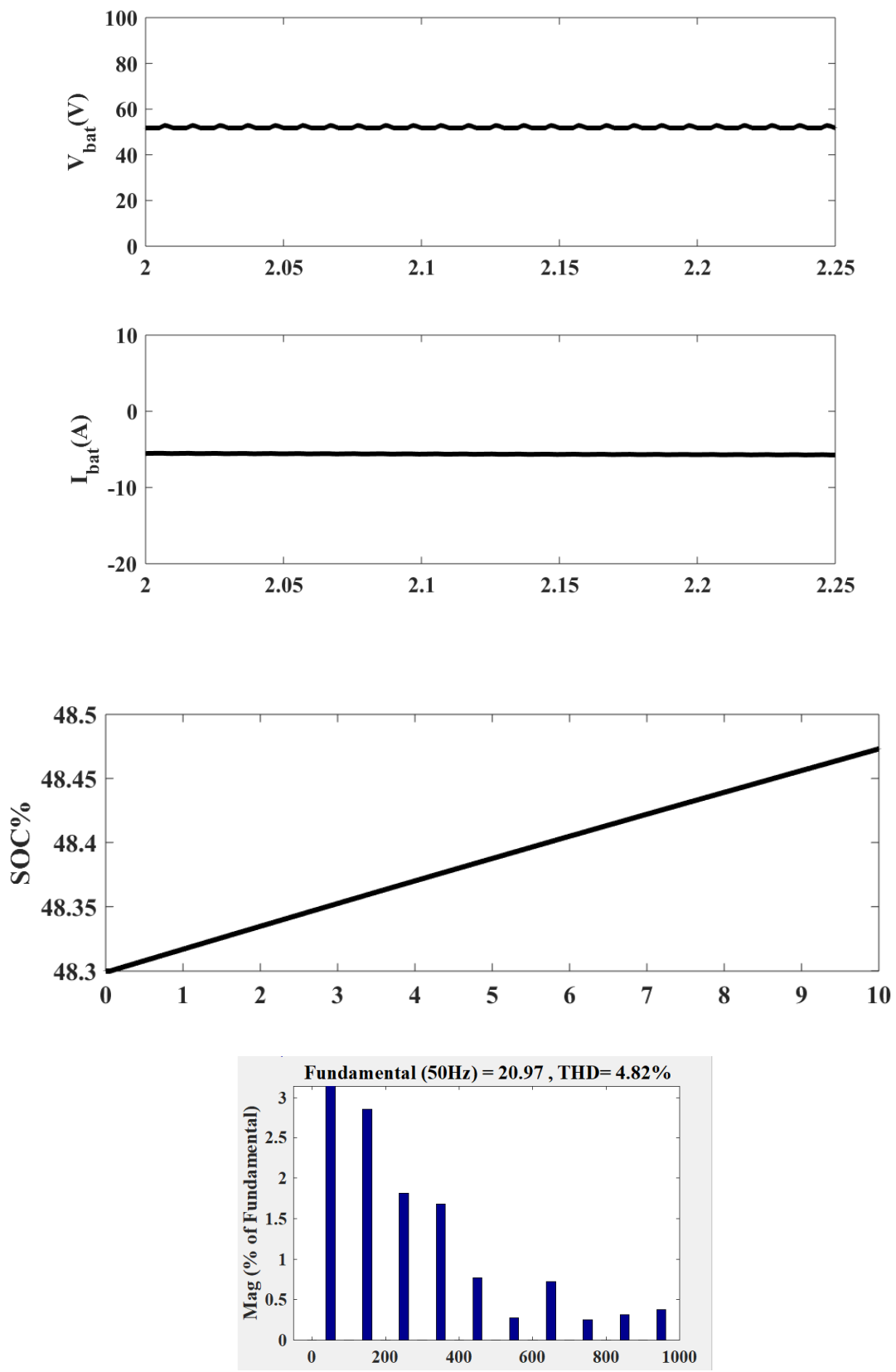
Fig 4.4. Results of modified CUK converter as PFC for charging

4.3 Modified Zeta Converter

A conventional Zeta converter although comes up with many advantages but at higher ratings the voltage stresses at PFC switches becomes high so in order to overcome these problems a new modified configuration came in picture having two additional switches and two additional clamping diodes in order to rectify the problems arisen due to switching stresses. Modified configurations provide When compared to standard link voltages, DC link voltages have a lower duty ratio. There is no inclusion of any extra capacitors or inductors which could increase the size and thereby increasing power density of the whole system which could suppress the advantages of using modified converter as PFC.

4.3.1 Working and Design considerations

The design configuration of modified Zeta converter as PFC is exhibited in Fig 4.5 which consists of a DBR, PFC converter followed by flyback converter which is helpful in reducing furthermore ripples as it is having high frequency transformer and high switching frequency. Modified Zeta converter is reducing THD as well as reducing stress at DBR switches also because of its design. The rearrangement of diodes and extra switches involved can be clearly depicted from Fig 4.5.
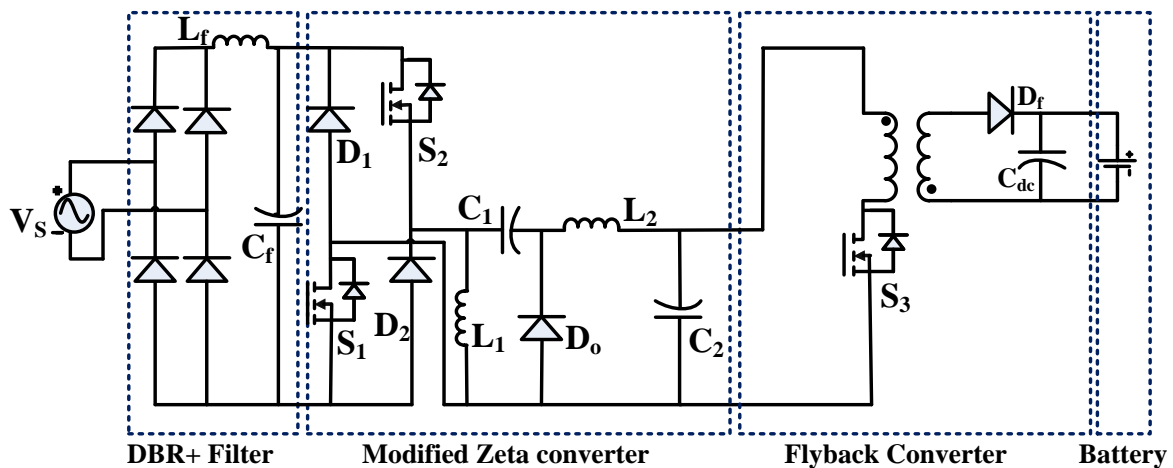
Fig 4.5 Modified Zeta Converter

4.3.2 Modes of operation

> **Mode-1:** This mode operation involves switches S_1, S_2 switched simultaneously while inductor L_1 starts charging via supply. Diode D_o is in non-conducting state. As inductor L_2 is storing energy, at the same time voltage across capacitor C_1 starts reducing as can be seen from Fig 4.6 (a).

43
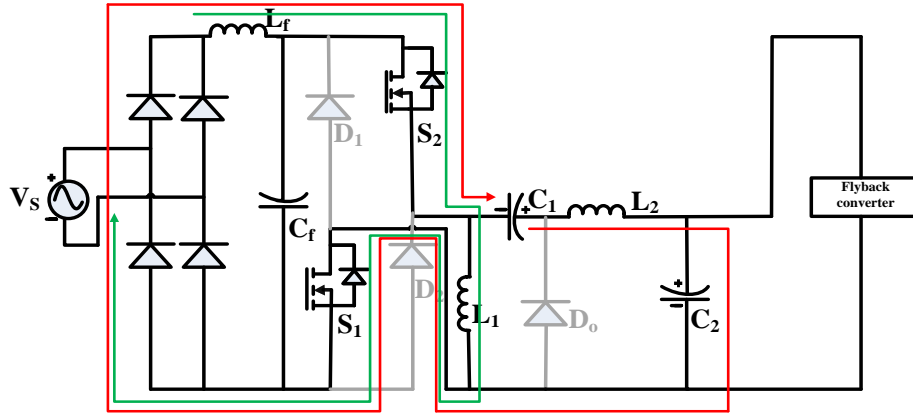
Fig 4.6 (a) Mode 1 of modified Zeta converter

➢ **Mode-2:** From Fig 4.6 (b) it can be observed that switch S_1, S_2 both are in off condition in mode 2 while diodes D_1, D_2 and clamping diodes become forward biased. Capacitance C_1 is getting charged through D_o diode. Inductor L_1 is getting discharged by diodes D_1 and D_2. Inductor L_2 supplies rest of the part of system with the help of capacitor C_2 and diode D_o.
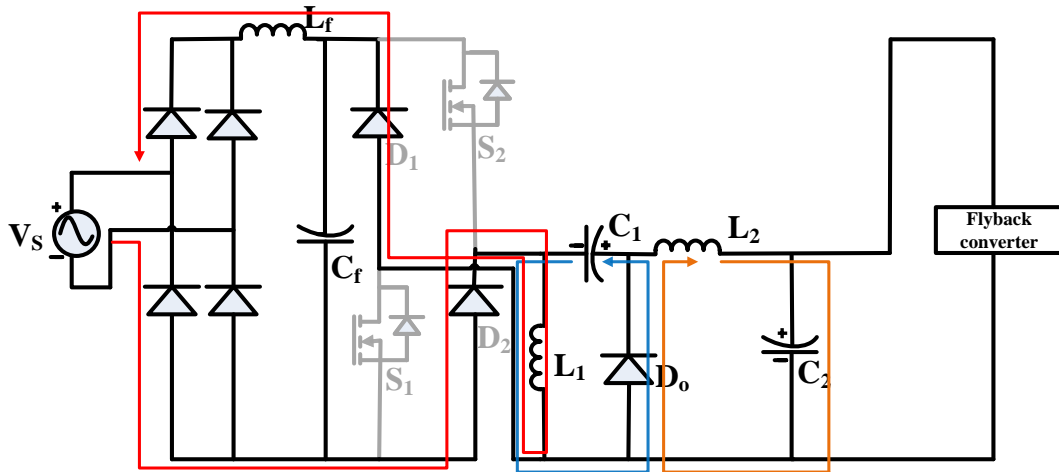
Fig 4.6 (b) Mode 2 of modified Zeta converter

• **Mode-3:** In this mode, system enters in DCM mode or in other words freewheeling period as clamping diodes and both switches remains in off state as per Fig 4.6 (c). Inductances L_1 and L_2 has currents in such a way that current in diode is tend to be zero. C_1 i.e., the transfer capacitance supplies energy requirement of load via L_2 and C_2.

Switches S_1, S_2 and diodes have peak voltages quite less than the conventional converter and is given by:

$$V_{S1} = V_{S2} = V_S \qquad (4.17)$$
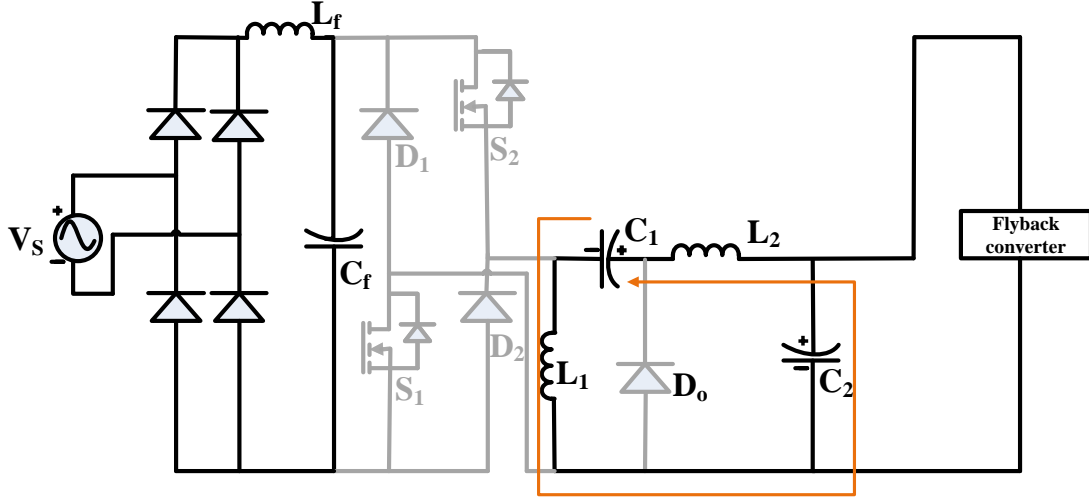
Fig 4.6 (c) Mode 3 of modified Zeta converter

The design of modified Zeta converter is illustrated in following equations given by:

To make Zeta converter work in DCM mode, Duty cycle is calculated as:

$$D(t) = \frac{V_s}{V_2 + \sqrt{2}V_s} \qquad (4.18)$$

where V_2 is the DC link voltage at Zeta converter

Critical value of Input Inductance L_1 is calculated as:

$$L_1 = \left(\frac{V_{s\,min}{}^2}{P} \right) \left(\frac{V_s}{V_2 + \sqrt{2}V_s} \right) \frac{T_s}{2} \qquad (4.19)$$

where T_s is the switching time period of Zeta converter.

Critical value of Series capacitance is given by:

$$C_1 = \frac{P}{\mu f \left(V_2 + \sqrt{2}V_{s\,max} \right)} \qquad (4.20)$$

where μ is the ripple factor for series capacitance

Critical value of inductance 'L$_2$' is given by:

$$L_2 = \left(\frac{V_{s\,min}^{\,2}}{P}\right)\left(\frac{V_s}{V_2 + \sqrt{2}V_s}\right)\frac{1}{\lambda f}$$

(4.21)

where λ is the ripple factor for current in inductor.

Critical value of DC-link capacitance for Zeta converter is given by:

$$C_2 = \frac{I_2}{4\pi f \Delta V_2}$$

(4.22)

Filter is designed to improve the current profile at the input of Zeta converter. It has an inductance and capacitance designed accordingly to decrease the ripples in input current. Critical value of filter capacitance is designed as:

$$C_{f\,max} = \frac{P\tan\theta}{2\pi f_c V_s^{\,2}}$$

(4.23)

Filter inductance 'L_f' is calculated as:

$$L_f = \left[\frac{1}{4\pi f_c^{\,2} C_f}\right] - \left[\frac{\left(0.04 V_s^{\,2}\right)}{2\pi f P}\right]$$

(4.24)

where f_c is filter's cut off frequency which is chosen to be 1/10 times of the frequency of converter.

In design of flyback converter magnetizing inductance plays an important role. Chosen value of the magnetising inductance should be lower than the predicted critical value.. Magnetizing inductance's critical value is given by:

$$L_m = \frac{\left(D_f V_2\right)^{\,2}}{2 f_{sw} I_{dc} V_{dc}}$$

(4.25)

where 'f_{sw}' is flyback converter's switching frequency.

All designed values for modified Zeta converter is mentioned in Table 4.2.

46

Table 4.2-Designed values for modified Zeta converter

	Parameters of Modified Zeta Converter	Designed values
9.	Input Inductance 'L_1'	110μH
10.	Input Series capacitor 'C_1'	0.88μH
11.	Output capacitor 'C_2'	2mF
12.	Output Inductance 'L_2'	2.8mH
13.	Filter Inductance 'L_f'	4mH
14.	Filter capacitance 'C_f'	580nF
15.	DC link capacitor 'C_{dc}'	3mF
16.	Magnetizing inductance 'L_m'	130μH
17.	Zeta converter Switching frequency 'f'	20kHz
18.	Flyback converter Switching frequency 'f_{sw}'	50kHz

4.3.3 Control Technique

The control technique this charging model is having two separate PI loops for each i.e., Flyback converter is being operated on cascaded loop of PI control which tracks battery voltage as well as keeps battery current in limits as shown in Fig 4.7(a). Battery voltage is being compared with reference voltage to produce an error signal fed to voltage PI controller which in turn is generating error signal to feed into current controller, further pulses are generated with PWM generator unit and switches S_3 while Modified Zeta converter has single PI loop control. It feedbacks DC link voltage after getting compared with reference voltage and gives the pulse for switching S_1 and S_2 used in modified Zeta converter as per Fig 4.7(b).
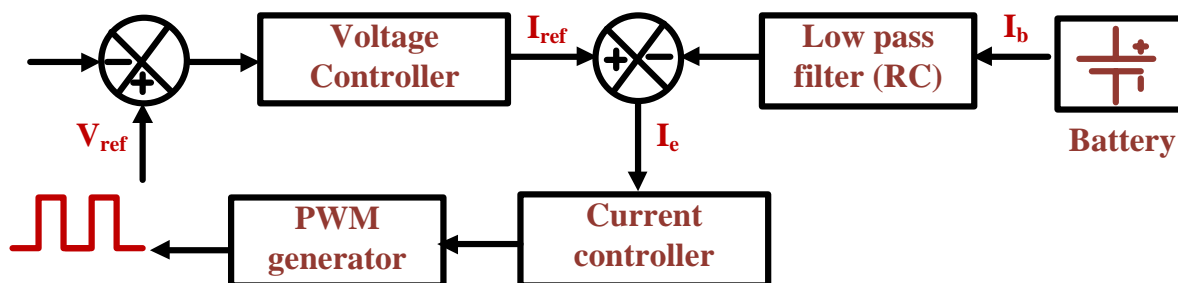
Fig 4.7 (a) Control for flyback converter
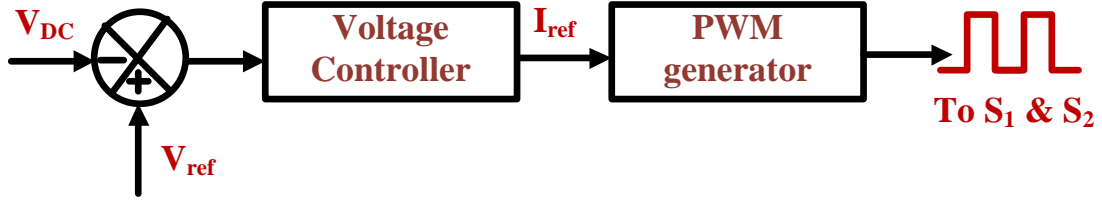
Fig 4.7 (b) Control for modified Zeta converter

4.3.4 Calculations of K_p and K_I

Let A_1, A_2, A_3 be the state space matrix of mode 1, mode 2 and mode 3 respectively. For state space matrix inductor currents and capacitor voltages are chosen as variables. Using KVL and KCL equations for each mode state space matrix can be generated.

Let $x_1 = I_{L1}$, $x_2 = I_{L2}$, $x_3 = V_{C1}$, $x_4 = V_{C2}$ (4.26)

For mode 1 matrix A_1 is given by: $x_1 = A_1 x + B_1$

$$\dot{x}_1 = \frac{V_S}{L_1} \tag{4.27}$$

$$\dot{x}_2 = \frac{V_S}{L_2} + \frac{x_3}{L_2} - \frac{x_4}{L_2} \tag{4.28}$$

$$\dot{x}_3 = \frac{x_1}{C_1} \tag{4.29}$$

$$\dot{x}_4 = \frac{x_1}{C_2} - \frac{x_4}{RC_2} \tag{4.30}$$

$$A_1 = \begin{bmatrix} 0 & 0 & 0 & 0 \\ 0 & 0 & \frac{1}{L_2} & -\frac{1}{L_2} \\ \frac{1}{C_1} & 0 & 0 & 0 \\ \frac{1}{C_2} & 0 & 0 & -\frac{1}{RC_2} \end{bmatrix}$$

Similarly, for mode 2 matrix A_2 can be calculated as:

48

$$\dot{x}_1 = \frac{V_S}{L_1} \tag{4.31}$$

$$\dot{x}_2 = \frac{x_4}{L_2} \tag{4.32}$$

$$\dot{x}_3 = \frac{x_1}{C_1} \tag{4.33}$$

$$\dot{x}_4 = \frac{x_2}{C_2} - \frac{x_4}{RC_2} \tag{4.34}$$

$$A_2 = \begin{bmatrix} 0 & 0 & 0 & 0 \\ 0 & 0 & \dfrac{1}{L_2} & -\dfrac{1}{L_2} \\ \dfrac{1}{C_1} & 0 & 0 & 0 \\ 0 & \dfrac{1}{C_2} & 0 & \dfrac{1}{RC_2} \end{bmatrix}$$

For mode 3 A_3 can be calculated as:

$$\dot{x}_1 = \frac{x_4}{L_1} + \frac{x_3}{L_1} \tag{4.35}$$

$$\dot{x}_2 = \frac{x_4}{L_2} + \frac{x_3}{L_2} \tag{4.36}$$

$$\dot{x}_3 = \frac{x_2}{C_1} \tag{4.37}$$

$$\dot{x}_4 = \frac{x_2}{C_2} - \frac{x_4}{RC_2} \tag{4.38}$$

$$A_3 = \begin{bmatrix} 0 & 0 & \dfrac{1}{L_1} & \dfrac{1}{L_1} \\ 0 & 0 & \dfrac{1}{L_2} & \dfrac{1}{L_2} \\ 0 & \dfrac{1}{C_1} & 0 & 0 \\ 0 & \dfrac{1}{C_2} & 0 & -\dfrac{1}{RC_2} \end{bmatrix}$$

For DCM mode:

$$\text{Average } A = A_1 \, d_1 + A_2 \, d_2 + A_3 \, (1 - d_1 - d_2) \tag{4.39}$$

where d_1, d_2 are duty ratios for mode 1 and mode 2 respectively. Matrix 'A' is generated after solving equation (4.23). This is used to find out transfer function of the respective model. Tuning of PI can be done using various methods. This model includes tuning via Zeigler Nicholas method where transfer function is calculated with the help of steady state analysis and state space modelling. The critical value of 'K_{cr}' can be calculated using Routh Hurwitz criteria which is consisting of auxiliary equation helpful in finding out the value of 'T_{cr}'. By Zeigler Nicholas method, values of 'K_p' and 'K_I' can be calculated as:

$$K_p = 0.45 K_{cr} \tag{4.40}$$

$$K_I = \frac{1.2 K_p}{T_{cr}} \tag{4.41}$$

$$T_{cr} = \frac{2\pi}{\omega_{cr}} \tag{4.42}$$

Critical value of 'K_{cr}' can be calculated by Routh-Hurwitz criteria.

4.3.5 Simulation Results

The simulation results for charging battery by using modified Zeta converter as a PFC unit is shown in Fig 4.8 below which shows peak value of 311V as supply voltage (V_s), supply current (I_s) having peak value 14.42A, Inductor 2 current (I_{l2}), capacitor 2 voltage (V_{C2}), battery voltage (V_{bat}), battery current (I_{bat}), State of charge (SOC%) and THD% respectively.
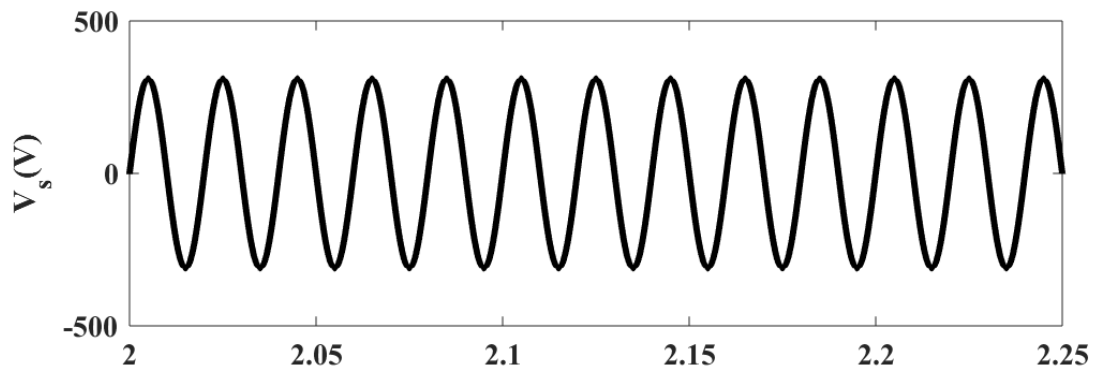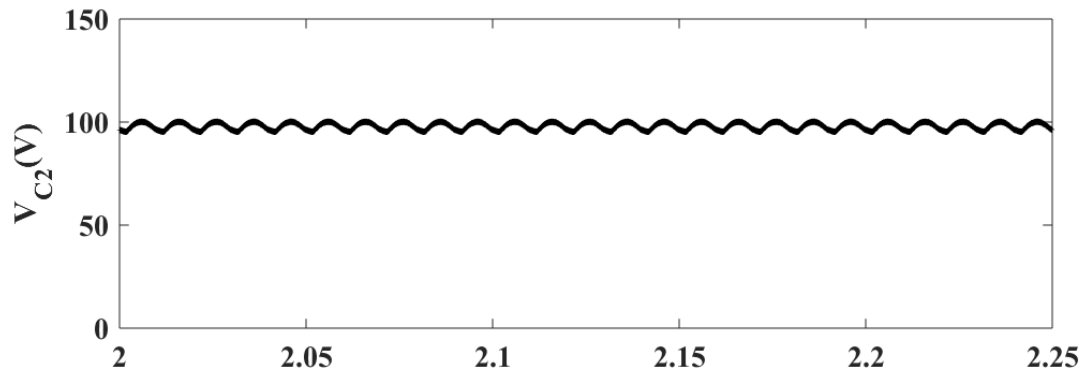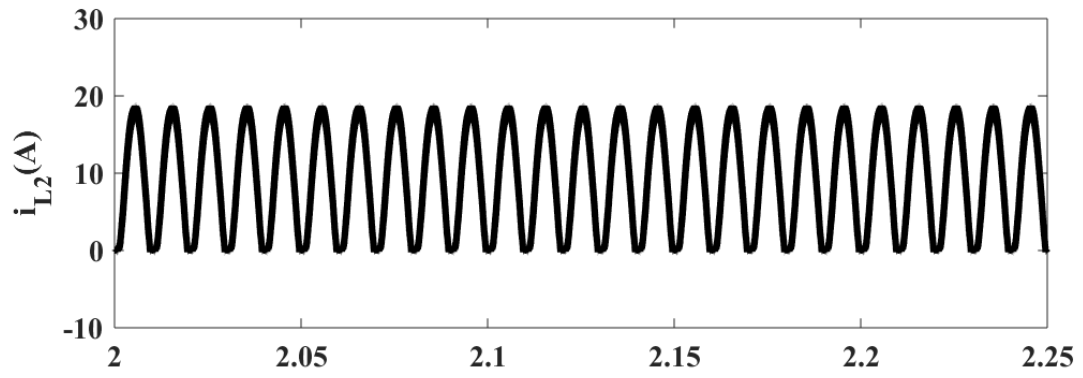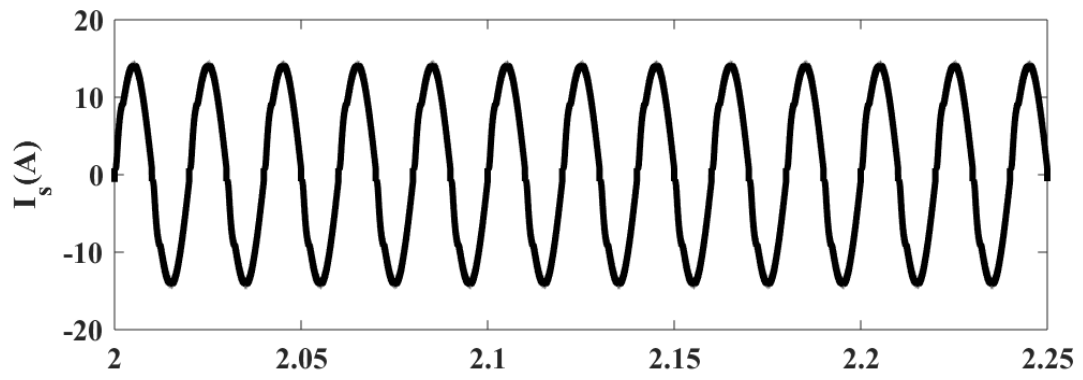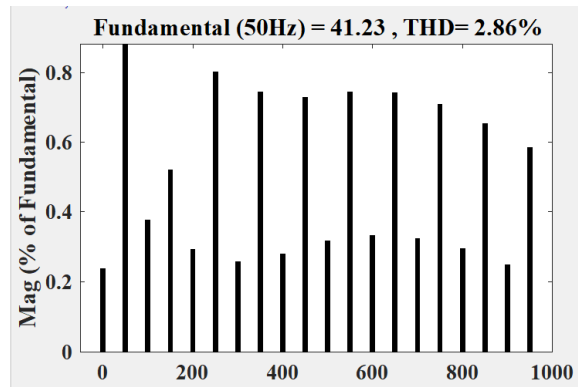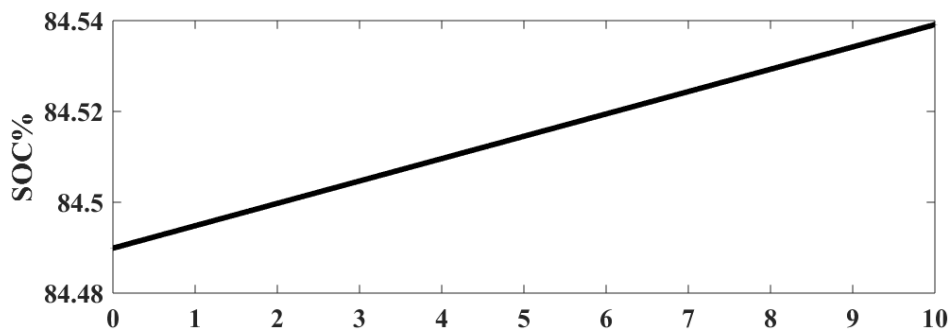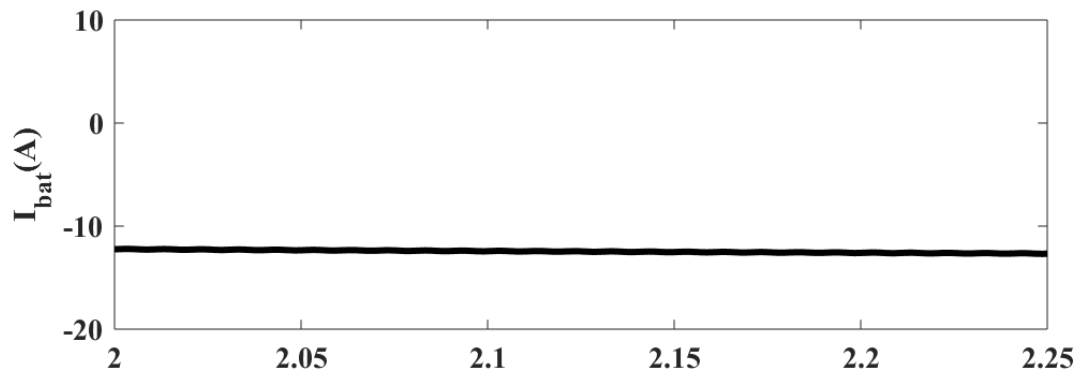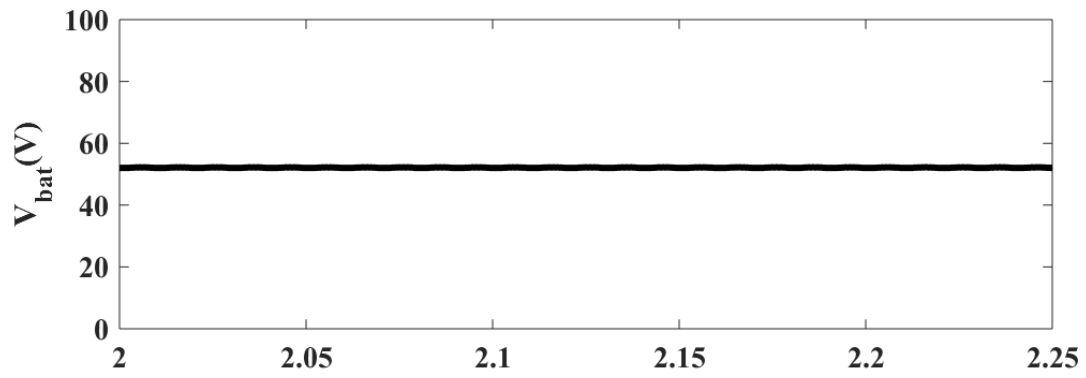
Fig 4.8 Results for modified Zeta as PFC for battery charging

4.4 Conclusion

Modified converters are better in improving current profile of input current as compared to conventional converters as we can observe it from the results due to their bridgeless nature DBR stresses gets reduced in the circuit. Along with these other modifications like rearrangement of diodes and inductor, capacitors resulting in an improvement in overall efficiency of the circuit charging the battery. Hence, they are more effective in improving THD.

CHAPTER-V

MODELLING AND ANALYSIS OF INTERLEAVED CONVERTERS

5.1 Introduction

Interleaved converters are the improved converter forms of various conventional converters. Interleaving is also known as 'multi-phasing' i.e., a technique useful for the filter components size reduction. These converters are generally $180°$ out of phase. It can be made by interleaving the two converters in combination of one which is helpful in improving power factor correction features thereby making it a low-cost efficient component to be used in EV for charger applications.

5.2 Interleaved Luo

Interleaved Luo is the configuration made by interleaving two converter cells into one and converting them into parallel combination of two Luo converters. The operation of converter takes place with a shift of $180°$. The converter has an inbuilt property of ripple cancellation within the circuit due to its interleaving structure and arrangement of two Luo converters in systematic manner which makes it more suitable for working as a PFC converter in charging.

5.2.1 Working and Design considerations

Interleaved Luo converter's design is illustrated in Fig 5.1. which shows two Luo converters are made to work as one by connecting them in parallel and this configuration is followed by a flyback converter having high transformer frequency thereby charging a battery.
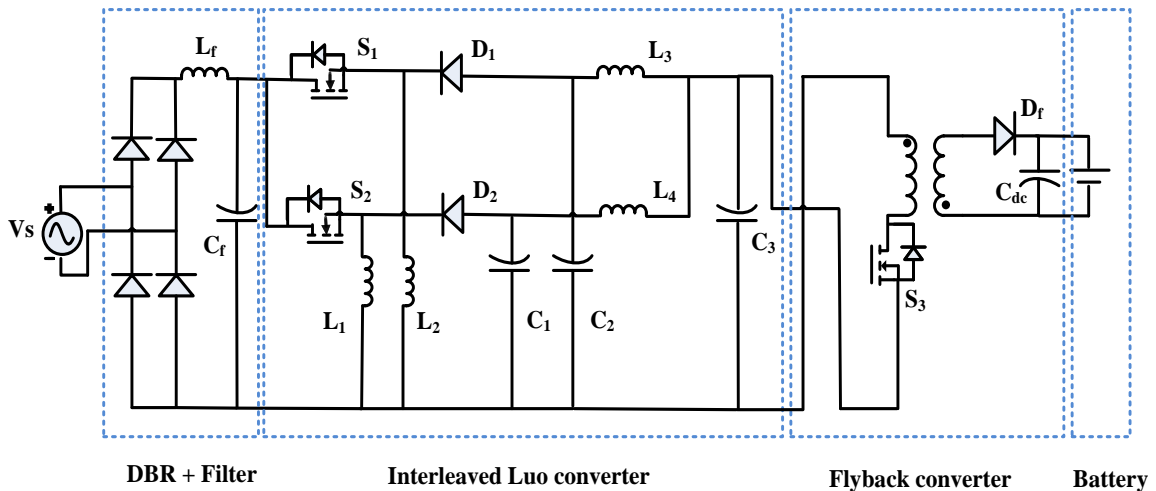
Fig 5.1 Interleaved Luo Converter Configuration

5.2.2 Modes of Charging

➤ **Mode-1:** As mentioned in Fig 5.2 (a), when the switch S_1 is turned on, the inductor L_2 begins charging and stores energy from the supply mains, while the inductor L_1 is discharging via diode D_2 (forward biased) by transferring energy to it. Capacitor C_1 is getting charged and resulting in increase of voltage across it while capacitor C_2 is discharging through L_3.
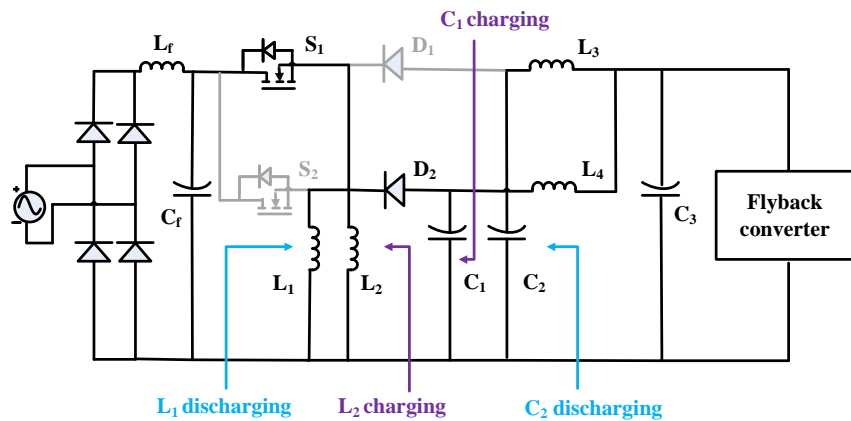
Fig 5.2 (a) Mode 1

➤ **Mode-2:** This mode's operation is shown in Figure 5.2 (b) where S_1 is the lone switch that is conducting and thus L_2 is storing energy through the supply lines. During this procedure, the inductor L_1 is totally depleted and enters DCM mode. In this mode, the diode D_1 is reverse biased and begins to discharge C_1 and C_2.
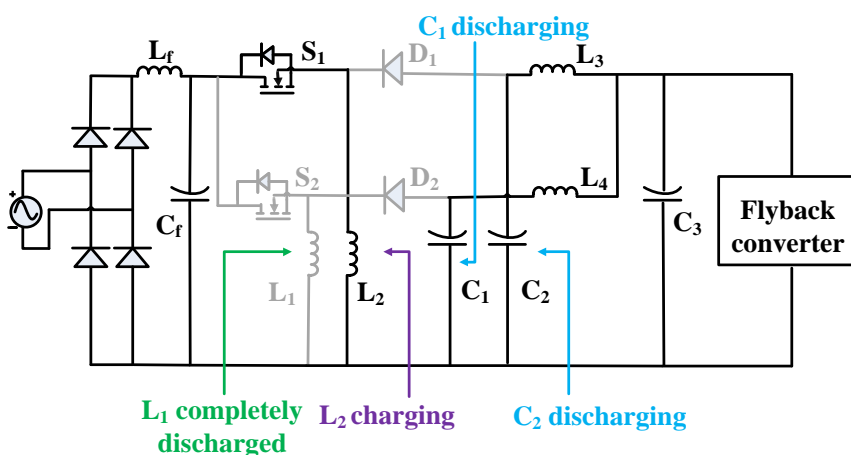
Fig 5.2 (b) Mode 2

➢ **Mode-3:** S_1 and S_2 both switches are acting in off condition as illustrated in Fig 5.2 (c) Inductor L_2 is still in DCM mode and starts discharging via diode D_1 as it is conducting. Immediate charging of capacitor C_2 starts meanwhile the voltage across capacitor C_1 starts decreasing as it is discharging via L_4.
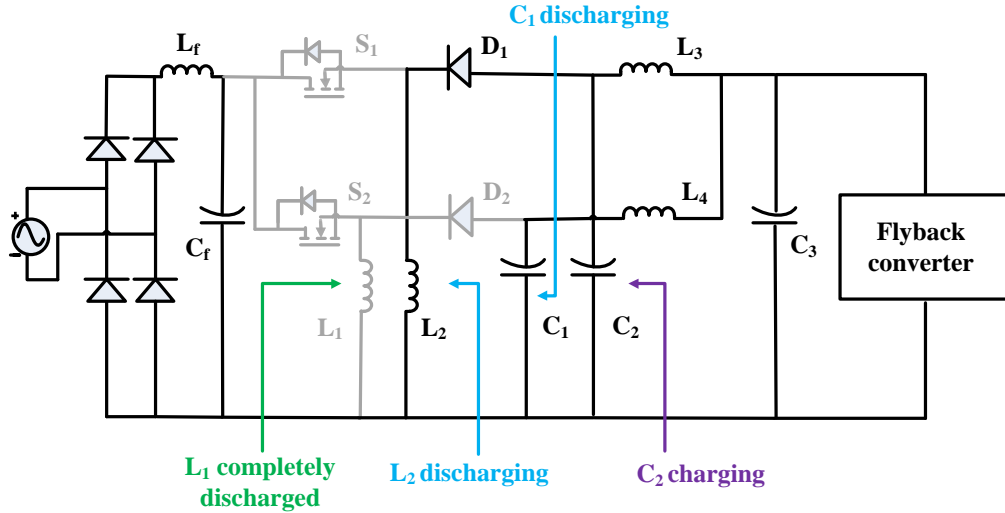
Fig 5.2 (c) Mode 3

➢ **Mode-4:** In Fig 5.2 (d) the moment when the switch S_2 is made on, voltage across C_2 starts rising and diode D_1 and inductor L_2. whereas inductor L_1 is gaining energy via supply mains meanwhile C_1 discharges through L_4 and current is supplied to the battery.

Fig 5.2 (d) Mode 4

56
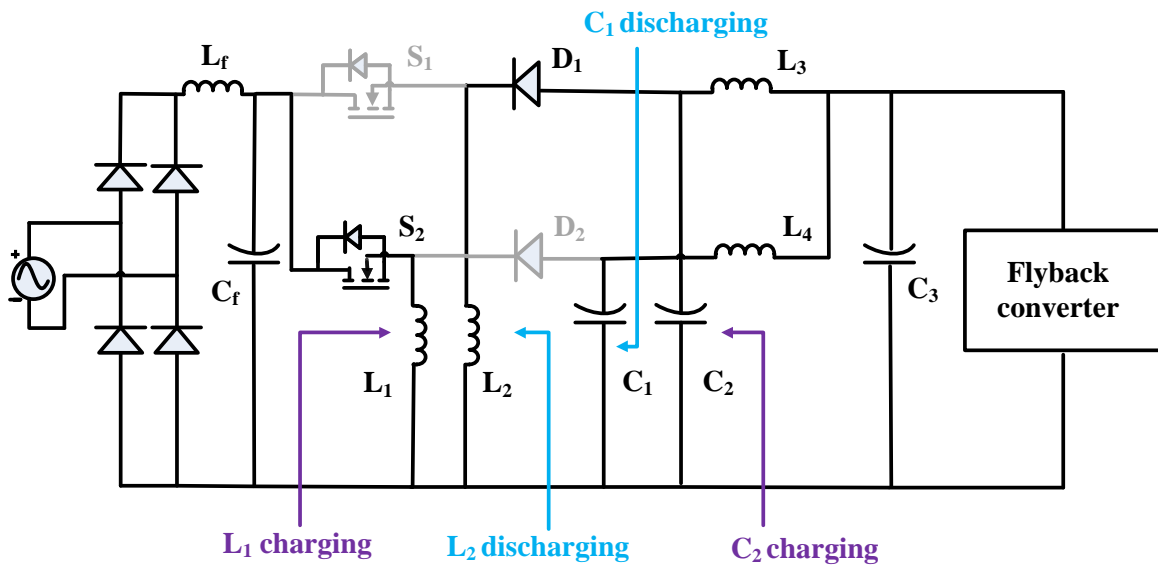
➢ **Mode-5:** In this mode diode D_1 and switch S_1 are non-conducting in nature which shows that inductor L_2 energy is completely discharged and current starts decreasing through it while switch S_2 is still in on mode as per Fig 5.2(e). Current in L_1 keeps on increasing as it is charging. Both C_1 and C_2 are getting discharged through L_3 and L_4.
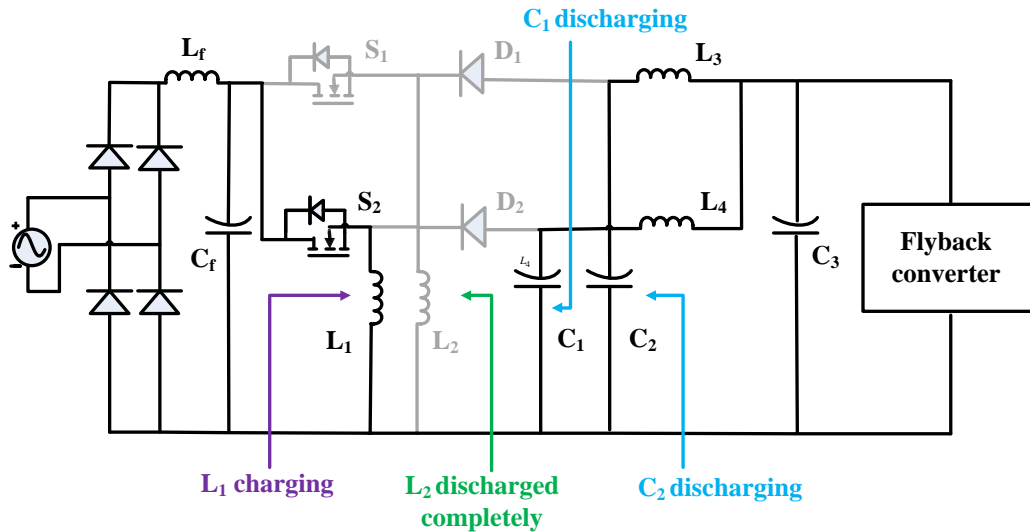
Fig 5.2 (e) Mode 5

➢ **Mode-6:** Switches S_1 and S_2 as well as diode D_1 remains off in this mode as per the illustration in Fig 5.2(f). Inductor L_2 is discharged completely as it enters in DCM mode while diode D_2 starts conducting gradually. Capacitor C_1 is charging via L_4 and voltage starts building up across the capacitor.
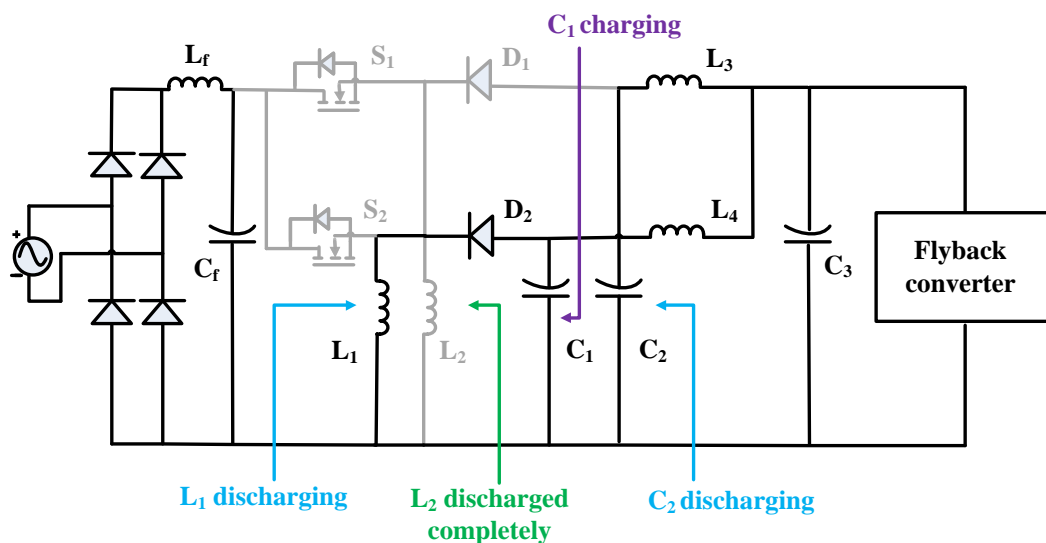
Fig 5.2 (f) Mode 6

The DC voltage generated at DBR's output is the average voltage V_{in} given by equation (5.1) Design of interleaved Luo converter in the charging of battery is defined by the following equations discussed below:

$$V_{in} = \frac{2\sqrt{2}V_s}{\pi}$$ (5.1)

V_s is the supply voltage. The output and input voltage are interconnected as per equation (5.2)

$$D = \frac{V_a}{V_a + V_{in}}$$ (5.2)

where V_a is the voltage generated at DC link of Luo converter and D is the duty cycle of interleaved converter. It varies between a minimum value of 0.56 to maximum value of 0.66. Converter has two inductors L_1 and L_2 at the input, they are made to work in DCM mode. So, the critical value of L_1, L_2 is calculated as follows:

$$L_{1,2} = \frac{D_{min}(1 - D_{min})}{2f_s I_{bat}}$$ (5.3)

where f_s is the Interleaved Luo converter switching frequency while I_b is the current which can be calculated as per equation (5.4).

$$I_b = \frac{P}{V_a}$$ (4.4)

The critical value of mid capacitors C_1 and C_2 is given by:

$$C_{1,2} = \frac{V_a D_{max}}{2f_s(\delta/2)R_L}$$ (5.5)

where δ is the capacitor voltage ripple and R_L is the load resistance.

The output capacitors of converter i.e., L_3 and L_4 have the critical values as given by:

$$L_{3,4} = \frac{I_{bat} D_{max}}{16f_s{}^2 C_{1,2}(\sigma/2)}$$ (5.6)

where σ is considered as ripple in current of inductor. Output capacitor C_3 of Luo converter i.e., DC link generated at output of Interleaved Luo converter is given by:

$$C_3 = \frac{I_{bat}}{2\omega\Delta V_3} \tag{5.7}$$

where ΔV_3 is the ripple voltage at C_3.

Flyback converter design consists of a transformer providing isolation, a diode D_f, a capacitor C_{DC} at output and a switch S_3. The selection of magnetizing inductance L_m plays an important role in high frequency transformer operation as well as flyback converter operation. It is chosen to be very less than the calculated critical value. Value of L_m is given as:

$$L_m = \frac{(V_a D_{fb})^2}{2fV_{bat}I_{bat}} \tag{5.8}$$

Duty cycle D_{fb} for flyback converter operation is given by:

$$D_{fb} = \frac{V_a}{(n_s/n_p)V_{bat} + V_a} \tag{5.9}$$

Where (n_s/n_p) is secondary to primary turn ratio and is considered as $(1/3)$ here. For the minimal ripple in the output current, an output DC link capacitor C_{DC} is employed. It can be estimated as:

$$C_{DC} = \frac{D_{fb}V_{bat}}{f(V_{bat}^2/P)\mu} \tag{5.10}$$

where μ represents the battery voltage ripple.

All designed values for interleaved Luo converter are mentioned in Table 5.1.

Table 5.1-Designed values for Interleaved Luo converter

	Parameters of Interleaved Converter	Designed values
1.	Supply voltage V_s	220V
2.	Average output voltage V_{in}	198V
3.	Duty ratio (Interleaved Luo) D	0.56-0.66
4.	Switching frequency f_s	20kHz
5.	Input inductors $L_{1,2}$	150μF
6.	Mid capacitors $C_{1,2}$	0.44μF
7.	Output inductors $L_{3,4}$	2.35mH
8.	DC link capacitor C_3	800μF
9.	Magnetizing inductance L_m	130μH
10.	Switching frequency f	50kHz
11.	Duty ratio (Flyback) D_{fb}	0.394
12.	Output DC link capacitor C_{DC}	1500μF

5.2.3 Control Technique

The suggested system uses a balanced control topology to deliver pulses to an Interleaved Luo converter that are 180 degrees phased apart. As shown in Fig 5.3(a), the DC link voltage produced at the output of the interleaved Luo converter is compared to the reference DC voltage controlling and fed to the voltage PI controller. As per Fig 5.3(b), the switching of a flyback converter involves a dual loop control of PI in which the battery voltage is detected and compared to a fixed voltage taken as reference, and the compared value is fed to a voltage PI controller and cascaded with a current PI controller, which in turn generates controlled pulses for the flyback converter switch.
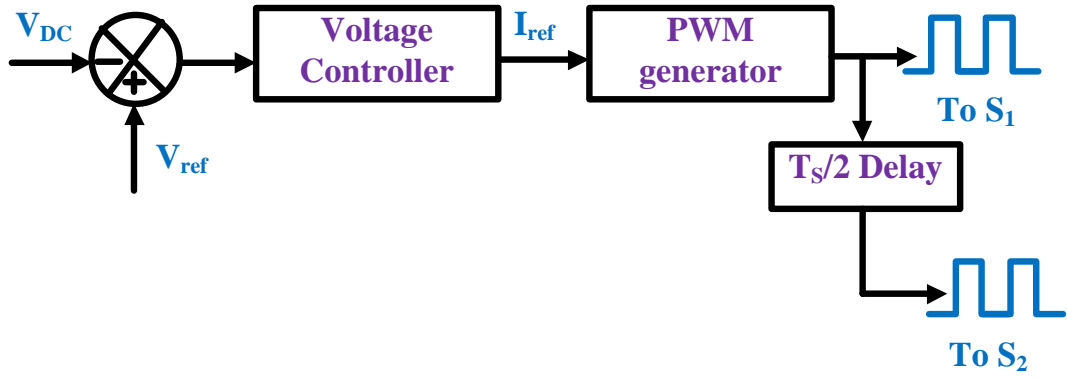
Fig 5.3 (a) Control for Luo converter
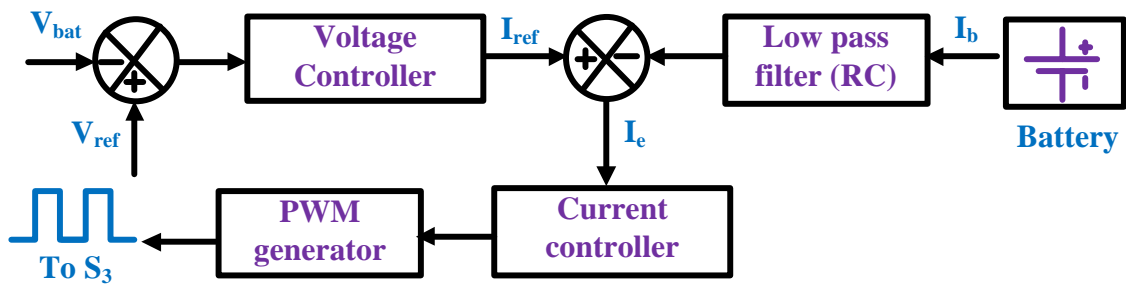
Fig 5.3 (b) Control for Flyback converter

5.2.4 Simulation Results

The simulation results for charging battery by using modified Zeta converter as a PFC unit is shown in Fig 5.4 below which shows supply voltage (V_s) with a peak voltage of 311V, supply current (I_s) with a peak value of 22.37A, Inductor 3 current (I_{L3}), Inductor 4 current (I_{L4}), battery voltage (V_{bat}), battery current (I_{bat}), State of charge (SOC%) and THD% as 4.66% respectively.
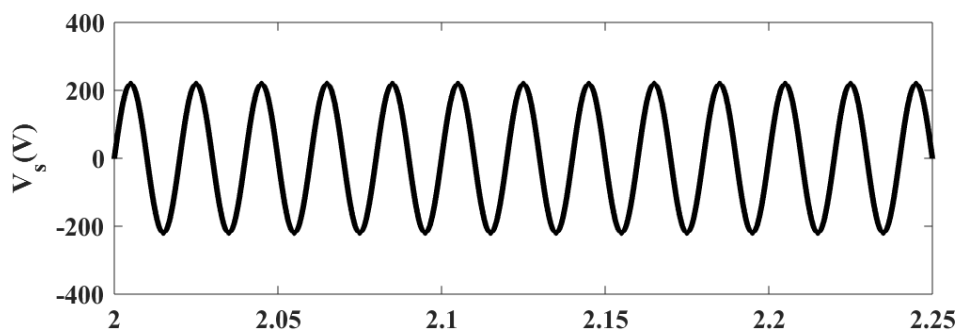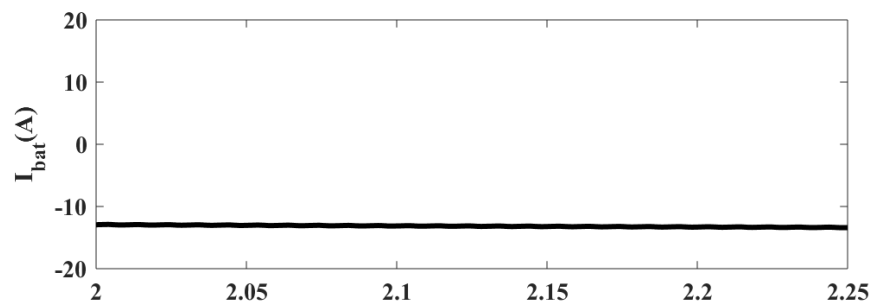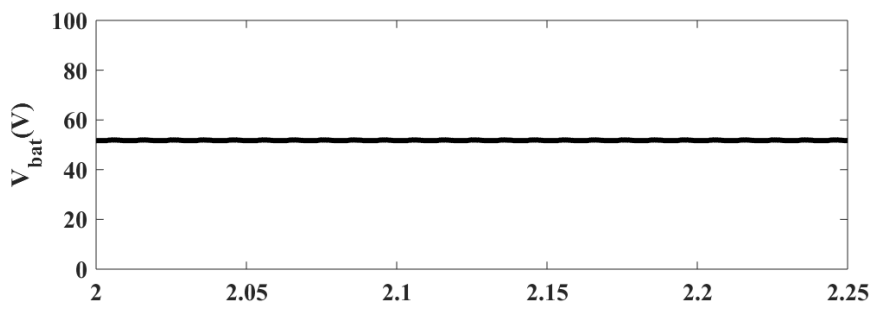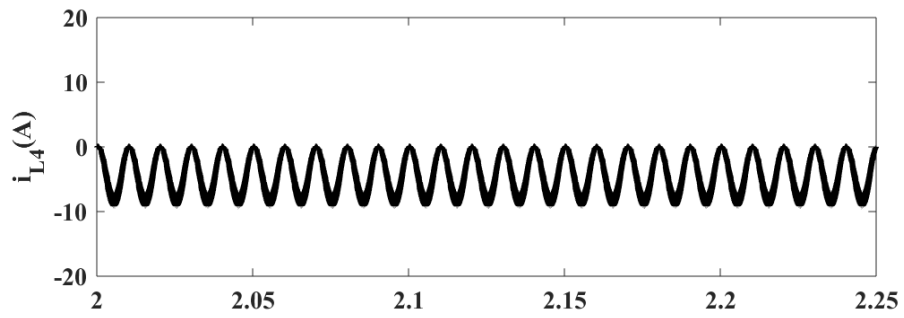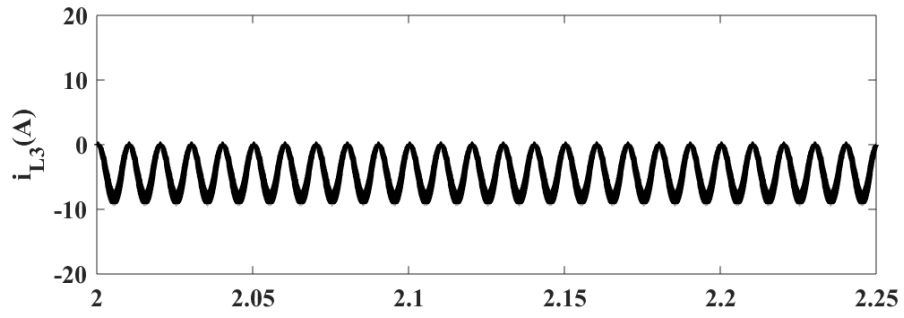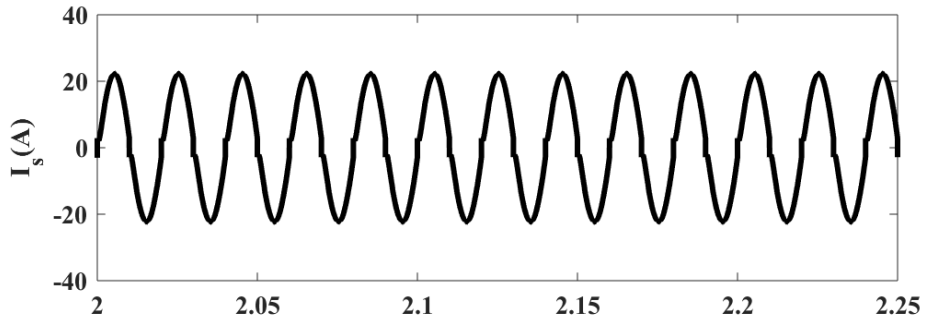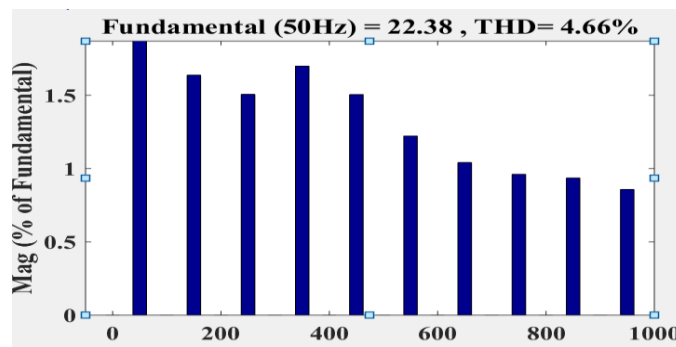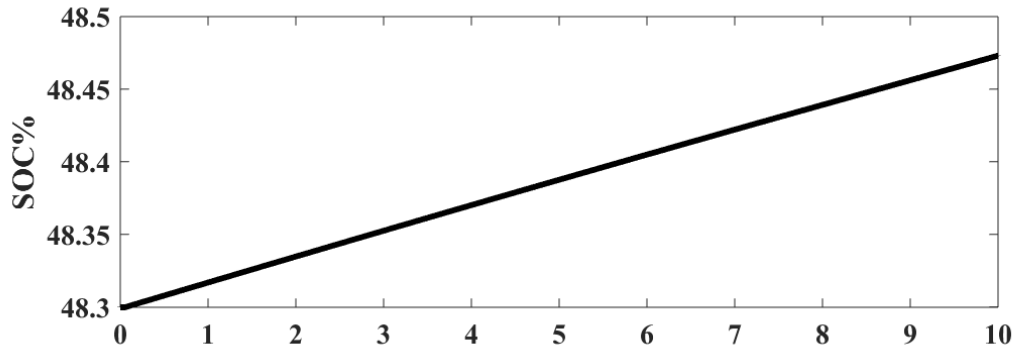
Fig. 5.4. Results for interleaved Luo as PFC for battery charging

5.3 Conclusion

Interleaved converters give excellent results as compared to conventional converters and also better for modified converters in some cases. As it can be seen from above analysis that THD has been reduced to great extent as well as power factor tends to unity which is desirable in charging of EV.

CHAPTER-VI

HYBRID EV CHARGING SYSTEM

6.1 Introduction

The basic charging system deals with DC-DC converter as power factor correction unit to lower down THD and improving power factor but as per the technology advancements research towards hybrid systems of charging is shifted which include sources like solar apart from AC mains or grid to charge the battery. It can boost up the process of charging and can be helpful in case of lack of supply also. So basically, hybrid systems can improve reliability of the whole charging process and hence of vehicle. Such a system is discussed in further sections in this chapter. According to a thumb rule, it is required to have 10 metre square area for installing a solar capacity of 1 kW. So, in LEV's area constraints are there which restricts the installation of higher capacity panels on their rooftop. Still their efficiency can be improved even with low power solar PV installations up to 500W and in some cases if vehicle can accommodate more panel, then it can be up to 700W. In hybrid systems which includes use of supercapacitors, Flywheels, Fuel cells etc. Supercapacitor is a new and willing area for further researches in charging system of EV. A general layout of hybrid charging system topology having supercapacitor is shown in Fig 6.1.
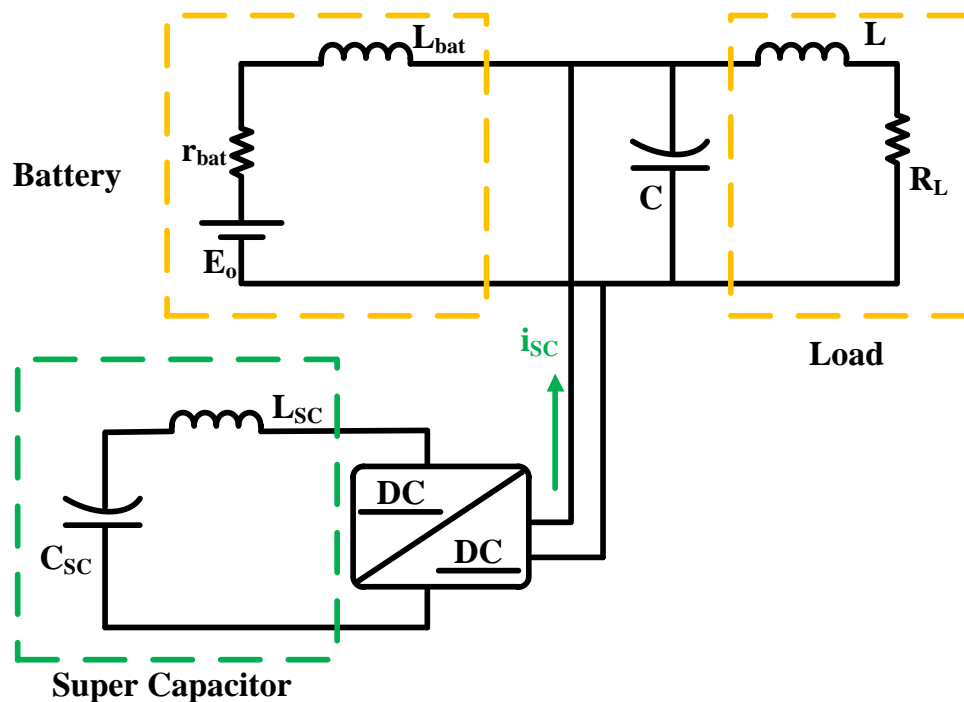
Fig 6.1 Supercapacitor in battery charging

6.2 Bridgeless Isolated Zeta Converter aided with Solar photovoltaic system

An onboard battery charger with a bridgeless isolated Zeta converter as a PFC unit is aided with solar PV for battery charging in this configuration. Bridgeless system is used because of elimination of DBR in its circuit leads to reduction in conduction losses at input thereby improving the battery charging process. The solar PV aided system can charge the battery in the absence of AC power and can also increase battery charging in the presence of power and a PFC circuit. The CUK converter in a solar PV circuit reduces the DC voltage generated at the PV input to the desired level by varying the duty cycle of the switch.

6.2.1 Working and Design Considerations

The PFC converter works in three modes depending on the basis of switching of S_1 and S_2. Isolation polarity decides the on and off working of the components at output side of bridgeless isolated Zeta converter. The designed converter is made to work in DCM mode. Fig 6.2 depicts the configuration for how an integrated system operates to meet the needs of a dependable system.
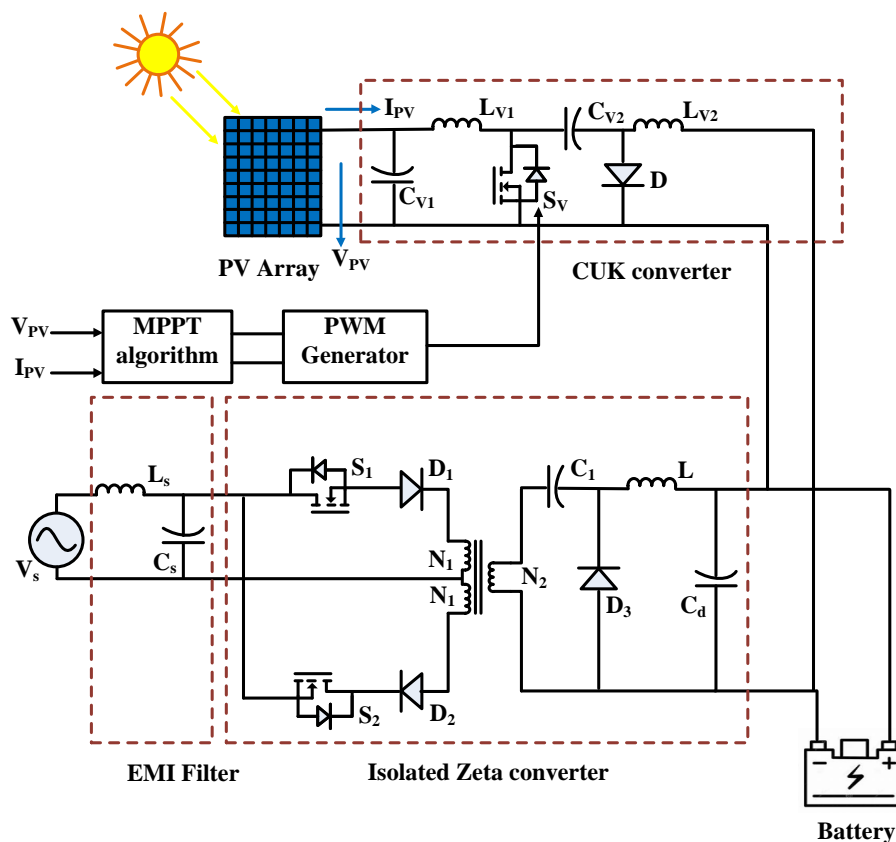
Fig 6.2 Isolated Zeta with PV Configuration

➢ **Mode-1:** Fig 6.3(a) and Fig 6.3(b) represents mode 1 during positive and negative half cycles respectively. Positive half cycle's operation includes switch S_1 becomes on and consequently upper half of the transformer is in working mode i.e.; energy is stored in magnetizing inductance causing capacitor C_1 to be in charging mode whereas diode D_3 is in non-conducting state. Battery is charged via C_1 and L as illustrated in Fig 6.3(a). In case of Fig 6.3(b) during negative cycle switch S_2 is on and upper half is non-working. Diode D_3 is in forward biased and in working condition. Charging voltage is supplied by the output capacitor in this mode.
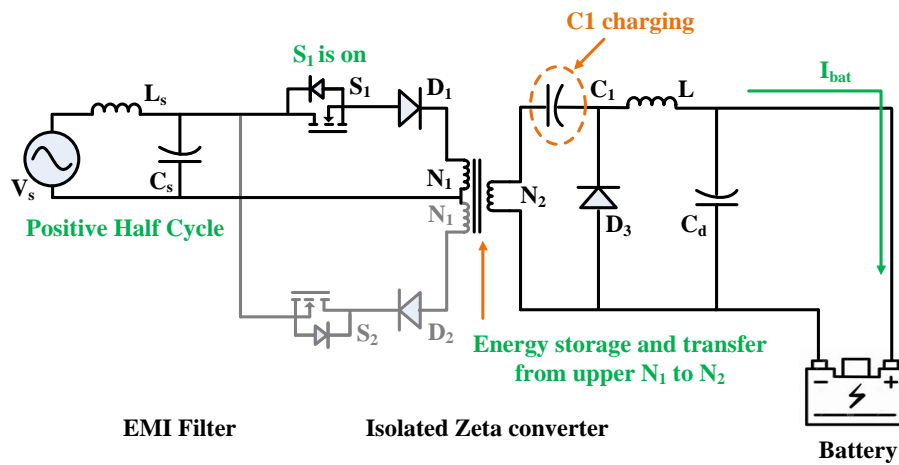
Fig 6.3 (a) Mode 1(a)
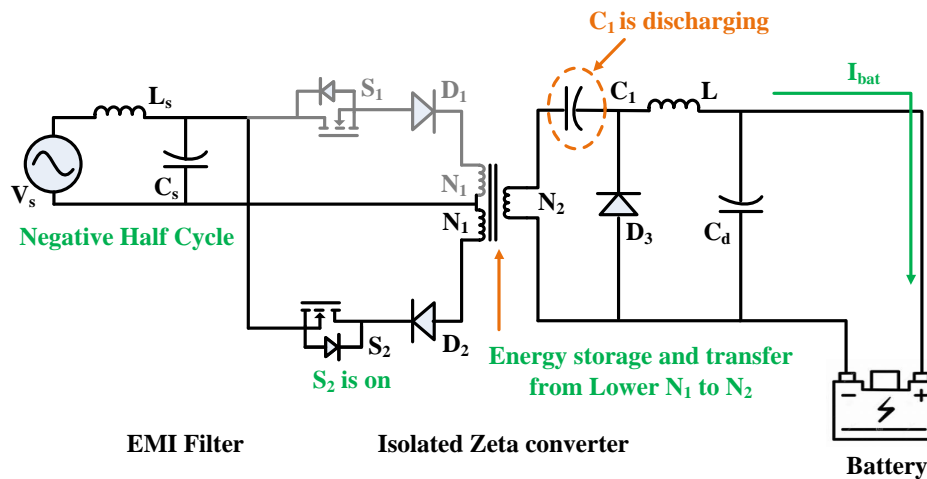
Fig 6.3 (b) Mode 1(b)

➢ **Mode-2:** After mode 1 both the switches are made to turn off in mode 2 as shown in Fig 6.3(c). In this charging of the battery is ensured by the output inductor as both the switches are in off condition and magnetizing inductance is also getting discharged.
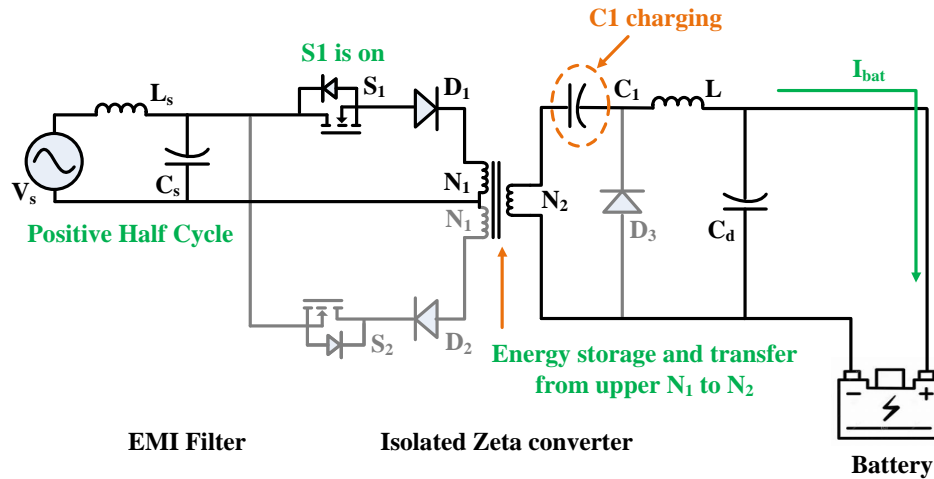
Fig 6. (c) Mode 2

➢ **Mode-3:** The magnetising inductance has been discharged fully in mode 3 and isolation is created from primary side of the transformer as can be seen in Fig 6.3(d) and the charging of battery is now completely the task of output inductor.
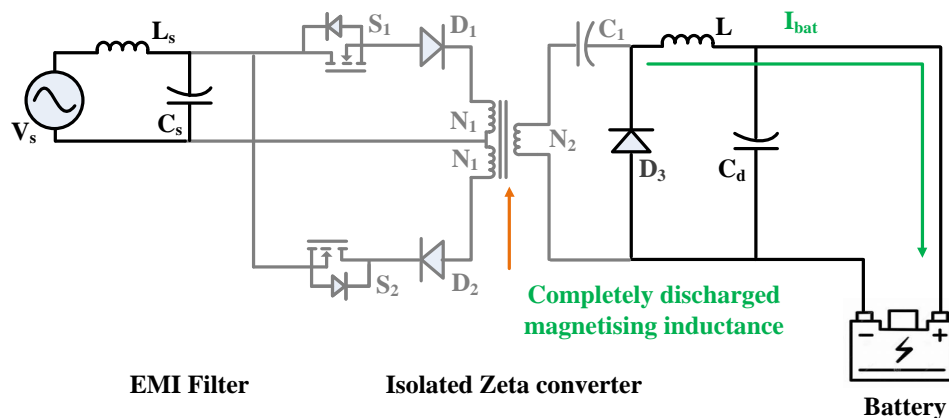
Fig 6.3 (d) Mode 3

A battery of 48V is getting charged with the help of PFC fed circuit as well as from solar fed circuit having CUK converter in it. The bridgeless isolated zeta converter is supplied by input supply as defined by:

$V_S(t) = V_m \sin \omega t$; where ω is $2\pi f$ and frequency f is given by 50 Hz. Output equation for charging is given by:

$$V_o = \left(\frac{N_2}{N_1} \right) \left(\frac{D}{1-D} \right) V_{in} \qquad (6.1)$$

where $\left(\dfrac{N_2}{N_1}\right)$ is the transformer turns ratio considered as 1:2 here and V_{in} is the average voltage given as:

$$V_{in} = \frac{2V_S}{\pi} \tag{6.2}$$

The critical magnetizing inductance value can be calculated as per the given equation (5.3) and the chosen inductance value should be very lower than the critical value.

$$L_m = \frac{\left(V_o^2\Big/P\right)(1-D)^2}{2Df_s\left(N_2\Big/N_1\right)^2} \tag{6.3}$$

where f_s is PFC converter's switching frequency. The capacitor C_1 present at the middle of the circuit and is found with the help of equation (6.4).

$$C_1 = \frac{V_oD}{\Delta V_{C_1} f_s\left(V_o^2\Big/P\right)} \tag{6.4}$$

The inductor L at output has specifications given by:

$$L = \frac{V_o(1-D)}{f_s\Delta I_L} \tag{6.5}$$

where, ΔI_L is the ripple in inductor current and it is regarded as 10% of inductor current. Output inductor value is high as it fulfils the energy requirement of load during the entire switching process. The DC link capacitor C_d at the output of PFC converter is calculated with the help of equation (6.6).

$$C_d = \frac{I_o}{2\omega\Delta V_d} \tag{6.6}$$

where ΔV_d is the DC link's voltage ripple which is chosen as 2% of the capacitor's DC link voltage.

Filter capacitance C_s and L_s are given by the equations (6.7) and (6.8) respectively. The calculated value is the maximum value of filter capacitance and chosen value should be less than calculated one.

$$C_s = \frac{P\sqrt{2}/V_S}{\omega V_m} \tan \theta \qquad (6.8)$$

Where θ is the angle of displacement in supply voltage and current at mains.

$$L_s = \frac{1}{4\pi^2 f_c^2 C_s} \qquad (6.9)$$

Where f_c is filter's cut off frequency which is chosen as $1/10^{th}$ of the converter frequency.

The design of CUK converter used in Solar PV circuit for getting the desired voltage for battery charging are given as follows: Inductors L_{v1} and L_{v2} are calculated by the formulas as per equations (6.10) and (6.11):

$$L_{v1} = \frac{(1-D)}{2Df}\left(V_o^2/P\right) \qquad (6.10)$$

$$L_{v2} = \frac{(1-D)}{2f}\left(V_o^2/P\right) \qquad (6.11)$$

The capacitors C_{v1} and C_{v2} are given by the equations (6.12) and (6.13).

$$C_{v1} = \frac{DV_o}{\Delta V_{c_{v1}} f\left(V_o^2/P\right)} \qquad (6.12)$$

$$C_{v2} = \frac{(1-D)V_o}{8\Delta V_{c_{v2}} f^2 L_{v2}} \qquad (6.13)$$

All the calculated values for designing of isolated Zeta converter is mentioned in Table 6.1 while for CUK converter used in PV is mentioned in Table 6.2.

Table 6.1-Designed values for Isolated Zeta converter

	Parameters of Isolated Zeta Converter	Designed values
1.	Supply voltage V_s	220V
2.	Average output voltage V_{in}	198V
3.	Switching frequency f_s	20kHz
4.	Filter capacitance C_s	330nF
5.	Filter Inductance L_s	3mH
6.	Output Capacitor C_1	330nF
7.	Output Inductor L	0.8mH
8.	DC link capacitor C_d	10mH
9.	Magnetizing Inductance L_m	50μH

Table 6.2-Designed values for CUK converter used in PV

	Parameters of CUK converter used in PV	Designed values
1.	Input Inductor L_{v1}	2.3mH
2..	Output Inductor L_{v2}	2.5mH
3.	Input Capacitor C_{v1}	100μF
4.	Output Capacitor C_{v2}	5μF

6.2.2 Control Strategy

Isolated Zeta converter has two switches S_1 and S_2 which are controlled using cascaded PI loop as shown in Fig 6.4, in which battery voltage is then compared to a voltage that has been taken as a reference voltage and voltage controller is fed with error voltage. The output signal of voltage PI controller is compared with the current PI controller receives the battery current which in turn generates pulses with the help of PWM generator. For PI tuning method opted here is Zeigler Nicholas. Before finding the values of K_p and K_I it is important to obtain transfer function of the system which has been achieved using the aid of steady-state simulations and using state space method. After finding out transfer function, Routh Hurwitz method is used to find out the critical value of K_{cr} afterwards equations (6.14), (6.15) and (6.16) can be used to find out the values of K_p and K_I.

$$T_{cr} = \frac{2\pi}{\omega_{cr}} \tag{6.14}$$

$$K_I = \frac{1.2K_P}{T_{cr}} \tag{6.15}$$

$$K_P = 0.45K_{cr} \tag{6.16}$$

In solar PV system, the switch S_v is controlled with the assistance of maximum power point tracking (MPPT) algorithm which is P&O technique here. The flow chart in Fig 6.5 shows the working of this technique in proper manner. Maximum power from PV array is extracted by using CUK converter as shown in Fig 6.2 and variation in duty cycle is used to achieve the maximum point of power in P-V curve at the concerned irradiation.
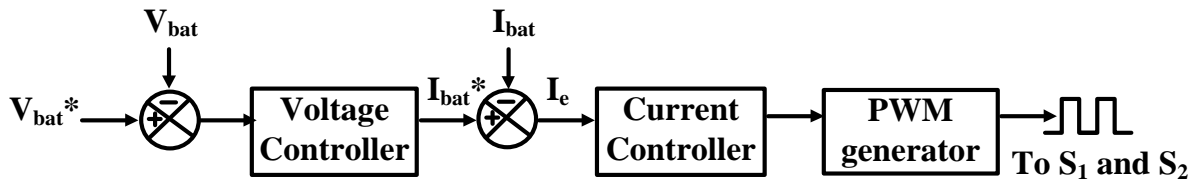
Fig 6.4 Control for Isolated Zeta converter
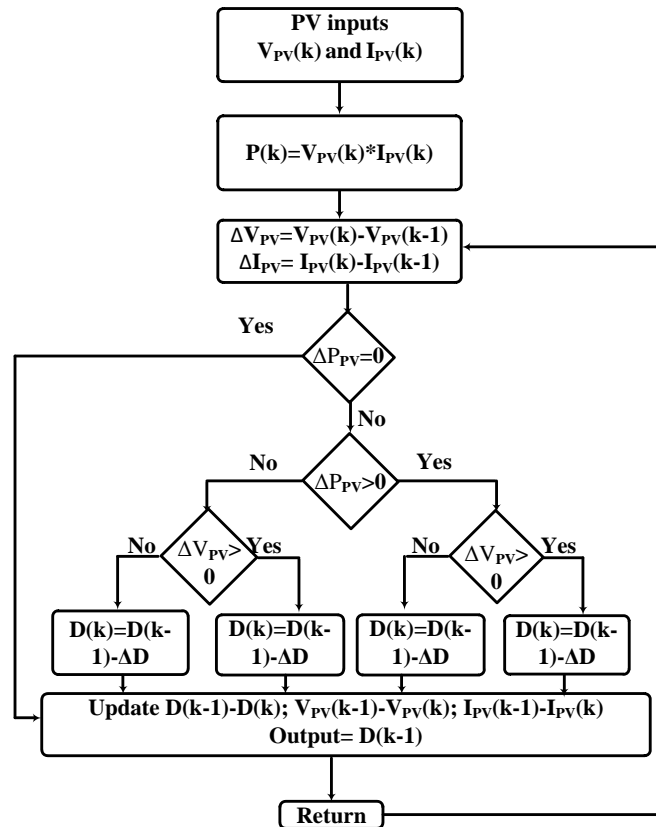
Fig 6.5 P&O algorithm

6.2.3 Simulation Results & Discussion

The results for PFC Zeta converter are as shown in Fig 6.6. It can be clearly observed that supply voltage and supply current are in phase showing the power factor closer to unity. Constant battery voltage is showing the charging of battery constantly. Negative battery current is a sign of charging of battery and hence li-ion battery of 48V,100Ah is getting charged with a constant current of 10A. Increasing SOC% is another parameter showing charging of battery as in Fig 6.6. THD of input supply current is found to be 1.30% which represents reduction in ripple to a large extent in the circuit. Overall battery is getting efficiently charged with the help of bridgeless PFC Zeta converter. In Fig 6.6. charging via solar fed CUK converter has been illustrated at solar irradiation of 1000W/¬m^2.
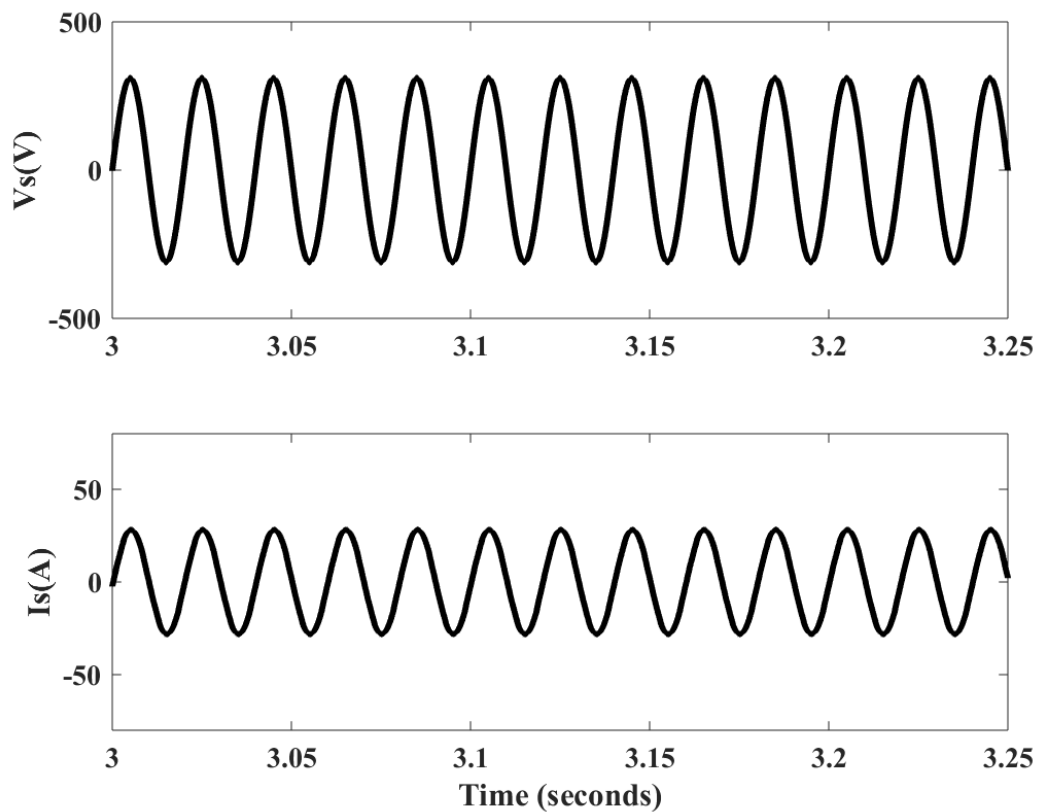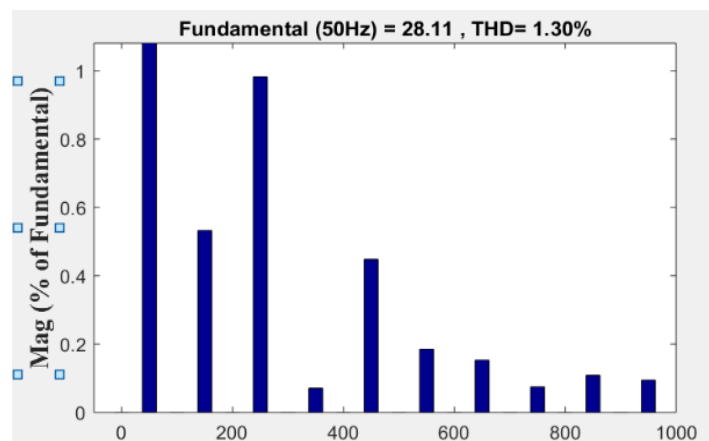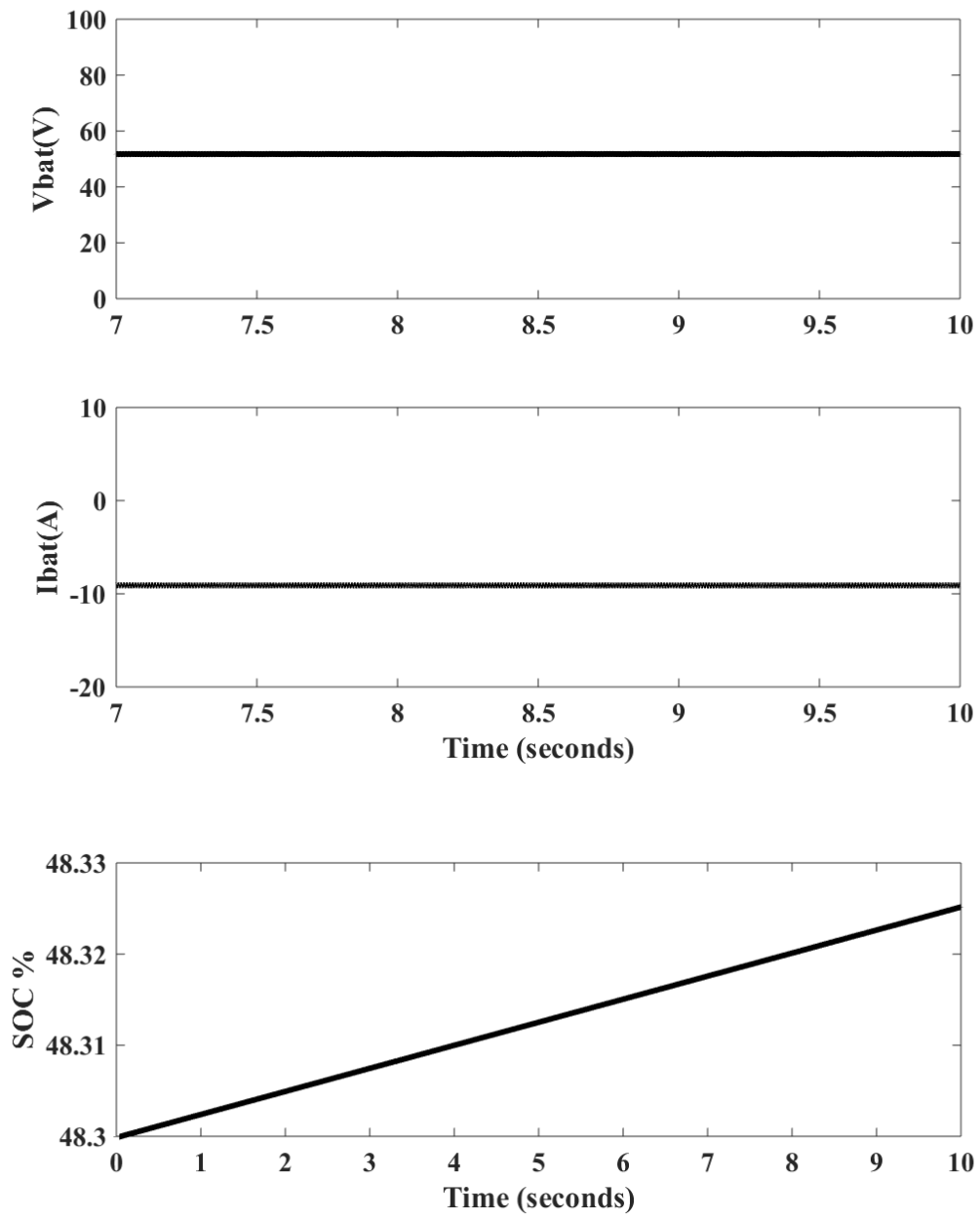
Fig 6.6 Results for Hybrid system battery charging
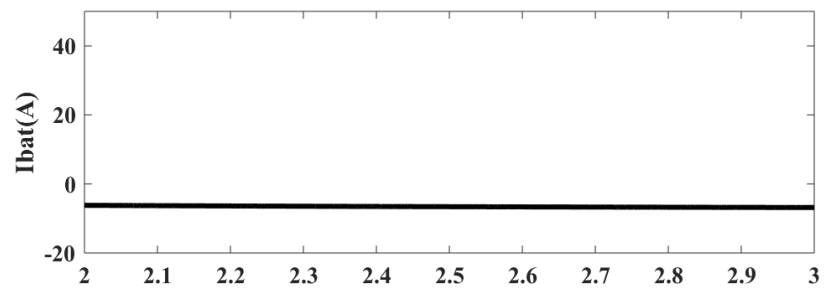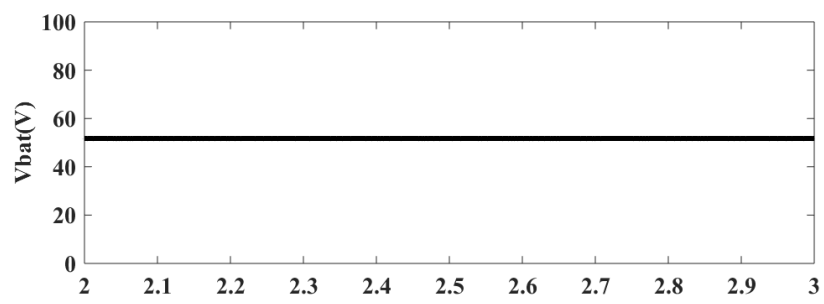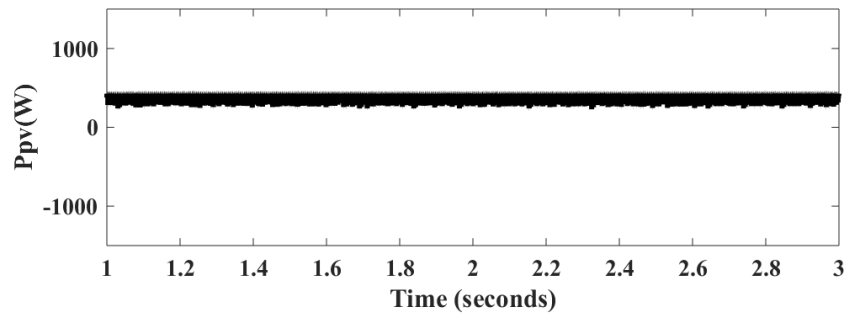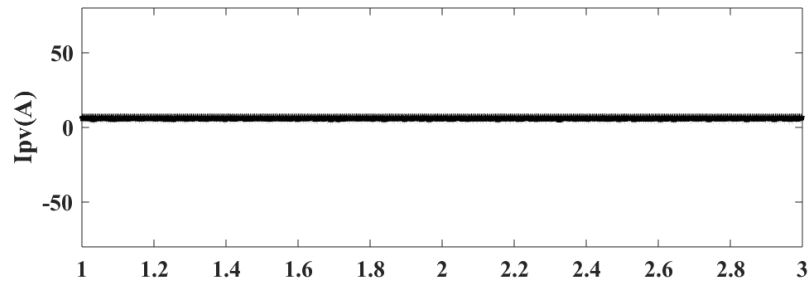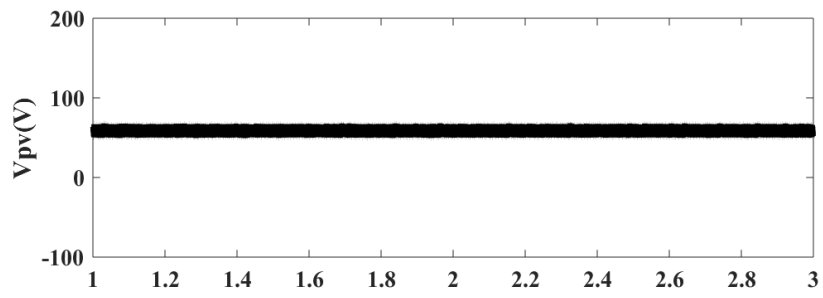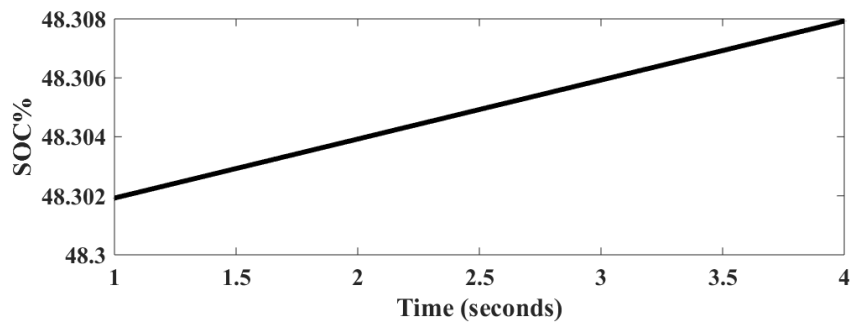
Fig 6.7 Charging characteristics of solar fed CUK converter charging at solar irradiation 1000W/m^2: Vpv (V), Ipv(A), Ppv(W), Vbat(V), Ibat(A), SOC%

6.3 Conclusion

An assisted solar PV charging has been presented in this repot which is a cost-effective and efficient approach for the charging of battery in LEV's. The effectiveness and reliability of system has been improved by utilizing the grid power as well as solar power to enhance the battery charging. THD of the system has been reduced to 1.30% while using PFC bridgeless isolated Zeta converter and in addition to this power factor is closer to unity while battery is getting charged with this prototype.

CHAPTER-VII

CONCLUSION AND FUTURE SCOPE OF WORK

This work reflects how EV charging system works and what are the charging techniques and configurations which can be used in onboard battery charging of EV. All the possible topologies and configurations have been studied to understand the working and design of EV charging system and it is found out that which topology works better inside onboard battery charger which can reduce THD to an extent where it can come under specified norms i.e., THD <5% according to IEC 61000-3-2 standards. All the models have been simulated in MATLAB/Simulink and results have been presented within each chapter. Mainly the DC-DC converters are being focussed under onboard battery charging, which are responsible for the improvement in power factor of the circuit w.r.t charger. So broadly we have discussed following converters so far:

- ❖ Conventional Converters
- ❖ Modified Converters
- ❖ Isolated Converters
- ❖ Bridgeless Converters
- ❖ Interleaved Converters
   New techniques involve:
- ❖ Switched Capacitor/Inductor
- ❖ Hybrid charging systems
- ❖ Supercapacitors
- ❖ Combinational Converters

All the systems are simulated in MATLAB to get the results for voltage, current and SOC% of battery which is being charged. A negative current and increasing SOC% shows the charging of battery while positive current and decreasing SOC% illustrates discharging of a battery.

It has been noted that although buck-boost converter gives good results in conventional converters but to improve power factor further other modified converters have been used and they have reflected the good results performance. Main results that show reliable and sound operation of converter is THD of input current and power factor (should be closer to unity or unity) is illustrated in Table 7.1. In the circuit where DBR is replaced or rearranged,

it can be seen that stresses on input switches becomes very less and charger's operation is smooth.

Table 7.1: Comparison of different converters as PFC

Converter	Type	THD%	Power Factor
Boost	Conventional	9.06%	0.957
Buck-Boost	Conventional	6.55%	0.968
CUK	Conventional	7.43%	0.964
SEPIC	Conventional	7.66%	0.963
Zeta	Conventional	5%	0.975
CUK	Modified	4.82%	0.976
Zeta	Modified	7.67%	0.963
Zeta	Isolated	1.30%	0.994
Luo	Interleaved	4.66%	0.977

On a concluding note, the quality of input current improves as the modifications in the respective conventional converters are made. As it can be observed from the comparison chart analysis illustrated in Fig 7.1 in relevance of CUK converter, Zeta converter and Luo converter for various configurations. It shows that how THD reduces and power factor reaches closer to unity as per Fig 7.2, on making changes in the PFC converter.
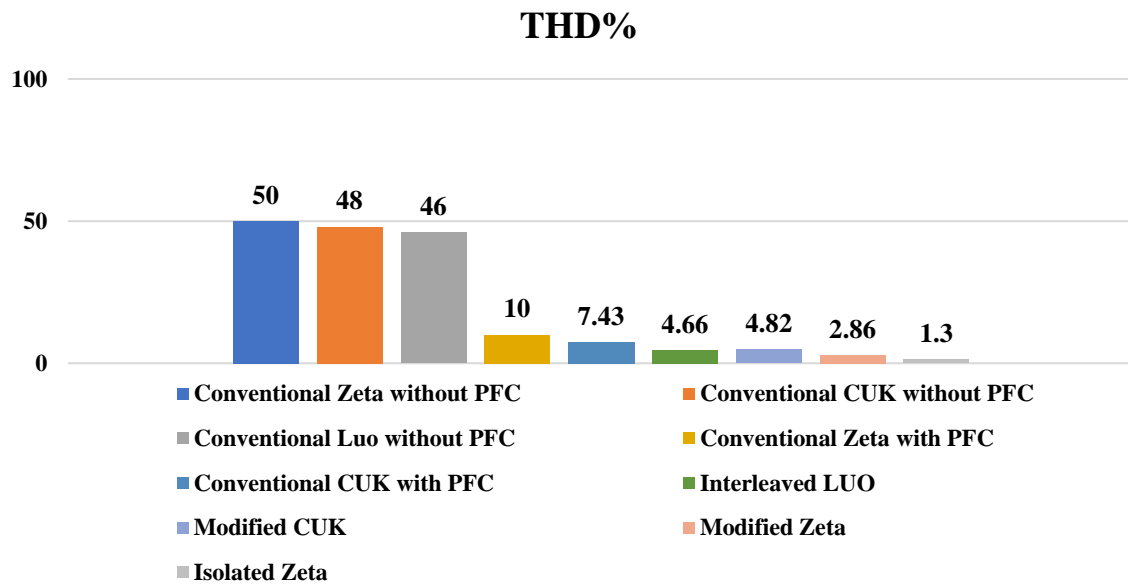
Fig 7.1 Comparison chart for THD%
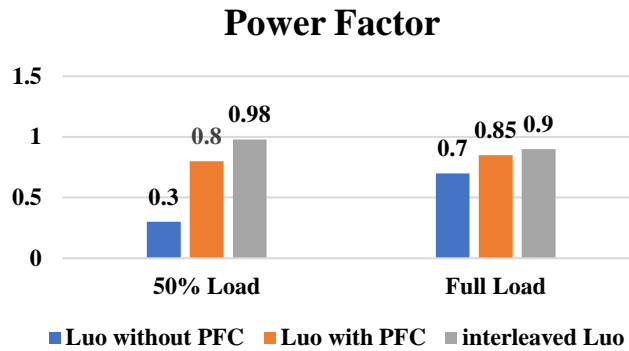
Power Factor

Fig 7.2 Comparison chart for power factor at different load

The future scope work includes study, implementation and understanding of the following work:

❖ Study and implication of bidirectional charging of Electric Vehicle.

Till now the work in this report is concise to unidirectional onboard charging only. As bidirectional charging involves flow in both directions, it is becoming very popular in EV charging area which needs to be studied.

❖ Working on new techniques like switched capacitor/inductor etc.

❖ Exploring more in hybrid systems.

❖ Hardware implementation of the simulated models.

REFERENCES

1. C. Shi, Y. Tang and A. Khaligh, "A Three-Phase Integrated Onboard Charger for Plug-in Electric Vehicles," in *IEEE Transactions on Power Electronics*, vol. 33, no. 6, pp. 4716-4725, June 2018.

2. N. Tutkun and A. N. Afandi, "Design of a PV Powered Charging Station for PHEVs,"*6th International Renewable and Sustainable Energy Conference (IRSEC)*, pp. 1-5, Dec 2018.

3. S. Kim, F.S. Kang, "Multifunctional Onboard Battery Charger for Plug-in Electric Vehicles," in *IEEE Transactions on Industrial Electronics*, vol. 62, no. 6, June 2015.

4. G. Su, C. White and Z. Liang, "Design and evaluation of a 6.6 kW GaN converter for onboard charger applications," *IEEE 18th Workshop on Control and Modelling for Power Electronics (COMPEL)*, pp. 1-6, July 2017

5. A. S. Daniel and K. R. M. V. Chandrakala, "Design of an Isolated Onboard Plug-in Electric Vehicle Charger," *7th International Conference on Electrical Energy Systems (ICEES)*, pp. 147-149, Feb 2021.

6. H. V. Nguyen and D. Lee, "An Improved Low-Voltage Charging Circuit for Single-Phase Onboard Battery Chargers," *IEEE Applied Power Electronics Conference and Exposition (APEC)*, pp. 3325-3331, March 2019.

7. S. S. Indalkar and A. Sabnis, "Comparison of AC-DC Converter Topologies Used for Battery Charging in Electric Vehicle," *2nd International Conference on Intelligent Computing, Instrumentation and Control Technologies (ICICICT),* pp. 1624-1627, July 2019.

8. B. Singh, B. N. Singh, A. Chandra, K. Al-Haddad, A. Pandey and D. P. Kothari, "A review of single-phase improved power quality AC-DC converters," in *IEEE Transactions on Industrial Electronics*, vol. 50, no. 5, pp. 962-981, Oct. 2003.

9. I. Subotic and E. Levi, "A review of single-phase on-board integrated battery charging topologies for electric vehicles, "*IEEE Workshop on Electrical Machines Design, Control and Diagnosis (WEMDCD),* pp. 136-145, march 2015.

10. A. V. J. S. Praneeth, L. Patnaik and S. S. Williamson, "A Variable DC Link Voltage in On-board Battery Chargers for Electric Vehicle Charging Application", *IEEE International Conference on Power Electronics, Drives and Energy Systems (PEDES),* pp. 1-6, Dec 2018.

11. S. Singh, B. Singh, G. Bhuvaneswari, Vashist Bhist, "Improved power quality switched mode power supply using buck-boost converter", *IEEE Trans. on industry application, International Conference on Power Electronics, Drives and Energy Systems (PEDES), pp.1-6, Dec 2014.*

12. R. Philip and C. Sreeja, "Single phase PFC using Buck-Boost converter "*Annual International Conference on Emerging Research Areas: Magnetics, Machines and Drives (AICERA/iCMMD)*" pp. 1-5, July 2014.

13. S. S. Indalkar and A. Sabnis, "An OFF Board Electric Vehicle Charger Based On ZVS Interleaved AC-DC Boost PFC Converter," *8th International Conference on Power Systems (ICPS),* 2019, pp. 1-6, Dec 2019.

14. P. S. R. Nayak, K. Kamalapathi, N. Laxman and V. K. Tyagi, "Design and Simulation Of BUCK-BOOST Type Dual Input DC-DC Converter for Battery Charging Application in Electric Vehicle," *International Conference on Sustainable Energy and Future Electric Transportation (SEFET)*, 2021, pp. 1-6, Jan 2021.

15. J. Panchal, R. Bajaga, P. Aswar, R. Sonawane and M. Murali, "Design and implementation of an integrated, non-isolated, inverted DC-DC buck-boost converter for battery charging," *Second International Conference on Electrical, Computer and Communication Technologies (ICECCT)*, 2017, pp. 1-6, Feb 2017.

16. N. Tiwari and A. N. Tiwari, "Performance Analysis of Unidirectional and Bidirectional Buck-Boost Converter Using PID Controller," 2nd *International Conference on Electronics, Materials Engineering & Nano-Technology*, pp. 1-6, may 2018.

17. R. Kushwaha and B. Singh, "A Modified Bridgeless Cuk Converter based EV Charger with Improved Power Quality," *IEEE Transportation Electrification Conference and Expo (ITEC), Detroit, MI, USA*, pp. 1-6, June 2019.

18. H. N. Shoumi, I. Sudiharto and E. Sunarno, "Design of the CUK Converter with PI Controller for Battery Charging*," International Seminar on Application for Technology of Information and Communication (iSemantic)*, 2020, pp. 403-407, Sep 2020.

19. R. Nithya and R. Sundaramoorthi, "Design and implementation of SEPIC converter with low ripple battery current for electric vehicle applications," *International Conference on Emerging Trends in Engineering, Technology and Science (ICETETS),* pp. 1-4, Feb 2016.

20. R. Kushwaha and B. Singh, "Power Factor Improvement in Modified Bridgeless Landsman Converter Fed EV Battery Charger," *in IEEE Transactions on Vehicular Technology*, vol. 68, no. 4, pp. 3325-3336, April 2019.

21. A. M. Khatab, M. I. Marei and H. M. Elhelw, "An Electric Vehicle Battery Charger Based on Zeta Converter Fed from a PV Array," *IEEE International Conference on Environment and Electrical Engineering and 2018 IEEE Industrial and Commercial Power Systems Europe (EEEIC / I&CPS Europe)*, 2018, pp. 1-5, June 2018.

22. R. Kushwaha and B. Singh, "An Improved Battery Charger for Electric Vehicle with High Power Factor," *IEEE Industry Applications Society Annual Meeting (IAS)*", pp. 1-8, Sep 2018.

23. A. Jha and B. Singh, "Portable Battery Charger for Electric Vehicles," *International Conference on Sustainable Energy and Future Electric Transportation (SEFET)*, pp. 1-6, Jan 2021

24. R. Kushwaha, B. Singh and V. Khadkikar, "An Improved PQ Zeta Converter with Reduced Switch Voltage Stress for Electric Vehicle Battery Charger," *IEEE Energy Conversion Congress and Exposition (ECCE)*, pp- 858-863, Oct 2020.

25. R. Kushwaha and B. Singh, "*Bridgeless Isolated Zeta–Luo Converter-Based EV Charger with PF pre regulation,*" in IEEE Transactions on Industry Applications, vol. 57, no. 1, pp. 628-636, Jan.-Feb. 2021.

26. Nagesha C, A. Sreedevi and M. Gopal, "Simulation and hardware implementation of 24 watt multiple output Flyback converter," *International Conference on Power and Advanced Control Engineering (ICPACE)"*, Bengaluru, pp. 366-370, August 2015.

27. S. J. Thomson, P. Thomas, A. R. and E. Rajan, "Design and Prototype Modelling of a CC/CV Electric Vehicle Battery Charging Circuit," *International Conference on Circuits and Systems in Digital Enterprise Technology (ICCSDET)*, pp. 1-5, Dec 2018.

28. S. S. Indalkar and A. Sabnis, "Comparison of AC-DC Converter Topologies Used for Battery Charging in Electric Vehicle,"*2nd International Conference on Intelligent Computing, Instrumentation and Control Technologies (ICICICT)*, pp. 1624-1627, July 2019.

29. E. L. Carvalho, E. G. Carati, J. P. da Costa, C. M. de Oliveira Stein and R. Cardoso, "Analysis, design and implementation of an isolated full-bridge converter for battery charging," *Brazilian Power Electronics Conference (COBEP)*, pp. 1-6, Nov 2017.

30. R. Kushwaha and B. Singh, "A Modified Bridgeless Cuk Converter based EV Charger with Improved Power Quality," *IEEE Transportation Electrification Conference and Expo (ITEC), Detroit, MI, USA*, pp. 1-6, June 2019.

31. R. Kushwaha, B. Singh, "Design and Development of Modified BL Luo Converter for PQ Improvement in EV Charger," in *IEEE Transactions on Industry Applications*, vol. 56, no. 4, pp. 3976-3984, July-Aug 2020.

32. K. Mishra, M. K. Pathak and S. Das, "Isolated converter topologies for power factor correction — A comparison*," International Conference on Energy, Automation and Signal*, Bhubaneswar, pp. 1-6, 2011.

33. B. Singh and R. Kushwaha, "A PFC Based EV Battery Charger Using a Bridgeless Isolated SEPIC Converter," in *IEEE Trans. on Industry Applications*, vol. 56, pp. 477-487, Jan.-Feb. 2020.

34. J. Gupta and B. Singh, "Single Stage Isolated Bridgeless Charger for Light Electric Vehicle with Improved Power Quality," *IEEE International Conference on Power Electronics, Drives and Energy Systems (PEDES)",* Dec 2020.

35. A. Kumar, U. Sharma and B. Singh, "PMBLDC Motor Based Ceiling Fan Using an Isolated PFC Zeta Converter*," IEEE International Conference on Power Electronics, Smart Grid and Renewable Energy (PESGRE2020)"*, pp. 1-6, Jan 2020.

36. B. Singh and R. Kushwaha, "An EV battery charger with power factor corrected bridgeless zeta converter topology," *7th India International Conference on Power Electronics (IICPE),* pp. 1-6, Nov 2016.

37. R. Kushwaha, B. Singh, "Design and Development of Modified BL Luo Converter for PQ Improvement in EV Charger," in *IEEE Transactions on Industry Applications*, vol. 56, no. 4, pp. 3976-3984, July-Aug 2020.

38. R. Kushwaha and B. Singh, "Interleaved Landsman Converter Fed EV Battery Charger with Power Factor Correction," *IEEE 8th Power India International Conference (PIICON)*, Dec 2018.

39. B. Singh and R. Kushwaha, "Power Factor Pre regulation in Interleaved Luo Converter-Fed Electric Vehicle Battery Charger," in *IEEE Transactions on Industry Applications*, vol. 57, no. 3, pp. 2870-2882, May-June 2021.

40. R. Kushwaha and B. Singh, "An Isolated Bridgeless Cuk-SEPIC Converter Fed Electric Vehicle Charger," *IEEE Industry Applications Society Annual Meeting*, pp. 1-7, Oct 2020.

41. A. M. S. S. Andrade, L. Schuch and M. L. da S. Martins, "Design and implementation of boost-zeta module-integrated converter for PV power applications," *17th European Conference on Power Electronics and Applications (EPE'15 ECCE-Europe),* pp. 1-10, Sep 2015.

42. J. Gupta, B. Singh and R. Kushwaha, "A Rooftop Solar PV Assisted On-Board Enhanced Power Quality Charging System for E-Rickshaw*," International Conference on Power, Instrumentation, Control and Computing (PICC),* Dec 2020.

43. P. H. Kumar and K. Bhaskar, "Electrical Energy Extraction from Unused Heat Energy of Hybrid EVs by Using Peltier Panel for Auxiliary Loads," *IEEE International Power and Renewable Energy Conference*, 2020, pp. 1-6, Nov 2020.

44. B. Bose, V. Kumar Tayal and B. Moulik, "Multi-loop Multi-objective Control of Solar Hybrid EV Charging Infrastructure for Workplace," *2nd International Conference on Advances in Computing, Communication Control and Networking (ICACCCN),* 2020, pp. 491-496, Dec 2020.

45. A. Verma and B. Singh, "Integration of Solar PV-WECS and DG Set for EV Charging Station," *IEEE International Conference on Power Electronics, Smart Grid and Renewable Energy (PESGRE2020)*, pp. 1-6, Jan 2020.

46. Y. J. Nattymol and T. N. Shanavas, "Power Quality Analysis of Single-Phase Transformer-less Buck-Boost Inverter for Compressor load," *IEEE International Conference on Intelligent Techniques in Control, Optimization and Signal Processing (INCOS),* pp. 1-4, April 2019.

47. J. Gupta, R. Kushwaha and B. Singh, "Improved Power Quality Transformer Less Single-Stage Bridgeless Converter Based Charger for Light Electric Vehicles," in *IEEE Transactions on Power Electronics*, vol. 36, no. 7, pp. 7716-7724, July 2021.

48. C. Patnaik, M. M. Lokhande and S. B. Pawar, "Hybrid Energy Storage System using supercapacitor for Electric Vehicles," *Innovations in Power and Advanced Computing Technologies (i-PACT),* pp. 1-5, March 2019.

49. S. Ruddell, U. K. Madawala and D. J. Thrimawithana, "A Wireless EV Charging Topology with Integrated Energy Storage," *in IEEE Transactions on Power Electronics,* vol. 35, no. 9, pp. 8965-8972, Sept. 2020.

50. V. V. Joshi, N. Mishra and D. Malviya, "A Vector Control Based Supercapacitor Current Control Algorithm for Fuel Cell and Battery - Supercapacitor Integrated Electric Vehicles," *IEEE 8th Power India International Conference (PIICON)*, pp. 1-6, Dec 2018.

51. P. J. Kollmeyer et al., "Real-Time Control of a Full-Scale Li-ion Battery and Li-ion Capacitor Hybrid Energy Storage System for a Plug-in Hybrid Vehicle," in *IEEE Transactions on Industry Applications*, vol. 55, no. 4, pp. 4204-4214, July-Aug. 2019.

52. N. Tiwari and A. N. Tiwari, "Performance Analysis of Unidirectional and Bidirectional Buck-Boost Converter Using PID Controller," 2nd International Conference on Electronics, Materials Engineering & Nano-Technology, pp. 1-6, may 2018.

53. W. Zhang and J. Wang, "Research on V2G Control of Smart Microgrid," *International Conference on Computer Engineering and Intelligent Control (ICCEIC)*, 2020, pp. 216-219, Nov 2020.

54. U. C. Chukwu, "The Impact of V2G on the Distribution System: Power Factors and Power Loss Issues," *SoutheastCon*, pp.1-4, April 2019.

55. P. Mahure, R. K. Keshri, R. Abhyankar and G. Buja, "Bidirectional Conductive Charging of Electric Vehicles for V2V Energy Exchange," *IECON 2020 The 46th Annual Conference of the IEEE Industrial Electronics Society*, pp. 2011-2016, Oct 2020.

56. V. K. Singh, Y. Sahu, P. K. Mishra, P. Tiwari and R. Maurya, "Charging of electric vehicles battery using bidirectional converter," *International Conference on Electrical and Electronics Engineering (ICE3)*, pp. 82-88, Feb 2020.

57. C. K. gowda, V. G. Khedekar, N. Anandh, L. R. S. Paragond and P. Kulkarni, "Bidirectional on-board EV battery charger with V2H application," *Innovations in Power and Advanced Computing Technologies (i-PACT),* 2019, pp. 1-5, March 2019.

58. A. K. Chauhan, M. Raghuram, A. K. Tripathi, S. K. Singh, X. Xiong and P. Xuewei, "A High Gain DC-DC Converter based on Switched Capacitor/Switched Inductor Arrangement," *IEEE International Conference on Power Electronics, Drives and Energy Systems (PEDES)*, pp. 1-6, 201

59. M. Vinduja, A. T. Surendran and M. N. Madhu, "A high step-up DC-DC converter based on integrated coupled inductor and switched capacitor," *International Conference on Power, Signals, Control and Computation (EPSCICON), Thrissur India*, pp. 1-5, Jan 2018.

60. S. Moury and J. Lam, "An Integrated PV-Battery Soft-switched Power Converter with MPPT and Voltage Regulation," *IEEE Energy Conversion Congress and Exposition (ECCE), Baltimore, MD, USA,* pp. 3433-3440 Oct 2019.

List of Publications

I.   C. Chaudhary, S. Mishra, U. Nangia, "Design and Analysis of Fly-back DC-DC Converter for Battery Charging with Improved Power Factor," 2021 *Latest Trends in Civil, Mechanical, and Electrical Engineering (LTCMEE), MANIT Bhopal*, April 2021.

    (**Accepted and presented)**

II.   C. Chaudhary, S. Mishra, U. Nangia "A Modified-Zeta Converter based Onboard Battery Charging with Improved THD," *2021 8th International Conference on Signal Processing and Integrated Networks (SPIN 2021), Amity university*, 26-27 Aug 2021.

    (**Accepted for oral presentation).**

III.   C. Chaudhary, S. Mishra, U. Nangia "Unidirectional Onboard Battery Charging for Electric Vehicle using Interleaved Luo Converter," *2021 8th International Conference on Signal Processing and Integrated Networks (SPIN 2021), Amity university*, 26-27 Aug 2021.

    (**Accepted for oral presentation).**

IV.   C. Chaudhary, S. Mishra, U. Nangia "A Bridgeless Isolated Zeta Converter for Battery Charging Aided with Solar Photovoltaic System," *2021 International Conference on Smart Generation Computing, Communication and Networking" (SMARTGENCON 2021), University of Pune*, Oct 2021.

    (**Accepted for oral presentation)**